UNIVERSIDADE FEDERAL DO PARÁ
INSTITUTO DE GEOCIÊNCIAS
PROGRAMA DE PÓS-GRADUAÇÃO EM GEOLOGIA E GEOQUÍMICA

TESE DE DOUTORADO

GEOMORFOLOGIA, MUDANÇAS NA FONTE DE MATÉRIA ORGÂNICA E VEGETAÇÃO EM PLANÍCIES DE MARÉ PRÓXIMAS A FOZ DO RIO AMAZONAS DURANTE O HOLOCENO

Tese apresentada por:

JOSÉ TASSO FELIX GUIMARÃES
Orientador: Prof. Dr. Marcelo Cancela Lisboa Cohen (UFPA)

BELÉM
2011

Dados Internacionais de Catalogação-na-Publicação (CIP)
Biblioteca Geólogo Raimundo Montenegro Garcia de Montalvão

G963g Guimarães, José Tasso Felix

Geomorfologia, mudanças na fonte de matéria orgânica e vegetação em planícies de maré próximas a foz do rio Amazonas durante o Holoceno / José Tasso Felix Guimarães**;** Orientador: Marcelo Cancela Lisboa Cohen – 2011

xviii, 126 f.: il.

Tese (doutorado em geologia) – Universidade Federal do Pará, Instituto de Geociências, Programa de Pós-Graduação em Geologia e Geoquímica, Belém, 2011.

1. Sedimentologia – Amapá (AP). 2. Estratigrafia. 3. Palinologia. 4. Holoceno. 5. Planícies de maré. I. Cohen, Marcelo Cancela Lisboa, *orient*. II. Universidade Federal do Pará. III. Título.

CDD 22º ed.: 552.5098116

Universidade Federal do Pará
Instituto de Geociências
Programa de Pós-Graduação em Geologia e Geoquímica

GEOMORFOLOGIA, MUDANÇAS NA FONTE DE MATÉRIA ORGÂNICA E VEGETAÇÃO EM PLANÍCIES DE MARÉ PRÓXIMAS A FOZ DO RIO AMAZONAS DURANTE O HOLOCENO

TESE APRESENTADA POR

JOSÉ TASSO FELIX GUIMARÃES

Como requisito parcial à obtenção do Grau de Doutor em Ciências na Área de GEOLOGIA

Data de Aprovação: 11/11/2011

Banca Examinadora:

Prof. Dr. MARCELO CANCELA LISBOA COHEN
(Orientador - UFPA)

Prof. Dr. AFONSO CÉSAR RODRIGUES NOGUEIRA
(Membro - UFPA)

Prof.ª Dr.ª MARIA INÊS FEIJÓ RAMOS
(Membro – MPEG)

Prof.ª Dr.ª SUSY ELI MARQUES GOUVEIA
(Membro – UFPA)

Prof. Dr. LUIZ CARLOS RUIZ PESSENDA
(Membro - USP)

A OXALÁ,
aos meus pais Hélio e Lourdes,
e meu irmão Marcelo Guimarães

AGRADECIMENTOS

Ao Prof. Dr. Marcelo Cancela Lisboa Cohen pelos ensinamentos, amizade, sugestões e críticas para o bom andamento do trabalho. Ao Prof. Dr. Afonso César Rodrigues Nogueira pela atenção, paciência, amizade e críticas que auxiliaram este "paleobotânico" a admirar imensamente a estratigrafia e sedimentologia. Ao Prof. Dr. Werner Truckenbrodt pelos ensinamentos sobre processos e respostas em sistemas sedimentares dominados por maré. Ao Prof. Dr. Luiz Pessenda pela amizade e apoio nas discussões isotópicas. Ao Prof. Dr. Hermann Behling pela contribuição nas discussões palinológicas.

Marlon Carlos França e Yuri Friaes pela amizade, dedicação e auxílio nos trabalhos de campo. À MSc. Any Terra pelo carinho e esforço durante o desenvolvimento desta tese. Aos membros do Grupo Análise de Bacias Sedimentares da Amazônia (GSED), dentre eles Luiz Saturnino e Max Rozo pela amizade e discussões. Á Suyanne Flávia pela amizade e apoio nas questões mineralógicas e geoquímicas. À Cleida Freitas pela amizade e eficiência com os assuntos da secretaria do PPGG.

Aos membros Laboratório de Dinâmica Costeira - UFPA e Laboratório de Carbono 14 - Centro de Energia Nuclear na Agricultura (CENA) dentre eles Álvaro Júnior e Jaime Júnior, Universidade de São Paulo-USP pela amizade e suporte. Ao Conselho Nacional de Desenvolvimento Científico e Tecnológico (CNPQ) pela concessão da bolsa de estudos (Processo 143518/2008-9). Este estudo foi financiado pelo CNPQ (Processo 562398/2008-2.

RESUMO

Dados geomorfológicos, fácies sedimentares, pólen, esporos, isótopos do carbono e nitrogênio, razão C/N e datações por ^{14}C permitiram a identificação e discussão sobre a relação entre os principais processos morfológicos, sinais climáticos e suas influências nos padrões de vegetação das planícies de maré próximas a foz do Rio Amazonas durante os últimos 5500 cal anos AP. Assim, os resultados da margem do Rio Amazonas (área da cidade de Macapá, Amapá) indicam influência marinha relacionada à presença de manguezal em planícies lamosas de maré entre 5560 - 5470 anos AP e 5290 - 5150 anos AP. Posteriormente, a área de manguezal retraiu seguindo o retorno de condições mais úmidas e aumento da descarga do Rio Amazonas. Um processo comum de retrabalhamento da planície de maré através da migração lateral de um canal meandrante ocorreu na área de estudo, com desenvolvimento subseqüente de uma vegetação transicional sob influência de água doce. Seguindo a sucessão natural da vegetação em condições climáticas e hidrológicas estáveis, a expansão das florestas de várzea (vegetação inundada por água doce) ocorreu desde 600 - 560 cal anos AP até o presente. Além disso, considerando as planícies de maré localizadas a oeste da foz do Rio Amazonas (área da cidade do Amapá, Amapá), estas condições estáveis também favoreceram a permanência do manguezal nas planícies de maré com deposição de matéria orgânica marinha durante, pelo menos, os últimos 2350 - 2300 cal anos AP. Dados de geomorfologia, salinidade da água, altura máxima de inundação, séries históricas de chuvas e fácies sedimentares foram utilizadas na análise das unidades morfológicas e geobotânicas, e suas mudanças de curto período para entender os principais processos atuantes em planícies de maré a noroeste da foz do Rio Amazonas (área da cidade de Calçoene, Amapá) durante os últimos 30 anos. Assim, esta área de estudo foi subdivida em planalto e planície costeira. O planalto costeiro apresenta uma superfície plana a levemente ondulada modelada por processos erosivos. Avulsão de canais aluviais e feição *birdfoot* possivelmente relacionada a seis lobos deltaicos foram também identificadas neste compartimento. A vegetação é representada por várzea e cerrado. A planície costeira tem um comprimento médio de 10 km, e apresenta canal fluvial de maré, paleocanais, lagos, várzea, campos herbáceos, manguezal, cadeias de *chenier*, barras lamosas alongadas de maré, planícies lamosas e mistas de maré (não vegetada). As fácies sedimentares indicam ambientes dominados por onda e maré. A presença de lagos e cinturão de lagos, coexistência dos campos herbáceos e manguezal na planície costeira podem estar relacionados ao abandono e preenchimento de canais de maré. A análise temporal destas feições indica redução da área do cerrado, expansão das áreas de várzea e manguezal, e formação de extensas planícies lamosas de maré durante os períodos

mais secos sob influência do El Niño. Os períodos mais úmidos sob influência do La Niña provavelmente favoreceu o aumento das áreas de várzea e lagos sobre as áreas de cerrado, e a expansão do manguezal. Desta forma, a diminuição dos índices de chuva durante o El Niño pode ter reduzido o influxo do Rio Calçoene e permitido um aumento da propagação da maré, transporte e deposição de lama ao longo do canal fluvial de maré e seus canais secundários com posterior desenvolvimento do manguezal e estabilização do substrato lamoso próximo a linha de costa durante o La Niña. Considerando uma escala de tempo maior, durante o Holoceno médio e superior, a análise dos dados de morfologia, fácies sedimentares, palinologia, isótopos do carbono e nitrogênio das planícies de maré da cidade de Calçoene-Amapá, indicou que esta planície apresentou alternâncias entre ambientes de supra e intermaré. A porção proximal desta planície está relacionada ao setor transicional entre o planalto e a planície costeira, e representa o estágio final de preenchimento de uma feição côncava para cima formada por um canal abandonado que contribui para o acúmulo de água sob fluxos de energia muito baixos, estabelecimento de pteridófitas e outros vegetais terrestres ao redor do lago formado desde 5280 - 5160 cal anos AP. Durante os últimos 2840 - 2750 cal anos AP, a fonte de lama cessou e matéria orgânica autóctone tornou-se predominante, assim como o aumento na contribuição de matéria orgânica terrestre (plantas C3), principalmente representada pela vegetação de várzea. Campos herbáceos já colonizavam a planície de maré durante os últimos 3170 - 2970 cal anos AP. Entretanto, parte da porção distal da planície de maré relacionada com os campos herbáceos foi coberta por cadeias de chenier entre 3170-2970 e 220-140 cal anos AP. O estabelecimento do manguezal, caracterizado por matéria orgânica estuarina, pólen de *Rhizophora* e *Avicennia*, ocorreu após 1350-1290 cal yr B.P e 220-140 cal anos AP na áreas do G3 e G2, respectivamente. Este padrão de empilhamento dos sedimentos indicando retrogradação, com fácies distais sobre fácies proximais, e transição gradual do depósito herbáceo para o depósito de manguezal sugere que a criação de espaço de acomodação pode ter sido produzida durante um aumento da ação de ondas, freqüência de inundação da maré e evolução de canais secundários na área de estudo como resultado de um aumento progressivo no nível relativo do mar. A integração de todos estes dados sugere que os processos morfológicos, padrões de vegetação e as fontes de matéria orgânica das planícies de maré de Calçoene, Amapá e Macapá foram influenciados pela interação entre o nível relativo do mar, mudanças climáticas e hidrológicas, e dinâmica dos canais de maré durante o Holoceno.

Palavras-chave: Sedimentologia - Amapá (AP). Estratigrafia. Palinologia. Holoceno. Planícies de maré

ABSTRACT

Geomorphological data, sedimentary facies, pollen, spores, carbon and nitrogen isotopes records, C/N ratio and radiocarbon dates allowed the identification and discussion about the relationship between the main morphological process, climatic signals and its influence on vegetation patterns of tidal flats near the mouth of the Amazon River during the last 5500 cal yr B.P. Therefore, data from the margin of Amazon River (Macapá site) indicate marine influence related to mangrove presence over a tidal mud flat between 5560 - 5470 cal yr BP and 5290 - 5150 cal yr BP. Afterward, the mangrove area shrank following the return of more humid conditions and increase of Amazon River discharge. A common reworking process of the tidal flat through the lateral migration of a meandering creek occurred in the study site, with later development of transitional vegetation under freshwater influence. Following the natural vegetation succession under stable climate and hydrological conditions, the expansion of *várzea* forests occurred since 600 - 560 cal yr BP until the present. Furthermore, regarding the tidal flats located west of the mouth of Amazon River (Amapá site), these stable conditions also allowed the mangrove maintenance over mudflats with deposition of marine organic matter during at least the last 2350 - 2300 cal yr BP. Processing and interpretation methods in optical and synthetic aperture radar (SAR) images, data of water salinity, maximum height of flood, historical rain series and sedimentary facies were used in the analysis of the morphological and geobotanical units, and its short-term changes to understand the main processes acting on the tidal flats downdrift of the Amazon River mouth (Calçoene site) during the last 30 years. Thus, the study area was subdivided in two main compartments: coastal plain and plateau. The coastal plateau presents a flat to gently undulated surface shaped by erosive process. Avulsion of alluvial channel and birdfoot feature possibly related to six deltaic lobes were also identified in this compartment. The vegetation is represented by *várzea* (flooded freshwater forests) and savannah. The coastal plain has an average length of 10 km, and it presents the tidal-fluvial channel, paleochannels, lakes, *várzea*, inundated field (herbaceous field), mangrove, chenier ridges, elongated tidal mud bars, tidal mud and mixed flat (non-vegetated). The sedimentary facies indicate tide and wave-dominated environments. The presence of lakes and lake belts, coexistence of herbaceous field and mangrove in the coastal plain may be related to silting and abandonment of tidal channels. The temporal analysis of these features indicates the savannah contraction, expansion of *várzea* and mangrove areas and formation of extensive mud tidal flats during drier period under the influence of El Niño. The wetter period under the influence of La Niña probably allowed the increase of *várzea* and lakes over the savannah areas, and the expansion

of mangrove. Therefore, the decrease of rainfall index during El Niño may have reduced the Calçoene River inflow and favored an increase of tidal propagation, transport and deposition of mud along the tidal-fluvial channel and its secondary channels with subsequent development of mangrove and stabilization of muddy substrate near the coastline in La Niña. Considering a longer time scale during the mid and late Holocene, the analysis of morphology, sedimentary facies, palynological, carbon and nitrogen isotopes, C/N and radiocarbon data from tidal flats in the Calçoene site, indicates that vegetation development during the mid and late Holocene occurred influenced by the interaction relative sea-level and tidal channel dynamic. The data indicate a mud-rich tidal flat that presents alternations between supra and intertidal environments. The proximal portion of the tidal flat is related to the transitional sector between the costal plateau and plain and represents the final filling stage of the concave-up feature formed by the abandoned channel that contributed to water accumulation under very low energy flows, fern and other terrestrial vegetation establishment surrounding the formed lake since 5280 - 5160 cal yr BP. During the last 2840 - 2750 cal yr BP, the source of mud ceased and autochthonous organic material became prevalent as well as the increase in contribution of terrestrial organic matter (C3 plants), mainly represented by *várzea* vegetation. Herbaceous field already colonized the tidal flat at least during the last 3170 - 2970 cal yr BP. However, part of distal portion of the tidal flat related to the herbaceous field was covered by chenier ridges between 3170-2970 and 220-140 cal yr BP. The mangrove establishment, characterized by estuarine organic matter, *Rhizophora* and *Avicennia* pollen, occurred after 1350-1290 cal yr B.P and 220-140 cal yr B.P. on G3 and G2 site, respectively. This stacking pattern of sediments indicating a retrogradation, with distal facies over proximal facies, and gradual transition of herbaceous to mangrove sediment (e.g. G3 site) suggesting that the creation of accommodation space may be produced during an increase of wave action, tidal inundation frequency and evolution of secondary channels in the study site as a result of progressive relative sea-level rise. The integration of all these data suggests that the morphological process, vegetation patterns and sources of organic matter from tidal flats of Calçoene, Amapá and Macapá sites was influenced and conditioned by the interaction between relative sea-level, climatic and hydrological changes, and tidal channel dynamic during the Holocene.

Keywords: Sedimentology - Amapá (AP). Stratigraphy. Palynology. Holocene. Tidal flats.

LISTA DE ILUSTRAÇÕES

1 CONSIDERAÇÕES INICIAIS

2 MID- AND LATE-HOLOCENE SEDIMENTARY PROCESS AND PALAEOVEGETATION CHANGES NEAR THE MOUTH OF THE AMAZON RIVER

3 EL NIÑO AND LA NIÑA EFFECTS ON TIDAL FLATS NEAR THE MOUTH OF THE AMAZON RIVER

4 MORPHOLOGICAL AND VEGETATION CHANGES ON TIDAL FLATS NEAR THE MOUTH OF THE AMAZON RIVER DURING LAST 5000 YR CAL YR B.P.

LISTA DE TABELAS

1 CONSIDERAÇÕES INICIAIS

2 MID- AND LATE-HOLOCENE SEDIMENTARY PROCESS AND PALAEOVEGETATION CHANGES NEAR THE MOUTH OF THE AMAZON RIVER

3 EL NIÑO AND LA NIÑA EFFECTS ON TIDAL FLATS NEAR THE MOUTH OF THE AMAZON RIVER

4 MORPHOLOGICAL AND VEGETATION CHANGES ON TIDAL FLATS NEAR THE MOUTH OF THE AMAZON RIVER DURING LAST 5000 YR CAL YR B.P.

SUMÁRIO

1 CONSIDERAÇÕES INICIAIS

1.1 INTRODUÇÃO

O desenvolvimento das planícies de maré mais extensas do Brasil, localizadas próximas da foz do Rio Amazonas, é caracterizado pela interação de processos morfológicos, hidrológicos e climáticos operando em diferentes escalas temporais e espaciais durante o Holoceno (e.g. Allison *et al*., 1995; Allison & Lee, 2004). Conseqüentemente, gigantescos bancos lamosos ligados à face litorânea alternando com cadeias de chenier arenosas dominam a costa, na qual possui história de mudanças na vegetação marcada por expansão/contração do manguezal (floresta inundada por água salobra) e várzea (floresta inundada por água doce), e coexistência de estratos arbóreos e herbáceos (Guimarães *et al*., 2010; Guimarães *et al*., no prelo).

Os manguezais próximos a foz do Rio Amazonas integram um sistema de *wetlands* que se estende por mais de 480 km e possuem a maior área de manguezais do mundo (Kjerve & Lacerda, 1993). A continuidade deste litoral de manguezal é interrompida por uma zona influenciada pelo influxo do Rio Amazonas, onde a várzea predomina (Cohen *et al*., 2009; Guimarães *et al*., no prelo). A zonação dos *wetlands* é produto da morfologia, gradientes da freqüência de inundação da maré, disponibilidade de nutrientes e salinidade ao longo da planície de maré (Wolanski *et al*., 1990; Gornitz, 1991; Semeniuk, 1994; Duke *et al*., 1998; Kao *et al*., 2004; Stuart *et al*., 2007; Krauss *et al*., 2008).

Mudanças na distribuição dos *wetlands* podem ser interpretadas como reflexo da geomorfologia (e.g. Blasco *et al*., 1996, Lara & Cohen, 2009; Fromard *et al*., 2004), uma vez que seu desenvolvimento e expansão são controlados pela interação continente-oceano, morfologia, regime de maré (Gornitz, 1991; Cohen & Lara, 2003) e fluxo de energia (Woodroffe *et al*., 1982). Assim, o manguezal, que ocupa a planície de intermaré, pode ser erodido e migrar rumo a áreas internas e mais elevadas da planície de maré (supramaré) devido a um aumento da freqüência de inundação. Assim, a vegetação de supramaré pode ser substituída por manguezal, resultando em geral, no empilhamento de fácies sedimentares distais sobre fácies sedimentares proximais (Cohen & Lara, 2003).

A interação destes fatores indica que os *wetlands* são considerados sensíveis a mudanças geomorfológicas, climáticas e no nível relativo do mar (e.g., Cohen *et al*., 2005a; Fromard *et al*., 2004; Alongi, 2008; Cohen *et al*., 2008, 2009; Lara & Cohen, 2009; Guimarães *et al*., 2010; Guimarães *et al*., no prelo). Considerando o nível relativo do mar, este pode também sofrer pequenas oscilações através de mudanças no influxo e descarga dos rios, que são controlados pelo clima (Mörner, 1999). Assim, em uma escala longa de tempo,

eventos secos seculares a milenares podem resultar em oscilações negativas no nível relativo do mar.

Considerando os processos hidrológicos e climáticos de longa escala na região Amazônica, muitos estudos têm indicado que o clima da Amazônia tem variado durante o Holoceno com flutuações significativas na precipitação (Absy *et al*., 1991; Desjardins *et al*., 1996; Ledru, 2001; Behling & Costa, 2000; Freitas *et al*., 2001; Pessenda *et al*., 2001; Weng *et al*., 2002; Bush *et al*., 2007; Pessenda *et al*., 2004a, 2004b; Mayle & Power, 2008), e no influxo dos rios como o Amazonas e seus tributários (Maslin & Burns, 2000; Latrubesse & Franzinelli, 2002). Seguindo esta interpretação, Toledo & Bush (2007) registraram um declínio na abundância de pólen de *Rhizophora* após 7000 cal anos AP, isto sugere uma diminuição da influência marinha, e, a partir de 5000 cal anos AP, a substituição de florestas com dossel fechado por campos herbáceos. Estes resultados podem indicar uma diminuição do influxo do Rio Amazonas devido a uma redução na precipitação da Amazônia durante o intervalo analisado.

No litoral do Amapá, as extensas planícies de maré desenvolvidas próximas ao Rio Amazonas e sua foz podem ser mais apropriadas para investigar mudanças da vegetação relacionada com variações no influxo do Rio Amazonas e nível relativo do mar durante o Holoceno. Entretanto, poucos estudos paleoecológicos baseados em dados de pólen foram realizados nesta área (Toledo & Bush 2007; Guimarães *et al*., 2010). Além disso, a interpretação de dados deve primeiramente considerar que as mudanças na vegetação ocorrem em várias escalas temporais e espaciais, e algumas destas mudanças são devido aos processos alóctones e autóctones (e.g. Bradley, 1999). Assim, dados morfoestratigráficos, $\delta^{13}C$, $\delta^{15}N$ e C/N devem ser utilizados em conjunto com os dados de pólen e esporos, uma vez que eles fornecem informações poderosas sobre os processos sedimentares, relação lateral entre os sedimentos, fontes de matéria orgânica e padrões da vegetação, no quais são necessários para isolar os sinais climáticos dos ruídos não climáticos e melhor interpretar os principais processos atuantes nas mudanças da vegetação (e.g. Dalrymple, 1992; Marzo & Puigdefabregas, 1993; Boutton *et al*., 1998; Behling & Costa, 2000; Cohen *et al*., 2005a; Wilson *et al*., 2005a, b).

Este trabalho apresenta uma descrição detalhada das mudanças geomorfológicas e da vegetação nas planícies de maré próximas a foz do Rio Amazonas durante os últimos 5500 cal anos AP, utilizando dados de morfologia, fácies sedimentares, palinologia, $\delta^{13}C$, $\delta^{15}N$, C/N e datações por ^{14}C. O objetivo é identificar e discutir a relação entre os principais processos climáticos, hidrológicos e morfológicos, e suas influências nos padrões da vegetação.

1.2 ÁREA DE ESTUDO

1.2.1 Configurações geológicas e fisiográficas

As áreas de estudo estão localizadas na Plataforma do Amapá e Bacia do Marajó que estão relacionadas a vários episódios de tectônica distensiva seguidos pela quebra do *Gondwana* e abertura do Atlântico Equatorial durante o Jurássico/Cretáceo Inferior (Szatmari *et al*., 1987; Azevedo, 1991). A Bacia do Marajó é limitada ao sul e a leste pelo arco de Gurupá e Tocantins, respectivamente (Figura 1a). A geologia regional apresenta rochas do Arqueano, Paleoproterozóico, Mesoproterozóico, Paleozóico e Quaternário (e.g. Horikava, 2003; Figura 1a). O Eon Arqueano está representado por rochas granítico - gnáissicas do Complexo Guianense e Cinturão Granulítico Tucumaque (Lima *et al*., 1974; Lima *et al*., 1992). A Era Paleoproterozóica abrange o Complexo Máfico - Ultramáfico Bacuri que intrude rochas do Complexo Guianense e rochas metavulcanossedimentares do Grupo Vila Nova (Pimentel *et al*., 2002; Lima *et al*., 1992). A Era Mesoproterozóica está relacionada com rochas vulcânicas félsicas do Grupo Iricoumé e rochas vulcânicas alcalinas do Grupo Maparí (Horikava, 2003). Rochas sedimentares do Paleozóico das Formações Trombetas (Siluriano) e Curuá (Devoniano) estão expostas na parte oeste do Estado do Amapá (Horikava, 2003), e areias e argilas avermelhadas, mosqueadas com conglomerados ferruginosos do Grupo Barreiras (Santos *et al*., 2004). Entretanto, Souza & Pinheiro (2009) e Souza (2010) demonstraram que estes depósitos formam terraços ferruginosos do Pleistoceno (80.000 a 30.000 anos A.P.) com orientação NW-SE, constituídos por pelitos, arenitos e cascalhos com predominância de ritmitos, acamamento *wavy*, estratificação heterolítica inclinada e estratificações cruzadas tabular e acanalada. Estas fácies foram agrupadas em canal fluvial, canal meandrante influenciado por maré e planície de maré. Assim, o modelo deposicional corresponde a um sistema costeiro com rios meandrantes influenciado pela maré com história geológica dominada por processos glacio-eustáticos, concomitantemente conduzidos por mudanças no nível do mar e interferências tectônicas durante os últimos 78 ka anos AP.

Do Pleistoceno ao Holoceno, mudanças climáticas, no nível do mar, e atividades neotectônicas resultaram em processos erosivos-deposicionais que modelaram o relevo até a sua atual configuração (Lima *et al*., 1991). Assim, ao longo da planície costeira adjacente ao Rio Amazonas, extensos terraços baixos e planos do Holoceno compostos de areia e lama foram desenvolvidos seguindo um padrão NW-SE, com diminuição na largura para noroeste (Figura 1b).

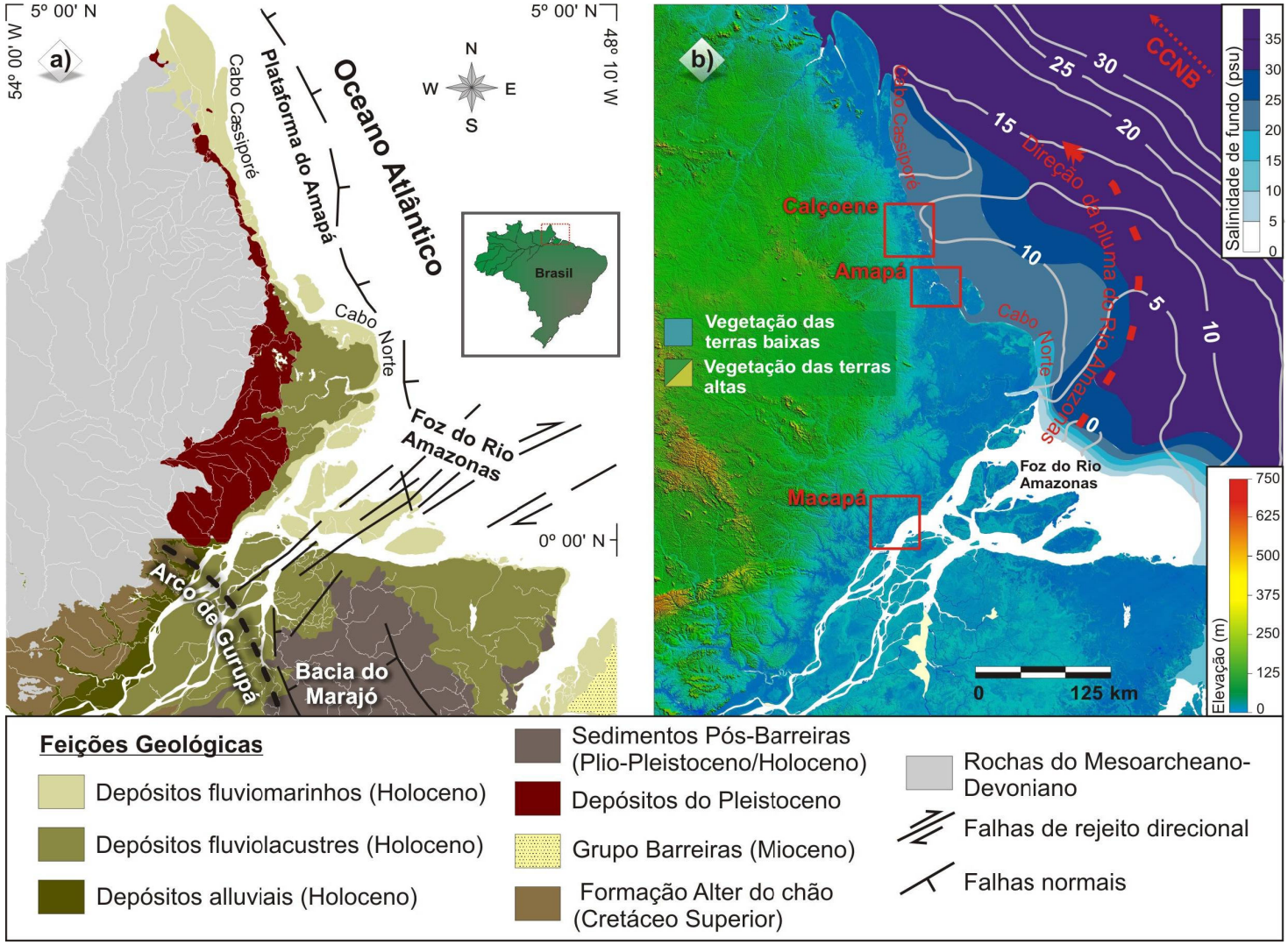

Figura 1 - a) Geologia regional da área de estudo na Bacia do Marajó e Plataforma do Amapá (modificado de Companhia de Pesquisa de Recursos Mineirais - CPRM, 2010 e Costa *et al*., 2002), e b) Mapa de elevação com salinidade de fundo e superficial da água, direção da pluma do Rio Amazonas e Corrente Costeira Norte do Brasil (CCNB) próximo ao litoral do Amapá (modificado de Vinzon *et al*., 2008 e

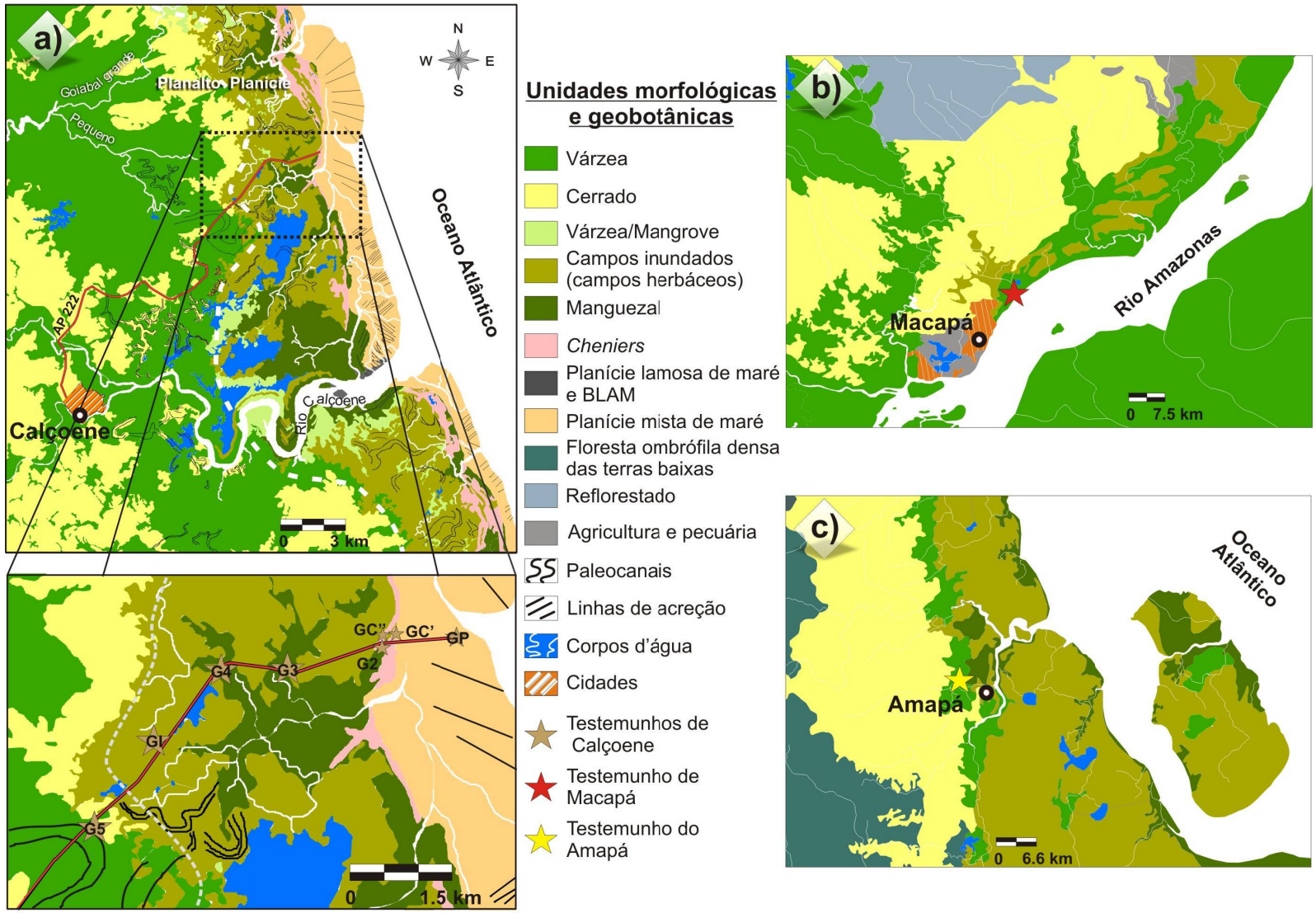

Figura 2 - Unidades morfológicas, geobotânicas e de uso da terra das áreas de estudo ao longo da costa do Estado do Amapá; a) Calçoene, b) Macapá e c) Amapá.

A planície costeira possui extensão média de 10 km, e apresenta canal estuarino, paleocanais, lagos, várzea, campos inundáveis, manguezal, *cheniers*, barras lamosas alongadas de maré (BLAM), planícies lamosas e mistas de maré (Figura 2a, b, c). As litologias e estruturas sedimentares predominantes são heterolíticos *flaser*, *wavy*, lenticular e inclinados, lamas inclinadas e bioturbadas, areias com laminações cruzadas, planas e truncadas de baixo ângulo, geradas em ambientes dominados por processos de maré e onda, influenciados pela descarga do Rio Amazonas, ventos alísios e regime de macromaré semidiurna. A presença de lagos e cinturão de lagos, juntamente com a coexistência de manguezal e campos inundados podem estar relacionados ao abandono e preenchimento de canais de maré (Guimarães *et al*., submetido).

Os tipos de solos são derivados das feições geológicas descritas na costa do Amapá, e podem ser classificados como Latossolos, Argissolos e Gleissolos conforme o Sistema Brasileiro de Classificação de Solos (Empresa Brasileira de Pesquisa Agropecuária - EMBRAPA, 2006).

Estudos florísticos de Costa Neto (2004), Costa Neto & Silva (2004) e Carvalho *et al*. (2006) descreveram intensamente as unidades geobotânicas e de uso da terra do estado do Amapá. Adicionalmente, um levantamento qualitativo da vegetação foi realizado na costa do Estado do Amapá. Assim, os padrões de vegetação descritos são caracterizados por cerrado no interior do continente, vegetação de várzea nas planícies aluviais, lacustres e de maré com influência de água doce, campos herbáceos na zona de supramaré, e manguezal na zona de intermaré próxima a linha de costa (Figura 2a, b, c; Tabela 1).

Tabela 1 - Principais espécies de planta identificadas na costa do Estado do Amapá. Unidades botânicas: AG/AP: agricultura e áreas de pasto; CA: cerrado arbustivo; V: Várzea; CI: Campo inundável (Herbáceo); MG: Manguezal.

(continua)

Família e Espécies	Forma Biológica	Unidades botânicas	Costa Neto (2004)	Carvalho et al. (2006)	Este estudo
Aizoaceae					
Sesuvium sp.	Erva	CI			
Anarcadiaceae					
Spondias mombin L.	Árvore	V			
Tapirira guianensis Aubl.	Árvore	V			
Aquifoliaceae					
Ilex sp.	Árvore	V			
Araceae					
Montrichardia arborescens L.	Erva	V			
Pistia stratioites L.	Erva	V, CI			
Arecaceae					

(continuação)

Euterpe oleracea Mart.	Árvore	V
Mauritia flexuosa L.f.	Árvore	V
Avicenniaceae		
Avicennia germinans L.	Árvore	MG
Cabombaceae		
Cabomba aquatica DC.	Erva	V, CI
Ceratopteridaceae		
Acrostichum sp	Erva	MG
Cobretaceae		
Laguncularia racemosa Gaertn.	Árvore	MG
Cyperaceae		
Cyperus giganteus Vahl.	Erva	CI
Cyperus luzulae (L.) Retz.	Erva	CI
Eleocharis emarginata Ness	Erva	CI
Eleocharis interstincta Vahl	Erva	CI
Eleocharis mutata L.	Erva	CI
Fimbristylis annua All.	Erva	CI
Rhynchospora barbata Vahl	Erva	CA
Scleria sp.	Erva	IF
Euphorbiaceae		
Alchornea sp.	Árvore	V
Hevea guianensis Aubl.	Árvore	V
Hura crepitans L.	Árvore	V
Manihot esculenta Crantz.	Shrub	AG/AP
Fabaceae		
Campsiandra laurifolia Benth.	Árvore	V
Chamaecrista sp.	Erva	CA
Machaerium lunatum SP.	Árvore	V
Macrolobium sp.	Árvore	V
Parkia nitida Miq.	Árvore	V
Pentaclethra sp.	Árvore	V
Vatairea guianensis Aubl.	Árvore	V
Helioconiaceae		
Heliconia sp.	Erva	IF
Malpighiaceae		
Byrsonima crassifolia L.	Árvore	AG/AP, CA
Byrsonima verbascifolia L.	Árvore	AG/AP, CA
Mascagnia sp.	Liana	FV
Malvaceae		
Pachira aquatica Aubl.	Árvore	V
Pseudobombax sp.	Árvore	V
Nymphaeceae		
Nymphaea sp.	Erva	V, CI
Poaceae		

(conclusão)

Hymenachne amplexicaule Nees	Erva	CA, CI	
Olyra latifolia L.	Erva	V, CI	
Paspalum sp.	Erva	CA	
Panicum laxum Sw.	Erva	CI	
Paspalum repens Berg.	Erva	CI	
Zea sp.	Erva	AG/AP	
Ponteridaceae			
Eichhornia azurea (Sw.) Kunth	Erva	CI	
Eichhornia crassipes Mart.	Erva	CI	
Rubiaceae	Erva		
Alibertia sp.	Árvore	FV	
Borreria sp.	Erva	CA, AG/AP	
Psychotria	Erva	CI	
Sapotaceae			
Pouteria sp.	Árvore	V	
Strelitziaceae			
Phenakospermum sp.	Erva	V	
Rhizophoraceae			
Rhizophora harrisonii Leechman	Árvore	MG	
Rhizophora mangle L.	Árvore	MG	
Rhizophora racemosa G. Mey.	Árvore	MG	

1.2.2 Clima e hidrologia

O clima da região é tropical/megatérmico caracterizado por estações secas (Setembro a Dezembro) e úmidas bem definidas (Janeiro a Julho) com uma média anual de precipitação e temperatura por volta de 3000 mm e 27.5 ºC, respectivamente (Bezerra *et al*., 1990). A descarga média do Rio Amazonas é de 170.000 m^3/s (na cidade de Óbidos), com vazão máxima e mínima de 270.000 e 60.000 m^3/s (ANA, 2003). O Estuário do Amazonas possui macromarés semidiurnas (Pugh, 1987), com amplitudes de 4 a 6 m. A pluma do Rio Amazonas é uma feição sazonal que apresenta extensão de ~ 3000 km através do Oceano Atlântico e cobre cerca de 2 x 10^6 km^2 (Cooley *et al*., 2007). A estrutura da pluma é controlada pela Corrente Costeira Norte do Brasil (CCNB), que induz um fluxo a noroeste com velocidades de 40 - 80 cm/s sobre a plataforma continental (Lentz, 1995), correntes de maré fortes (Beardsley *et al*., 1995), ventos alísios e Zona de Convergência Intertropical - ZCIT (Lentz & Limeburner, 1995). Conseqüentemente, a descarga do rio e as condições

hidrodinâmicas favorecem uma redução forte na salinidade da água ao longo de todo o Rio Amazonas e costa adjacente (Figura 2a, b; Vinzon *et al*., 2008; Rosario *et al*., 2009).

1.3 ESTRATÉGIA METODOLÓGICA, BASE PARA INTERPRETAÇÃO DOS DADOS E ELABORAÇÃO DE MODELOS EVOLUTIVOS

1.3.1 Sensoriamento remoto e processamento digital de imagens

O mapeamento, análise da distribuição espacial e temporal das unidades morfológicas e geobotânicas foram realizadas através do processamento e interpretação de imagens ópticas e SAR com auxílio de levantamentos de campo, relativos à geomorfologia e sedimentologia. Assim, um conjunto composto por seis imagens Landsat/TM referentes aos anos de 1987, 1997 e 2000 (225_58 e 225_68), uma imagem SAR/SRTM V2 de 2000 e duas imagens SLAR/GEMS 1000 de 1971 correspondentes as folhas NA22VD e NA22XC do projeto RADAM (Departamento Nacional de Produção Mineral - DNPM, 1971) foram utilizadas para a etapa de sensoriamento remoto. Algumas características destas imagens são descritas na Tabela 2.

Tabela 2 - Principais características dos dados dos sensores remotos.

Plataforma	**Sensor**	**Data de aquisição**	**Ângulo de incidência**	**Resolução espacial (m)**	**Condições da maré**
Twin-jet	GEMS 1000	1972 20/09/1987	45-77º	16	-
Landsat-5	TM	15/09/1997 28/08/2008	Nadir	30	Low
SRTM	InSAR	Fev. 2000	*off*-nadir	90	-

As imagens Landsat/TM, adquiridas do Instituto Nacional de Pesquisas Espaciais (INPE), foram processadas utilizando o *Spring* 4.3 (Câmara *et al*., 1996), geometricamente corrigidas através de 15 pontos de controle do terreno com o auxílio de um GPSMAP 60CSx, obtidos ao longo dos cruzamentos das principais vicinais do município de Calçoene. O erro quadrático médio foi menor que um *pixel* e a reamostragem foi realizada pelo método do vizinho mais próximo. A correção radiométrica para atenuação dos efeitos atmosféricos foi baseada na correção dos histogramas pelos valores mínimos no método de subtração do *pixel* escuro (Chaves, 1988). Um aumento linear de contraste foi aplicado para aumentar o contraste a partir da redistribuição dos valores na totalidade do histograma. Adicionalmente, uma transformação não-linear que considera a distribuição acumulativa da imagem original baseada na equalização dos histogramas foi realizada para gerar uma imagem resultante, cujo

histograma foi aproximadamente uniforme. Três bandas (TM 4-5-6) para a composição de cor *red-green-blue* (R-G-B) foram selecionadas baseado no *optimum index factor* (Chavez *et al*., 1982) e selecionadas para a interpretação visual. Estes dados foram posteriormente exportados no formato vetorial shapefile para análise espacial no ArcMap 9.2 (ESRI, 2006).

Os dados SRTM (banda C, λ = 5.6 cm) foram obtidos da *National Aeronautics and Space Administration* (NASA), *National Imagery and Mapping Agency* (NIMA), *German Space Agency* (DLR) e *Italian Space Agency* (ASI). O comprimento de onda da banda C interage com os elementos do dossel das árvores que resulta em elevações refletindo a combinação da morfologia do terreno e alturas das árvores (e.g. Hofton *et al*., 2006). Estes dados foram processados para melhorar o potencial da caracterização geomorfológica. Esta etapa consistiu na customização dos esquemas de sombreamento e paletas utilizando o *Global Mapper* 8 (GLOBAL Mapper LLC, 2009). O desenvolvimento das paletas foi realizado por abordagem interativa usando ferramentas de tela que permitiu destacar as características topográficas e morfológicas de interesse para este trabalho (e.g. Hayakawa *et al*., 2010). A análise morfométrica com base no perfil topográfico foi aplicada para aumentar o potencial de visualização das feições.

Os dados SLAR/GEMS1000 foram obtidos a partir da plataforma Carvelle com altitude média do levantamento de 12 km e a velocidade média da aeronave 690 km/h. O sistema imageador GEMS (*Goodyear Mapping System* 1000) operou na banda X (λ = 3 cm e freqüência entre 8 e 12,5 GHz). O levantamento foi realizado ao longo de linhas de vôo N-S com espaçamento de 27.5 km. A altitude da aeronave foi controlada por radar altímetro *Stewart-Warner*, com precisão de 50 m. O posicionamento do avião foi obtido com plataforma inercial do tipo *Litton*, apoiado em terra por estações SHORAN com alcance de 400 km e por estações de posicionamento via satélite TRANSIT, com precisão de aproximadamente 15 m, referidas ao *datum* geodésico de Córrego Alegre (DNPM, 1971). As folhas NA22VD e NA22XC foram digitalizadas em resolução alta para armazenar as respectivas imagens em formato digital matricial, que possibilitou o realce das informações através da aplicação do filtro gama e interpretação das feições do terreno.

1.3.2 Amostragem e descrição de fácies sedimentares

A análise de facies é tradicionalmente utilizada para definir características do sedimento formado sob certos processos (físicos, químicos e biológicos) e ambiente de sedimentação. Desta forma, cada ambiente deposicional possui uma assinatura no sedimento, resultando em fácies sedimentares singulares (Reineck & Singh, 1980; Walker, 1992; Reading, 1996).

A interpretação dos dados sedimentológicos deste trabalho é baseada nos modelos de processo-resposta para depósitos clásticos influenciados por maré (após Klein, 1971). Assim, o transporte de maré pode ser dividido em dez fases físicas (Tabela 3). Cada uma destas fases tende a desenvolver sua própria associação de estruturas sedimentares e feições texturais.

Tabela 3 - Modelos de processo-resposta para depósitos clásticos influenciados por maré (após Klein, 1971).

(continua)

Processo de transporte	**Critério**
A. Transporte de carga de fundo por correntes de maré com reversão bipolar-bimodal da direção do fluxo.	1. Estratificação cruzada com limites dos *sets* pronunciados (Klein, 1970a). 2. Estratificação cruzada espinha de peixe (Reineck, 1963). 3. Distribuição bimodal-bipolar da orientação da direção máxima do mergulho da estratificação cruzada (Reineck, 1963; Klein, 1967). 4. Lâminas paralelas (Van Strasten, 1954). 5. Organização interna complexa de dunas e *sand waves* (Klein, 1970a; Reineck, 1963). 6. Arredondamento supermaturo dos grãos de quartzo (Balazs & Klein, 1972).
B. Assimetria tempo-velocidade do transporte de carga de fundo por correntes de maré.	7. Superfícies de reativação (Klein, 1970a). 8. Freqüência de distribuição bimodal ou multimodal da espessura do *set* do estrato cruzado (Klein, 1970a). 9. Freqüência de distribuição bimodal do ângulo de mergulho do estrato cruzado (Klein, 1970a). 10. Distribuição unimodal da orientação da direção máxima do mergulho do estrato cruzado (Klein, 1970a). 11. Orientação dos estratos cruzados paralela a inclinação do corpo arenoso (Klein, 1970a). 5. Organização interna complexa de dunas e *sand waves* (Klein, 1970a; Reineck, 1963). 6. Arredondamento supermaturo dos grãos de quartzo (Balazs & Klein, 1972).
C. Último estágio de emersão do escoamento de vazante e emersão com súbitas mudanças na direção do fluxo em profundidades muito reduzidas (menor que 2 m).	12. Distribuição trimodal da orientação da direção máxima do mergulho do estrato cruzado (Klein, 1970a). 13. Distribuição quadrimodal da orientação da direção máxima do mergulho do estrato cruzado (Evans, 1965; Klein, 1967). 14. Pequenas *ripples* de corrente sobreposta a 90º ou obliqüamente em grandes *ripples* de corrente (Klein,

(continuação)

	1963, 1970a; Imbrie & Buchanan, 1965). 15. *Ripples* de interferência (Reineck, 1963, 1967). 16. *Ripples* de cristas duplas (Van Straaten, 1954). 17. *Ripples* de correntes com topo achatado (Tanner, 1958). 18. *Ripples* de corrente sobreposta a 90º e 180º na crista e *slip faces* de dunas, *sand waves*, e estratificação cruzada (Klein, 1970a). 19. Seqüências "B-C" das estratificações cruzadas recobertas por micro-lâminas cruzadas (Klein, 1970b). 20. *Ripples* simétricas (Reineck, 1963). 21. *Fetch marks* nas *slip faces* do estrato cruzado (Klein, 1970a). 22. Estruturas de *washout* (Van Straaten, 1954).
D. Alternância de transporte de carga de fundo por correntes de maré com deposição por suspensão durante período de quiescência.	23. Estratificação cruzada com *flasers* (Reineck & Wunderlich, 1968). 24. Acamamento *flaser* (Reineck & Wunderlich, 1968). 25. Acamamento *wavy* (Reineck & Wunderlich, 1968). 26. Acamamento lenticular (Reineck & Wunderlich, 1968). 27. Acamamento de maré (Reineck & Wunderlich, 1968). 28. Acamamento convoluto (Dott & Howard, 1962). 29. *Ripples* de corrente com calhas lamosas (Reineck & Wunderlich, 1968).
E. Deposição de lama em suspensão durante período de quiescência.	30. 23 (acima)
F. Escavação por maré.	31. Conglomerados de lama na base de *washouts* e canais (Reineck, 1963, 1967; Van Straaten, 1954). 32. Conglomerados residuais de conchas na base de *washouts* e canais (Reineck, 1963; Klein, 1963; Van Straaten, 1952). 33. *Ilots* (Macar & Ek, 1965). 34. Conglomerados intraformacionais (Reineck, 1963, 1967). 35. *Flutes* (Klein, 1970a). 36. Escorrimentos (Van Straaten, 1954; Reineck, 1967).

(conclusão)

G. Exposição e evaporação.	37. Gretas de contração (Van Straaten, 1954). 38. Marcas *Runzel* (Wunderlich, 1970). 34. Conglomerados intraformacionais e clastos *rip-up* (Reineck, 1963, 1967).
H. Escavação e diagênese.	39. Profundidade de escavação (Rhoads, 1967). 40. Rastros e trilhas (Van Straaten, 1954). 41. Restos de plantas (Van Straaten, 1954). 42. "Fauna empobrecida" (Van Straaten, 1954).
I. Compactação diferencial e reajuste hidroplástico.	28. Acamamento convoluto (Dott & Howard, 1962). 43. Estrutura de sobrecarga (Van Straaten, 1954). 44. Pseudonódulos (Macar & Antun, 1950).
J. Diminuição do fluxo de energia ao longo do tempo.	45. Gradação normal, seqüência granodecrescente ascendente (Evans, 1965; Reineck, 1963; Van Straaten & Kuenen, 1957; Klein, 1971).

Os modelos de planícies de maré geralmente consistem de uma seqüencia granodecrescente ascendente contendo três membros principais, nos quais podem ser utilizados, com cautela, como elementos arquiteturais para a identificação de depósitos de planícies de maré (Van Straaten 1961; Klein, 1977; Reineck & Singh 1980; Weimer *et al*., 1982; Dalrymple, 1992). O membro basal (submaré) consiste de areia composta por estratificação cruzada espinha de peixe, estratificação cruzada orientada unimodalmente, superfícies de reativação, *ripples* de corrente superpostas no topo do estrato cruzado ou dunas preservadas, *washout* e *ripples*. As estruturas e morfologia indicam um regime de transporte de carga de fundo por correntes de maré com possível assimetria tempo-velocidade, escoamento de emersão e exposição. O segundo membro (intermaré) consiste de litologias mistas de areia e lama intercalada, formadas em *ripples* de corrente, acamamentos lenticular, *wavy* e *flaser*. Os processos deposicionais envolvem a alternância de transporte de carga de fundo e suspensão. O membro superior apresenta lama com lâminas paralelas, gretas de contração e bioturbação. Isto representa o ambiente de supramaré dominado por processos ocasionais de suspensão e exposição subaérea.

Os trabalhos de campo foram realizados durante os meses de maio de 2009 (estação chuvosa) e dezembro de 2010 (estação seca) para caracterização e validação das informações extraídas a partir dos dados de sensoriamento remoto e identificação dos processos sedimentares atuantes na área de estudo. Os dados sedimentares são oriundos de terraços expostos, trincheiras e testemunhos descritos e amostrados da cidade de Macapá, Amapá e

Calçoene (Figura 2) com posição geográfica e topográfica do transecto obtido a partir de um modelo digital de elevação baseado na análise dos dados SRTM e Landsat/TM (Guimarães et al., submetido). Seguindo a proposta de Walker (1992), a análise de fácies incluiu descrições da cor, litologia, textura e estruturas. Radiografias (Raios X) auxiliaram na identificação das estruturas sedimentares. A interpretação dos dados sedimentológicos foi também baseada nos modelos de processo-resposta para depósitos clásticos influenciados por maré (após Klein, 1971; Tabela 3). As fácies sedimentares foram codificadas segundo Miall (1978). Conceitos morfoestratigráficos como a organização e correlação dos sedimentos com base na morfologia, coexistência lateral e superposição através do tempo geológico foram aplicados seguindo a análise geomorfológica da área de Calçoene (Guimarães *et al*., submetido). Adicionalmente, folhas dos gêneros mais abundantes foram coletadas a 2 m de altura, para identificar as assinaturas isotópicas do carbono.

Medições hidrotopográficas (Cohen, 2003) e da salinidade da água foram realizadas ao longo de 30 estações distribuídas em uma transecção ao longo da estrada do Goiabal, que intercepta as principais unidades geobotânicas da região. Estas medições utilizaram réguas graduadas com 2 m de altura e base estável, onde potes de acrílico de 10 ml foram vinculados em cada régua de 10 em 10 cm, para obtenção da máxima altura de inundação e salinidade da água durante a maior maré registrada para o ano de 2009 no litoral do Amapá (Diretoria de Hidrografia e Navegação - DHN, 2009). Dados mensais de precipitação da estação pluviométrica de Calçoene (administrada pela CPRM), entre janeiro de 1987 a dezembro de 2008 foram adquiridos através do HidroWeb (Agência Nacional das Águas - ANA, 2010). Baseado nos dados pluviométricos mensais, dois padrões sazonais distintos foram definidos, com estação chuvosa de janeiro a junho, e estação seca de junho a novembro. As médias pluviométricas sazonais (médias mensais do período chuvoso e seco) e anuais (soma das médias sazonais) foram comparadas com anomalias positivas (El Niño) e negativas (La Niña) entre os anos de 1986 a 2008 obtidas pelo Índice Oceânico Niño (*Climate Prediction Center*/ *National Oceanic and Atmospheric Administration* - CPC/NOAA, 2010), para identificar o grau de influência dos eventos El Niño e La Niña no regime de chuva, e conseqüentemente, na configuração morfológica e geobotânica da costa de Calçoene.

1.3.3 Palinologia

A palinologia atualmente está designada a análise dos materiais biológicos (palinormorfos) de dimensões compreendidas entre 5 e 500 μm, compostos de quitina e esporopolenina, que podem ser estudados através de técnicas palinológicas. Entretanto, os

grãos de pólen e esporos são dominantes nos espectros palinomórficos (Hesse *et al*., 2008). O pólen é o gametófito masculino das angiospermas e gimnospermas, formado nas anteras das flores de monocotiledôneas e dicotiledôneas e nos sacos polínicos dos cones (estróbilos) masculinos das gimnospermas, como pinheiros, abetos, ciprestes, araucárias, ginkgos e cicas. O esporo é o propágulo das plantas criptógamas (e.g. algas, musgos e samambaias).

A exina é uma espécie de envoltório externo do grão de pólen e esporo com grande resistência química, ornamentações variadas, estruturas complexas e vários tipos de abertura que permitem sua identificação (Heslop-Harrison, 1971). Muitas terminologias morfológicas são freqüentemente utilizadas como Erdtman (1952), Faegri & Iversen (1950) e Kremp (1965). Conforme Salgado-Labouriau (2007), as principais características morfológicas do pólen são:

Associação – Após a divisão meiótica que forma o pólen, cada célula-mãe se subdivide em quatro células haplóides. Estas células são geralmente separadas e cada grão fica isolado dos outros. Contudo, os grãos de pólen de alguns gêneros ficam unidos firmemente em grupos de dois grãos (díade), de quatro grãos (tétrade) de mais quatro grãos (políade). Os esporos estão sempre em grãos isolados e têm geralmente marcas (trilete ou monolete) na área da superfície onde houve a união dos grãos (pólo proximal) durante a fase de tétrade.

A posição dos grãos na tétrade inicial determina a polaridade do grão. O pólo proximal fica na parte de contato entre as células e pólo distal na parte mais afastada do centro da tétrade. Essa nomenclatura permanece nos grãos depois que se separam. O eixo que vai do centro de um pólo ao outro é o polar (diâmetro polar – P), enquanto que o eixo perpendicular ao eixo polar é o equatorial (diâmetro equatorial – E). A visão é polar quando o pólo está voltado para o observador, e a visão equatorial está 90º desta posição.

Forma – Os esporos, devido à cicatriz (lasura) no pólo proximal são denominados triletes, monoletes ou aletes. Os grãos de pólen apresentam a forma de um elipsóide de revolução com a adoção da nomenclatura matemática de oblato, esférico e prolato para descrever a forma, e utilização dos sufixos "per" e "sub" para subdividir estas formas com base na relação entre o diâmetro polar (P) e o diâmetro equatorial (E) do grão (Erdtman, 1952). Os limites de cada classe foram estabelecidos utilizando frações para tornar os dados quantitativos. Entretanto, devido à propriedade elástica da exina, uma descrição rigorosa da forma não tem sentido, uma vez que ela varia dentro de um limite, se o grão está ou não hidratado, se está ou não comprimido pela lamínula na preparação para microscopia. Adicionalmente, o elipsóide de revolução aplicado ao grão de pólen é uma forma abstrata, porque poucos tipos polínicos são um elipsóide perfeito (Salgado-Labouriau, 2007).

Abertura – As aberturas podem estar localizadas em um setor da exina (zonoaperturado) ou em toda a superfície do grão (pantoaperturado). A posição das aberturas do grão infere a localização dos pólos e dos diâmetros P e E. Poros, colpos e cólporos são os três tipos de aberturas dos grãos. O colpo é uma invaginação germinal (Erdtman, 1947) ou uma área delgada da exina (Faegri & Iversen, 1950). O poro é uma abertura, de forma arredondada a elíptica, ou simplesmente seções delgadas da exina, enquanto que a abertura composta denominada cólporo é constituída de um ou mais poros (Punt *et al*., 1994).

As aberturas são locais importantes para a saída do tubo polínico, na germinação do pólen para fecundação e servem como caminho para transferência de água e outras substâncias entre a célula e o exterior (Punt *et al*., 1994). Os esporos não têm aberturas, o trilete (em forma de Y) e o monolete (forma alongada) são cicatrizes de contato entre os grãos quando estavam em tétrade, após a divisão da célula-mãe do esporo. Esporos sem cicatrizes são denominados aletes.

Ornamentação – Ao microscópio ótico, a superfície do pólen pode ser estriada, reticulada, pilada, rugolada, foveolada, lisa ou ter saliências como espinhos, verrugas e pilos. A maioria das ornamentações pode ser negativa ou positiva. Ornamentação negativa é aquela onde as estruturas se encontram na parte interior da exina, em oposição às estruturas positivas, que estão localizadas sobre a superfície da parede celular.

As categorias negativas de ornamentação são: perforada, no qual o teto, microperforado, possui pequenas cavidades menores que 1 μm de diâmetro; foveolada, ornamentação caracterizada por cavidades ou depressões maiores que 1 μm; fossulada, caracterizada pela presença de sulcos alongados e irregulares.

As categorias positivas de ornamentação são: escabrada, quando o padrão de ornamentação é composto de grânulos de qualquer formato, mas com diâmetros menores que 1 μm; gemada, ornamentação com estruturas arredondadas (gemas); clavada, ornamentação com elementos esculturais alongados com diâmetro da parte superior maior que o da base, denominados clavas; verrucada, quando a ornamentação é composta de elementos não pontiagudos, semelhantes a verrugas, geralmente com diâmetros maiores que 1 μm; espinhosa, ornamentação composta de espinhos maiores que 1 um; rugolada, ornamentação constituída de elementos alongados, produzindo um padrão escultural intermediário entre a condição estriada e a reticulada (Iversen & Troels-Smith, 1950); estriada, ornamentação onde existem sulcos separando elementos esculturais salientes; e reticulada, ornamentação em forma de malha, constituída de cavidades (lúmens) cercadas de elementos mais estreitos que os lúmens (Punt *et al*., 1994; Kremp, 1965).

Estrutura interna – Erdtman (1952) denominou a camada externa e interna como sexina e nexina, respectivamente (Figura 3). Faegri (1956) demonstrou duas camadas que se coram diferencialmente com a fucsina básica: a ectexina, parte externa que se cora positivamente com a fucsina básica e endexina. Posteriormente, com o uso do MET foi reconhecido que as duas terminologias não são equivalentes.

A ectexina tem uma densidade eletrônica mais alta quando observada em preparações convencionais de cortes para observação em MET, e inclui a sexina e a parte superior da nexina de Erdtman (1952). A endexina (Faegri, 1956) é a parte mais interna da exina, praticamente não se cora com fucsina básica na microscopia óptica, tem densidade eletrônica baixa nos cortes observados em MET e corresponde à nexina 2 de Erdtman (1960). Para material sem corar observado em microscópio óptico é comum a utilização dos termos de Erdtman (1952), enquanto que a nomenclatura de Faegri & Iversen (1950) para material corado com fucsina básica ou observado em MET (Figura 4 e 5).

As columelas são pequenos cilindros ou bastões da sexina/ectexina que sustentam um teto (tectum). Bácula é um tipo de relevo que consiste em um elemento cilíndrico e livre na superfície da exina (Punt *et al*., 1994). O termo pila deve ser utilizado para cilindros livres que sustentam uma cabeça (caput).

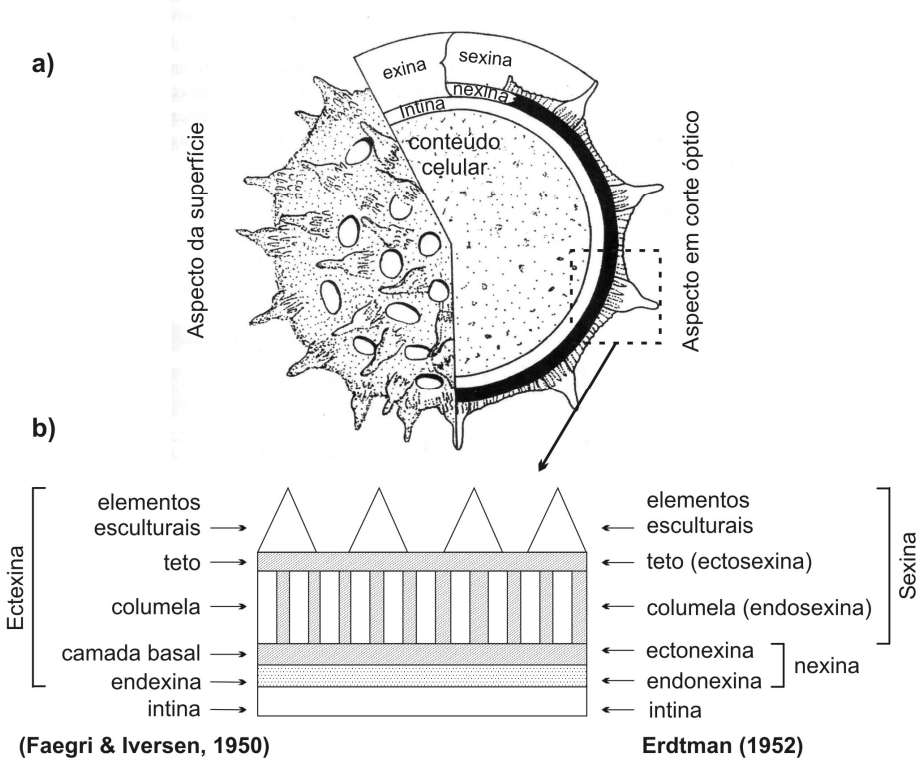

Figura 3 - a) Camadas da exina (modificado de Salgado-Labouriau, 1962) e b) terminologia das camadas da exina.

Tamanho – A distinção por tamanho é muitas vezes a única e possível forma para distinguir duas ou mais espécies com o mesmo tipo polínico. Mas este tipo de distinção tem que ser usado com muito cuidado nos grãos antigos ou fósseis, pois eles foram preservados em condições diferentes. Em sedimentos antigos, os grãos de pólen e esporos dobram ou se achatam como um disco ou podem abrir em duas ou mais partes. Em muitos casos as diferenças de tamanho e forma são pequenas ou existe uma gradação contínua entre os extremos.

A metodologia para interpretação paleoecológica, a partir da análise palinológica, está baseada no princípio de que todos os tipos polínicos preservados em sedimentos do Quaternário são sensíveis a comparação com gêneros modernos, uma vez que não ocorreram extinções de plantas durante este período (Traverse, 2007). A identificação dos palinomorfos até a menor categoria taxonômica é fundamental na análise palinológica, porque pode fornecer informações sobre os padrões da vegetação no momento da deposição do sedimento. Além disso, a delineação da área fonte dos grãos de pólen e esporos é essencial para o uso dos dados palinológicos na reconstrução dos padrões da vegetação.

Prentice (1985) e Sugita (1993) elaboraram um modelo de transporte e deposição do pólen baseado na dispersão de partículas pequenas. Este modelo revelou que cada táxon possui uma função de dispersão singular, na qual pode ser usada para avaliar a abundância de plantas e/ou padrões da vegetação. Na costa norte do Brasil, muitos estudos têm demonstrado que os dados de pólen de testemunhos de sedimentos obtidos de planícies de maré vegetadas representam a vegetação local (e.g. Behling & Costa, 2001; Behling *et al*., 2004; Cohen *et al*., 2009; Guimarães *et al*., 2010), e a força do sinal polínico de cada unidade da vegetação depende da distância do transporte (e.g. Davis, 2000).

Ao longo das fácies sedimentares dos testemunhos deste trabalho, 1 cm^3 de sedimento foram retirados em intervalos de 5 cm. Primeiramente, em cada amostra foram adicionados tabletes de marcadores exóticos, esporos de *Lycopodium* (Stockmarr, 1971), para o cálculo da concentração de pólen (grãos/cm^3) e a razão da acumulação de pólen (grãos/cm^2/ano). Todas as amostras foram preparadas utilizando técnicas analíticas para a extração dos grãos de pólen, incluindo acetólise (Faegri & Iversen, 1989). Os resíduos das amostras foram montadas em lâminas com gelatina glicerinada. Manuais para descrição morfológica de pólen e esporos foram consultados (Roubik & Moreno, 1991; Colinvaux *et al*., 1999, Hesse *et al*., 2008) juntamente com a coleção de referência do Laboratório de Dinâmica Costeira - UFPA para identificar grãos de pólen e esporos. De 300 a 400 grãos de pólen foram contados em cada amostra.

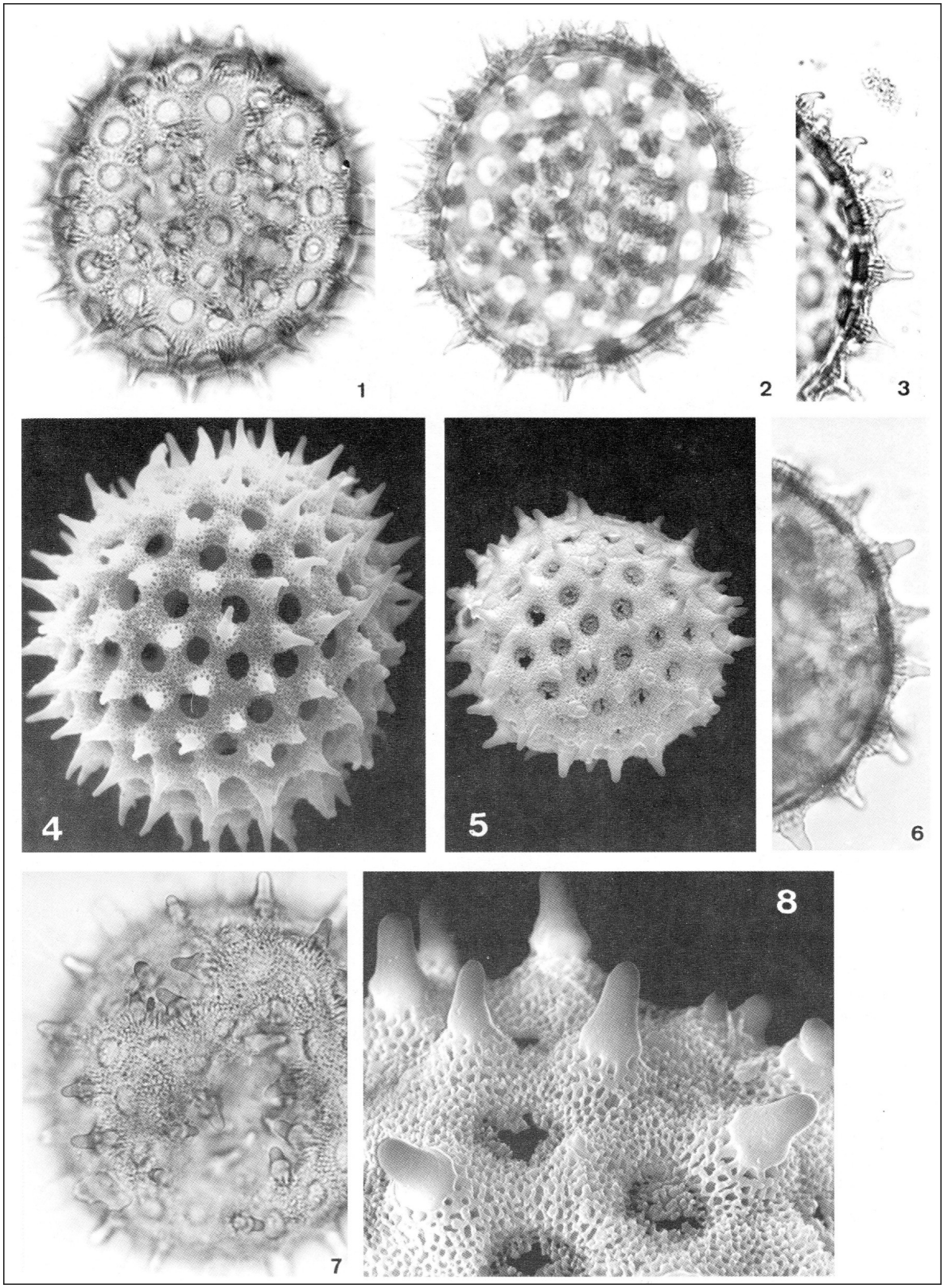

Figura 4 - Exemplos de grãos de pólen da região Amazônica e respectivas descrições morfológicas. Imagens 1-4: *Ipomea carajensis* D. Austin – forma esferoidal, pantoporados, superfície reticulada com espinhos. Diâmetro = ~ 107 µm. Imagens 5-8: *Ipomea cavalcantei* D. Austin – forma esferoida, pantoporados, superfície reticulada com espinhos. Diâmetro = ~ 120 µm (Modificado de Carreira & Barth, 2003).

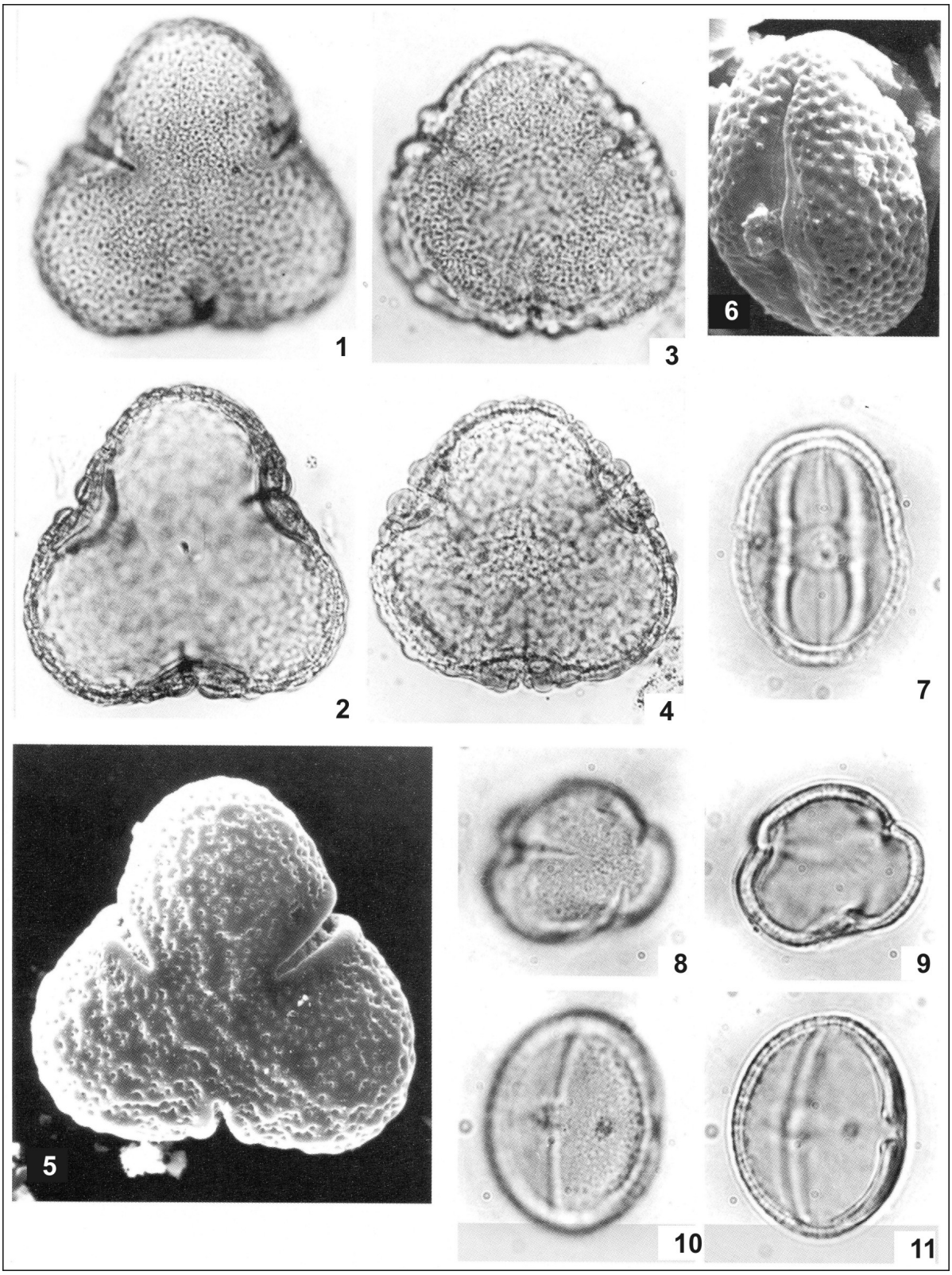

Figura 5 - Exemplos de grãos de pólen da região Amazônica e respectivas descrições morfológicas. Imagens 1-5: *Mabea angustifolia* Spruce ex Benth. – isopolares, 3-colporados, superfície faveolada. Diâmetro = ~ 125 µm. Imagens 6-11: *Maprounea guianensis* Aubl. – isopolares, forma prolata, 3-colporados, superfície reticulada. Diâmetro = ~ 30 µm (Modificado de Carreira & Barth, 2003).

Os dados de pólen e esporos são apresentados em diagramas polínicos como percentagens da soma total de pólen. Taxa foram agrupados em Manguezal, Campos inundáveis (herbáceos), Várzea e Transicional/Floresta Secundária (TFS). Os softwares Tilia e Tilia Graph foram utilizados para a análise estatística e plotagem dos diagramas polínicos (Grimm, 1987). Os diagramas foram estatisticamente subdivididos em zonas das assembléias de pólen baseado na transformação raiz quadrada dos dados percentuais e análise de agrupamento estratigraficamente restrita pelo método da soma total dos quadrados (Grimm, 1987).

1.3.4 Isótopos do carbono e nitrogênio e razão C/N

A fotossíntese, processo de conversão CO_2 atmosférico em compostos orgânicos, apresenta duas etapas distintas: dependente de luz, quando esta energia é absorvida por pigmentos fotossintetizantes (e.g. clorofila) e convertida em energia química; e não dependente de luz, quando esta energia química é utilizada para ligação do carbono a uma molécula orgânica (Raven *et al*., 1996). A classificação das plantas que realizam os ciclos fotossintéticos C3, C4 e CAM está relacionada às características fisiológicas e bioquímicas da etapa não dependente da luz e as diferenças entre estas plantas possuem implicações ecológicas, uma vez que representam adaptações a condições ambientais distintas.

Nas plantas C3, o CO_2 atmosférico é reduzido à fosfoglicerato (um composto de três átomos de carbono), via enzima ribulose bifosfatocarboxilase/oxilase (RUBisCO). As plantas do ciclo C4 reduzem esse o CO_2 à ácidoaspártico ou málico, (com quatro átomos de carbono), através da enzima fosfoenolpiruvato (PEP) carboxilase, enquanto que no ciclo CAM, as plantas utilizam tanto os ciclos C3 e C4 (Raven *et al*., 1996). Plantas do ciclo C3 são representadas por vegetação arbórea, mas algumas espécies de gramíneas de áreas úmidas também realizam este ciclo. As plantas do ciclo C4 são representadas predominantemente por gramíneas de ambientes com temperatura elevada e estresse hídrico (Sage & Monson, 1999).

Considerando os isótopos estáveis do carbono (^{12}C e ^{13}C), cerca de 98.9% do carbono é encontrado na natureza na forma de ^{12}C, enquanto a abundância do ^{13}C é de apenas 1.1% (O´Leary, 1988). Através da razão $^{13}C/^{12}C$ é possível determinar a contribuição relativa de espécies de plantas que realizam os ciclos fotossintéticos C3, C4 e CAM, uma vez que apresentam forma diferenciada de discriminação isotópica das plantas em relação ao CO_2 durante o processo fotossintético, que varia de acordo com a via enzimática empregada e gera diferentes assinaturas isotópicas.

Os isótopos do nitrogênio (^{14}N e ^{15}N) e a razão C/N apesar de serem menos utilizados em estudos paleoecológicos podem também fornecer informações sobre a diferenciação entre fontes de matéria terrestre e aquática (e.g. Thornton & McManus, 1994; Meyers, 1997), assim como, integrados aos dados de isótopos do carbono para estabelecer a origem da matéria orgânica preservada em ambientes transicionais (e.g. Graham *et al*., 2001; Byrne *et al*., 2001; Cloern *et al*., 2002). Além disso, grãos de pólen e esporos não são ocasionalmente encontrados em depósitos do Holoceno devido ao tamanho do sedimento ou corrosão química (Sangster & Dale 1961, 1964; Colinvaux *et al*., 1999; Cohen, 2003; Guimarães *et al*., 2010), e dados descontínuos nos diagramas polínicos podem limitar a interpretação paleoecológica (e.g. Wilson *et al*., 2005a, b). Assim, algumas variações nos valores de $\delta^{13}C$, $\delta^{15}N$ e C/N apresentados por diferentes vegetais são brevemente discutidos abaixo.

O ciclo fotossintético C3 realizado por plantas terrestres revela valores de $\delta^{13}C$ entre -32‰ e -21‰ e C/N > 12. As plantas C4 têm valores de $\delta^{13}C$ variando de -17‰ a -9‰ e C/N > 20 (Deines, 1980; Meyers, 1994; Tyson, 1995). Em ambientes dominados por plantas C3, algas de água doce apresentam valores de $\delta^{13}C$ entre -25‰ e -30‰ (Schidlowski *et al*., 1983; Meyers, 1994), e algas marinhas em torno de -24‰ a -16‰ (Haines, 1976; Meyers, 1994). Em ambientes dominados por plantas C4, algas podem ter valores de $\delta^{13}C \leq 16‰$ (Chivas *et al*., 2001). Bactérias possuem valores de $\delta^{13}C$ entre -12‰ a -27‰ (Coffin *et al*., 1989). Em geral, bactérias e algas têm C/N de 4-6 e <10, respectivamente (Meyers, 1994; Tyson, 1995). Os valores de $\delta^{13}C_{POC}$ fluvial são provenientes do fitoplâncton (-25‰ a -30‰) e matéria orgânica particulada terrestre (-25‰ a -33‰). Por outro lado, o $\delta^{13}C_{POC}$ varia de -23‰ a -18‰ (e.g. Barth *et al*., 1998; Middelburg & Nieuwenhuize, 1998). Fitoplâncton tem valores de C/N entre 5 e 10 (Meyers, 1994; Tyson, 1995). Peterson *et al*. (1994) encontrou valores de $\delta^{13}C_{DOC}$ marinho entre -22‰ e -25‰, e $\delta^{13}C_{DOC}$ de água doce entre -26‰ e -32‰. Thornton & McManus (1994), e Meyers (1997) usaram os valores de $\delta^{15}N$ para diferenciar matéria orgânica de origem aquática (>10.0‰) e terrestre (~0‰).

$\delta^{13}C$, $\delta^{15}N$ e razão C/N foram analisados nas amostras de sedimento (6-50 mg) extraídas em intervalos de 5 cm ao longo das fácies sedimentares. Os isótopos estáveis do carbono e nitrogênio assim como o carbono orgânico total (TOC) e nitrogênio (TN) foram analisados no Laboratório de Isótopos Estáveis do Centro para Energia Nuclear na Agricultura (CENA), Universidade de São Paulo (USP), usando um CF-IRMS (*Continuous Flow Isotopic Ratio Mass Spectrometer* - Espectrometria de Massa de Razões Isotópicas de Fluxo Contínuo). O carbono orgânico e nitrogênio são expressos como percentagem do peso seco e os resultados

do ^{13}C são dados com relação ao padrão *Viena Pee Dee Belemnite* (VPDB) e N_2 atmosférico utilizando as notações convencionais:

$$\delta^{13}C_{amostra} = \frac{R_{S1} - R_{PDB}}{R_{PDB}} x1000$$

$$\delta^{15}N_{amostra} = \frac{R_{S2} - R_{ar}}{R_{ar}} x1000$$

Onde R_{S1} e R_{S2} são, respectivamente, as razões $^{13}C/^{12}C$ e $^{15}N/^{14}N$ na amostra, R_{PDB} a razão $^{13}C/^{12}C$ para o padrão internacional VPDB e R_{ar} a razão $^{15}N/^{14}N$ para o ar atmosférico. Os resultados foram apresentados em δ ‰, com precisão analítica melhor que 0.2 ‰ (Pessenda *et al*., 2004a).

1.3.5 Datação por ^{14}C

A determinação da idade do isótopo radioativo ^{14}C está fundamentada na compreensão da origem, ciclagem e decaimento. A produção de ^{14}C na alta atmosfera ocorre ininterruptamente através da interação de nêutrons, provenientes de colisões de raios cósmicos, principalmente partículas α, com átomos de ^{14}N. O ^{14}C passa por um processo de oxidação formando $^{14}CO_2$, que posteriormente é disperso na atmosfera e suas camadas inferiores. Assim, o $^{14}CO_2$ pode ser fixado no processo de fotossíntese e os átomos de ^{14}C serão utilizados na constituição do vegetal e podem ser transferidos a outros setores da teia alimentar, ambos considerados reservatórios naturais de ^{14}C. Durante a vida do organismo, existe um equilíbrio entre a atividade específica do ^{14}C com relação à do ambiente, e a relação $^{14}C/^{12}C$ de todos os seres vivos apresenta a mesma proporção. A assimilação é constante durante a vida do organismo, devido à absorção contínua de CO_2 pelas plantas. Quando o equilíbrio é rompido (e.g. morte do organismo), ocorre apenas à desintegração radioativa do ^{14}C, que decai em taxa constante. Na desintegração radioativa do ^{14}C, a emissão da partícula β ocorre formando o ^{14}N estável (Libby *et al*., 1955).

A meia vida do ^{14}C de 5.730 ± 30 anos foi determinada com precisão pelo *National Bureau of Standard*, em 1961. Na 5ª Conferência sobre a Datação por ^{14}C, realizada nos Estados Unidos em 1962, foi adotado o valor de 5.568 ± 30 anos, que apresenta um erro de ~ 3%, uniformizando os resultados obtidos por diversos laboratórios durante a implantação do método em 1950.

A atividade de uma amostra depende do número total de núcleos radioativos presentes e de uma probabiblidade de decaimento (λ) constante para cada nuclídeo. A atividade do ^{14}C pode ser determinada por:

$$A=A_0e^{-\lambda t}$$

Onde, t = tempo decorrido após a morte do organismo,

A = atividade da amostra no tempo t qualquer,

Ao = atividade da amostra no tempo t = 0, sendo representada pelo padrão Ácido Oxálico NIST.

λ = constante de desintegração ($\ln 2/t_{1/2}$, e $t_{1/2}$ = meia-vida do ^{14}C)

Para $t_{1/2}$ de 5.568 anos temos:

$$\frac{1}{2}=\frac{t_{1/2}}{\ln 2}=8033$$

A idade da amostra é determinada por:

$$t=-8033\ln\frac{A}{A_o}$$

Onde, t = tempo decorrido desde que a amostra foi removida da condição de equilíbrio com o reservatório de ^{14}C.

A correção do fracionamento isotópico deve ser considerada na determinação da idade ^{14}C, uma vez que as plantas absorvem CO^2 atmosférico para realizar o processo de fotossíntese de forma discriminatória em relação ao ^{12}C e ^{13}C, que introduz erros no cálculo da idade ^{14}C (Stuiver & Polach, 1977). O cálculo deste fracionamento é feito por:

$$\delta^{13}C_{amostra}=\frac{R_{S1}-R_{PDB}}{R_{PDB}}x1000$$

O valor de $\delta^{13}C$ representa a proporção da razão $^{13}C/^{12}C$ de uma amostra em relação à do padrão VPDB (veja seção secundária 3.4).

A detecção da atividade do ^{14}C em amostras de origem ambiental pode ser realizada através de espectrômetros de cintilação líquida de baixo nível de radiação de fundo, contadores proporcionais gasosos e Espectrometria de Aceleração de Massa - *Accelerator Mass Spectrometry* (AMS). A grande vantagem que AMS possui sobre os outros métodos é o pequeno volume de amostra. Espectrômetros de aceleração de massa requerem de 20 a 500 mg para algumas amostras, enquanto que os métodos convencionais precisam, no mínino, de 10 g em amostras como madeira e carvão, e mais de 100 g em ossos e sedimentos. Além disso, medições AMS possuem maior precisão e menor ruído de fundo que outros métodos de datação radiométrica (Beta, 2010).

Quatorze amostra de sedimento de ~ 2 g cada foram utilizadas para datação por ^{14}C neste trabalho. As amostras foram pré-tratadas e o material residual foi extraído com 2% HCl

a 60°C durante 4 horas, lavado com água destilada-pH neutro e secadas (50 ºC). As amostras foram analisadas por AMS no *Center for Applied Isotope Studies*, *Athens* (*Georgia*, EUA) e *Physikalisches Institut*, *University of Erlangen* (*Nürnberg*, ALE). Os dados de ^{14}C são expressos em anos antes AD 1950 (anos A.P.), normalizado para $\delta^{13}C$ de -25‰VPDB e em cal anos AP com precisão de 2σ (Reimer *et al*., 2004).

2 MID- AND LATE-HOLOCENE SEDIMENTARY PROCESS AND PALAEOVEGETATION CHANGES NEAR THE MOUTH OF THE AMAZON RIVER*

José Tasso Felix Guimarães[1]*, Marcelo Cancela Lisboa Cohen[1], Luiz Carlos Ruiz Pessenda[2], Marlon Carlos França[1], Clarisse Beltrão Smith[1], Afonso César Rodrigues Nogueira[1]

[1] *Programa de Pós-Graduação em Geologia e Geoquímica, Instituto de Geociências, Universidade Federal do Pará (UFPA). Rua Augusto Correa 01, 66075-110, Belém/PA, Brasil*

[2] *Centro de Energia Nuclear na Agricultura (CENA), 13400-000, Piracicaba/SP, Brasil*

* Accepted for publication in The Holocene

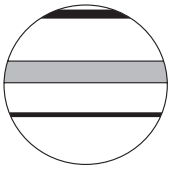

Research paper

The Holocene
1–12

DOI: 10.1177/0959683611423693
hol.sagepub.com
SAGE

Mid- and late-Holocene sedimentary process and palaeovegetation changes near the mouth of the Amazon River

José Tasso Felix Guimarães,[1] Marcelo Cancela Lisboa Cohen,[1] Luiz Carlos Ruiz Pessenda,[2] Marlon Carlos França,[1] Clarisse Beltrão Smith[1] and Afonso César Rodrigues Nogueira[1]

Abstract

The integration of sedimentary facies, pollen, spores, carbon and nitrogen isotopes records, C/N ratio and radiocarbon dates allowed the identification of changes in vegetation and the sources of organic matter accumulated on tidal flats near the mouth of the Amazon River during the mid and late Holocene. Data from the margin of Amazon River indicate marine influence related to mangrove presence over a tidal mud flat between 5560–5470 cal. yr BP and 5290–5150 cal. yr BP. Afterward, the mangrove area shrank following the return of more humid conditions and increase of Amazon River discharge. A common reworking process of the tidal flat through the lateral migration of a meandering creek occurred in the study site, with later development of transitional vegetation under freshwater influence. Following the natural vegetation succession under stable climate and hydrological conditions, the expansion of 'várzea' (flooded freshwater vegetation) forests occurred since 600–560 cal. yr BP until the present. Furthermore, regarding the tidal flats located west of the mouth of Amazon River, these stable conditions also allowed the mangrove maintenance over mudflats with deposition of marine organic matter during at least the last 2350–2300 cal. yr BP.

Keywords

Amazonia, C and N isotopes, climate changes, facies analysis, Holocene, palynology

Introduction

Morphological, climatic and hydrological factors have produced the formation of geobotanical units of the Amazonian coastal region leading to the development of a marine-influenced littoral (southeastern coastline), dominated by mangroves and saltmarsh vegetation, and a fluvial sector (northwestern coastline), characterized by 'várzea' (flooded freshwater forests) and herbaceous vegetation (Cohen et al., 2009).

Palaeoenvironmental research in the marine littoral shows mangrove establishment between 7500 and 5100 cal. yr BP (Behling and Costa, 2001; Behling et al., 2001; Cohen et al., 2005) during the Holocene reflecting the postglacial sea-level rise that invaded the coast embayed by rather shallow and broad valleys (Cohen et al., 2005; Souza Filho et al., 2006), while the fluvial littoral presents tidal flat deposits influenced by marine processes during the Holocene with vegetation history characterized by mangrove and 'várzea' expansion/contraction phases (Cohen et al., 2008; Guimarães et al., 2010).

Toledo and Bush (2007) recorded declining abundance of *Rhizophora* pollen after c. 7000 cal. yr BP, suggesting a weakening of the marine influence and, from 5000 cal. yr BP, the replacement of closed forest elements by open flooded savanna. Those findings indicate reduced discharge from the Amazon River, likely due to a marked decrease in precipitation in the Andes between 8000 and 5000 cal. yr BP.

Several studies indicate that Amazon climate has varied during the Holocene with significant fluctuations in precipitation (e.g. Absy et al., 1991; Behling and Costa, 2000; Desjardins et al., 1996; Ledru, 2001; Pessenda et al., 2001; Van der Hammen, 1974), and possibly, in the river water discharge such as Amazon River and its tributaries (e.g. Latrubesse and Franzinelli, 2002; Maslin and Burns, 2000).

In Amapá littoral, extensive tidal flat deposits developed adjacent to the Amazon River may be more appropriate to investigate vegetation changes related to variations of the Amazon River discharge during the Holocene. However, few palaeoecological studies based on pollen data were performed in this area (Guimarães et al., 2010; Toledo and Bush, 2007).

Considering the techniques applied in this work, the facies analysis is traditionally used to define characteristics of a sedimentary unit that formed under certain hydrodynamic processes and sedimentation environment. Thus, each depositional environment puts its own imprint on the sediment, resulting in a singular facies (e.g. Walker, 1992), while pollen records from vegetated tidal flats tend to represent local vegetation and the strength of the pollen signal from each phytophysiognomy is distance-weighted (e.g. Behling et al., 2004; Cohen et al., 2009; Guimarães et al.,

[1]Universidade Federal do Pará (UFPA), Brazil
[2]Centro de Energia Nuclear na Agricultura (CENA), Brazil

Received 18 March 2011; revised manuscript accepted 22 August 2011

Corresponding author:
José Tasso Felix Guimarães, Programa de Pós-Graduação em Geologia e Geoquímica, Instituto de Geociências, Universidade Federal do Pará (UFPA), Rua Augusto Correa 01, 66075-110, Belém/PA, Brazil.
Email: tasso@ufpa.br

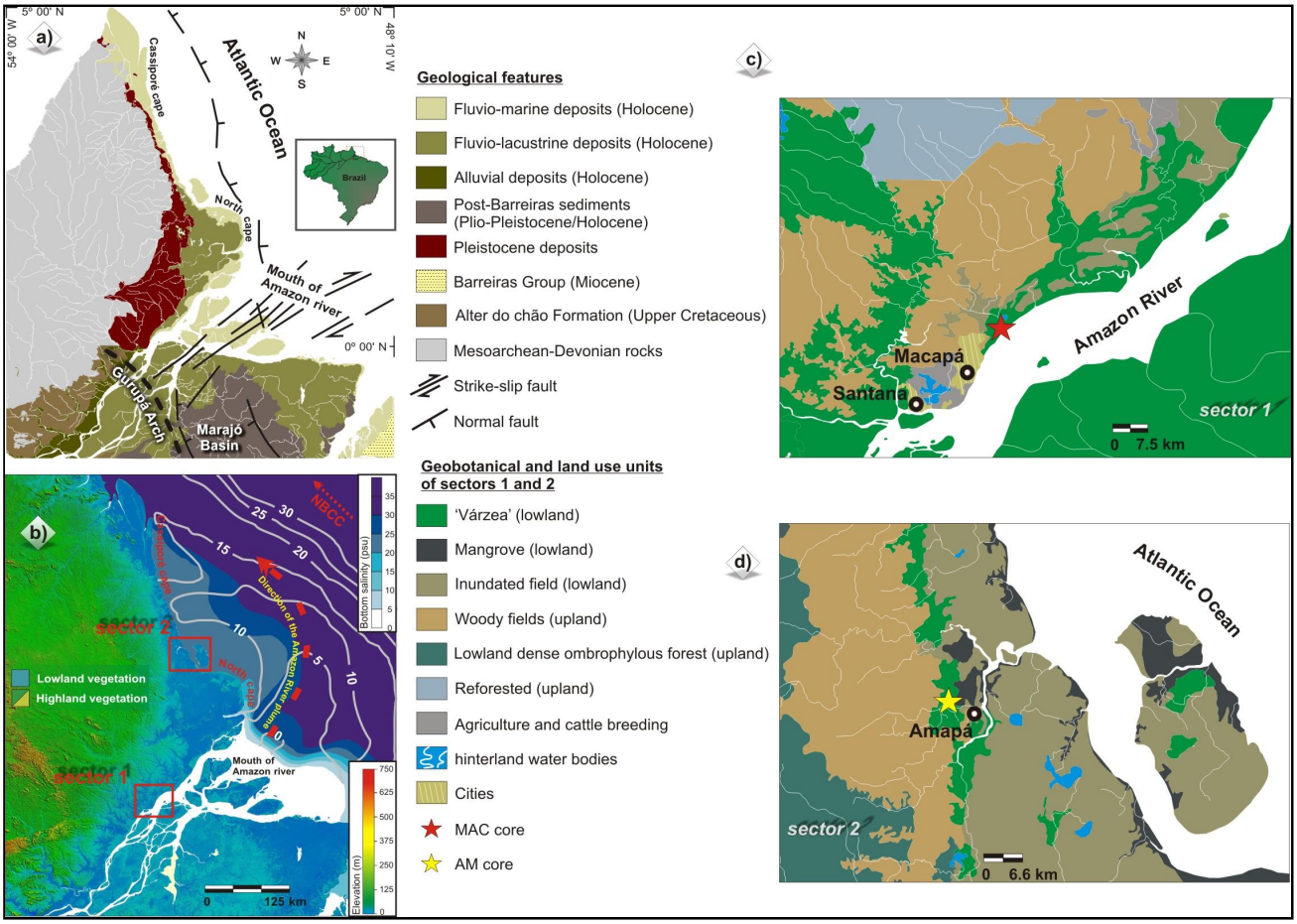

Figure 1. Study site: (a) regional geology of the study area in the Marajó basin (modified from CPRM, 2010 and Costa et al., 2002), (b) elevation map with bottom and surface water salinity, direction of the Amazon River plume and North Brazilian Coastal Current (NBCC) near the Amapá littoral (modified from Vinzon et al., 2008 and Rosario et al., 2009), (c) and (d) geobotanical and land use units of sectors 1 (Macapá) and 2 (Amapá) with sampling sites

2010). As additional information, carbon and nitrogen isotope ($\delta^{13}C$ and $\delta^{15}N$) and carbon to nitrogen ratios (C/N) can be used, since they can provide data about the origin of organic matter (e.g. Lamb et al., 2006).

Thus, an interdisciplinary approach based on facies analysis, isotopic and pollen records may provide better information about process and environment of deposition, and the origin of organic matter preserved in coastal deposits, respectively (Dalrymple and Choi, 2007; Lamb et al., 2006), which is required to isolate the climatic signal from the non-climatic noise and better interpret the main process acting on coastal systems as indications of hydrodynamic regime, river discharge, organic matter sources and vegetation patterns (e.g. Engelhart et al., 2007; Freycon et al., 2009; Horton et al., 2005). This interproxy study was applied in order to investigate the sedimentary process, vegetation changes and sources of organic matter accumulated on tidal flats near the mouth of Amazon River during the mid and late Holocene.

Study area

Geological and physiographic setting

The coastal zone of Amapá in the study area is located in the Marajó basin that is linked to the Gondwana break up and Equatorial Atlantic opening during Jurassic/early Cretaceous (Szatmari et al., 1987). This basin is limited to the south and west by Gurupá and Tocantins arches, respectively.

The regional geology includes Mesoarchean-Devonian Crystalline and Metassedimentary rocks to the western part, and Pleistocene sandstone and conglomerates in the eastern part interpreted as tidal depositional systems (Souza and Pinheiro, 2009). From the Late Pleistocene to Holocene, erosional and depositional processes due to Late Pleistocene and Holocene climatic and sea-level changes, along with tectonic processes, shaped the relief of the Amapá coast, resulting in its current configuration (Lima et al., 1991). Therefore, along the coastal plain adjacent to the Amazon River, extensive north–south trending Holocene terraces composed of sand and mud have developed (Figure 1a, b). The very flat, low-elevation landscape is characterized by flooded areas and both abandoned and active meandering channels (Figure 1b). The coast between Cassiporé and North Cape, which is part of the longest muddy coastline in the world (Figure 1a, b), is strongly influenced by Amazon River discharge (Allison et al., 2000).

Floristic studies of Costa Neto (2004), Costa Neto and Silva (2004), Carvalho et al. (2006) and Costa Neto et al. (2007) described geobotanical and land-use units (Figure 1c, d). For sectors 1 (freshwater influence) and 2 (brackish water influence) (Figure 1c, d and Table 1), a vegetation survey based on qualitative descriptions was carried out. The modern vegetation of Macapá region – sector 1 (Figure 1c) is represented by periodically inundated herbaceous-shrubs field (upland to supratidal zone) and permanently inundated herbaceous field (supratidal zone). The supratidal and intertidal zone are colonized by well-developed 'várzea' (flooded freshwater forests). The vegetation of Amapá region – sector 2 (Figure 1d) is characterized by well-developed mangrove forests near the coastline, herbs vegetation (supratidal zone), and 'várzea'.

Table 1. Main plant species identified in the study site

Family and species	Biological form	Macapá (sec. 1)	Amapá sec. 2)	Vegetation units
Aizoaceae				
Sesuvium sp.	Herb		X	IF
Anarcadiaceae				
Tapirira sp.	Tree	X	X	VF
Aquifoliaceae				
Ilex sp.	Tree	X		VF
Araceae				
Montrichardia sp.	Herb	X	X	VF
Arecaceae				
Euterpe sp.	Tree	X	X	VF
Mauritia sp.	Tree	X	X	VF
Avicenniaceae				
Avicennia sp.	Tree		X	MG
Cabombaceae				
Cabomba sp.	Herb	X	X	VF, IF
Ceratopteridaceae				
Acrostichum sp	Herb		X	MG
Cobretaceae				
Laguncularia sp.	Tree		X	MG
Cyperaceae				
Cyperus sp.	Herb	X	X	IF
Scleria sp.	Herb	X	X	IF
Euphorbiaceae				
Alchornea sp.	Tree	X	X	VF
Hevea sp.	Tree	X	X	VF
Fabaceae				
Macrolobium sp.	Tree	X	X	VF
Parkia nitida Miq.	Tree	X	X	VF
Helioconiaceae				
Heliconia sp.	Herb	X	X	IF
Malpighiaceae				
Mascagnia sp.	Climber	X	X	FV
Malvaceae				
Pachira sp.	Tree	X	X	VF
Pseudobombax sp.	Tree	X	X	VF
Nymphaeceae				
Nymphaea sp.	Herb	X	X	VF, IF
Poaceae				
Olyra latifolia L.	Herb	X	X	VF, IF
Panicum laxum Sw.	Herb	X	X	IF
Paspalum sp.	Herb	X	X	IF
Ponteridaceae				
Eichhornia sp.	Herb	X	X	IF
Rubiaceae	Herb			
Alibertia sp.	Tree	X	X	FV
Psychotria	Herb	X	X	IF
Rhizophoraceae				
Rhizophora sp.	Tree		X	MG
Strelitziaceae				
Phenakospermum sp.	Herb	X		VF

Vegetation units, VF, Varzea forest; IF, Inundated Field; MG, Mangrove.

Climate and hydrology

The regional climate is humid tropical characterized by well-defined dry (September to December) and wet (January to July) seasons, with annual average precipitation and temperature around 3000 mm and 27.5°C, respectively (Bezerra et al., 1990). The mean Amazon River discharge is about 170 000 m^3/s (at Óbidos city), with maximum and minimum outflow of 270 000 and 60 000 m^3/s (ANA, 2003). The Amazon estuary is classified as semi-diurnal macrotidal (Pugh, 1987), with a tidal range of 4 to 6 m (Gallo and Vinzon, 2005). The structure of the plume is controlled by the North Brazilian Current, which induces a northwestern flow with speeds of 40–80 cm/s over the continental shelf (Figure 1b; Lentz, 1995), strong tidal currents (Beardsley et al., 1995), trade winds and the Intertropical Convergence Zone (ITCZ; Lentz and Limeburner, 1995). Consequently, the river discharge and hydrodynamic conditions allow a strong reduction of water salinity along the Amazon River and adjacent coast (Figure 1b; Rosario et al., 2009; Vinzon et al., 2008).

Table 2. Carbon Isotopic ($\delta^{13}C$) signature of leaves from main genres of the study site showing C3 plant dominance (more depleted values ranging from −26.6 to −34.4)

Family	Species	$\delta^{13}C$ (‰) $_{VPDB}$
Aizoaceae	*Sesuvium* sp.	−13.9
Arecaceae	*Euterpe oleracea* Mart.	−34.4
Araceae	*Montrichardia arborescens* (L.) Schott.	−27.6
	Pistia stratioides L.	−26.6
Avicenniaceae	*Avicennia germinans* (L.) Stearn	−31
Cyperaceae	*Cyperus* sp.	−29.8
Heliconiaceae	*Heliconia* sp.	−29.7
Strelitziaceae	*Phenakospermum* sp.	−34.3
Nymphaeaceae	*Nymphaea* sp.	−27
Poaceae	*Panicum* sp.	−12
	Hymenachne amplexicaule (Rudge) Nees.	−29.2
	Olyra latifolia L.	−32
	Paspalum repens Berg.	−11
Pteridaceae	Acrostichum L.	−32
Rhizophoraceae	*Rhizophora mangle L.*	−33.5

Materials and methods

Sampling and facies description

The sediment cores were sampled from the city of Macapá – sector 1 (freshwater influence), and the city of Amapá – sector 2 (brackish water influence) (Figure 1c, d) using a Russian Sampler with the geographical position of each point determined by GPS (Reference Datum: Sad69). Following the proposal of Walker (1992), facies analysis included descriptions of color, lithology, texture and structures. X-ray radiographs aided the identification of sedimentary structures. The sedimentary facies was codified following Miall (1978). The interpretation of the sedimentological data is also based on clastic tidalite process-response models (after Klein, 1971). Leaves of the most abundant genera were collected to heights of up to 2 m, to identify the carbon isotopic signatures (Table 2). Sediment cores were sampled from tidal flats colonized by 'várzea' (sector 1 – MAC core to 2 m depth, 00°04′15″N, 51°02′15″W, ~5–7 m above mean sea level (a.m.s.l.), and 0.3 km from the Amazon River), and mangrove vegetation (sector 2 – AM core to 1 m depth, 02°03′08″N, 50°48′21″W, ~ 2–4 m a.m.s.l., 15 km away from the coastline and 150 km from the mouth of Amazon River).

Pollen and spore analyses

Throughout the sediment cores, 1 cm^3 of sediments were picked in 5 cm intervals. One tablet of exotic *Lycopodium* spores was added to each sample for the calculation of pollen concentration (grains/cm^3). All samples were prepared using standard techniques of pollen analysis including acetolysis (Faegri and Iversen, 1989). Handbooks of pollen and spores morphology were consulted (Colinvaux et al., 1999; Hesse et al., 2008; Roubik and Moreno, 1991) jointly with the reference collection of the 'Laboratório de Dinâmica Costeira – UFPa' to identify of pollen grains and spores. Samples were counted to a minimum of about 300 pollen grains. The total pollen sum only considers pollen grains and excludes algae, microforaminifers, fungal and fern spores. Forty pollen taxa were identified. Pollen and spore data are presented in pollen diagrams as percentages of the total pollen amount. Taxa were grouped into Vegetation units: Mangrove, Inundated field, 'várzea' and Transitional/Secondary Forest (TSF). The software Tilia and Tilia Graph were used for the calculation and plotting of pollen diagrams. The pollen diagrams were statistically subdivided into zones of pollen and spores assemblages based on square-root-transformation of the percentage data and stratigraphically constrained cluster analysis by the method of total sum of squares (Grimm, 1987).

C/N, carbon and nitrogen isotopes

The $\delta^{13}C$, $\delta^{15}N$ and elemental C and N (C/N) amounts were analyzed from sediment samples (6–50 mg) taken at 5 cm intervals along the cores. The stable carbon and nitrogen isotopes as well as the total organic carbon (TOC) and nitrogen (TN) were determined at the Stable Isotopes Laboratory of Center for Nuclear Energy in Agriculture (CENA), University of Sao Paulo (USP), using a Continuous Flow Isotopic Ratio Mass Spectrometer (CF-IRMS). Organic carbon and nitrogen are expressed as percentage of dry weight and ^{13}C and ^{15}N results are given with respect to VPDB standard and atmospheric N_2, respectively, using the conventional δ (‰) notation. Analytical precision is ± 0.1% and ±0.2‰, respectively.

The organic matter source will be environment-dependent with different $\delta^{13}C$, $\delta^{15}N$ and C/N compositions (e.g. Lamb et al., 2006), as follows: The C3 terrestrial plants shows $\delta^{13}C$ values between −32‰ and −21‰ and C/N ratio > 12, while C4 plants have $\delta^{13}C$ values ranging from −17‰ to −9‰ and C/N ratio > 20 (Deines, 1980; Meyers, 1994; Tyson, 1995). In C3-dominated environments, freshwater algae have $\delta^{13}C$ values between −25‰ and −30‰ (Meyers, 1994; Schidlowski et al., 1983) and marine algae around −24‰ to −16‰ (Haines, 1976; Meyers, 1994). In C4-dominated environments, algae can have $\delta^{13}C$ values ≤16‰ (Chivas et al., 2001). Bacteria have $\delta^{13}C$ values ranging from −12‰ to −27‰ (Coffin et al., 1989). In general, bacteria and algae have C/N ratios of 4–6 and <10, respectively (Meyers, 1994; Tyson, 1995).

Fluvial $\delta^{13}C_{POC}$ values result from freshwater phytoplankton (−25‰ to −30‰) and particulate terrestrial organic matter (−25‰ to −33‰). However, marine $\delta^{13}C_{POC}$ ranges from −23‰ to −18‰ (e.g. Barth et al., 1998; Middelburg and Nieuwenhuize, 1998). Peterson et al. (1994) found values from marine $\delta^{13}C_{DOC}$ between −22‰ and −25‰, and freshwater between −26‰ and −32‰. Thornton and McManus (1994) and Meyers (1997) used $\delta^{15}N$ values to differentiate organic matter from aquatic (>10.0‰) and terrestrial plants (~0‰).

Radiocarbon dating

Five bulk samples of ~ 2g each were used for radiocarbon dating (Table 3). The sediment samples were checked and physically cleaned under the microscope. The residual material was then extracted with 2% HCl at 60°C for 4 h, washed with distilled water until neutral pH and dried (50°C). The sediment organic matter was analyzed by Accelerator Mass Spectrometry (AMS) at the Center for Applied Isotope Studies (Athens, Georgia, USA). Radiocarbon ages are reported in years before AD 1950

Table 3. Radiocarbon dates (AMS) of the samples

Sample	Lab. number	Depth (cm)	Radiocarbon age (yr BP)	2σ calibration(cal. yr BP)	Dated material
MAC 20	UGAMS 5311	20	660 ± 25	600–560	sed. org. matter
MAC 145	UGAMS 5312	145	4470 ± 30	5290–5150	sed. org. matter
MAC 200	UGAMS 5313	200	4790 ± 30	5560–5470	sed. org. matter
AM 60	UGAMS 5314	60	1240 ± 30	1260–1080	sed. org. matter
AM 100	UGAMS 5315	100	2270 ± 25	2350–2300	sed. org. matter

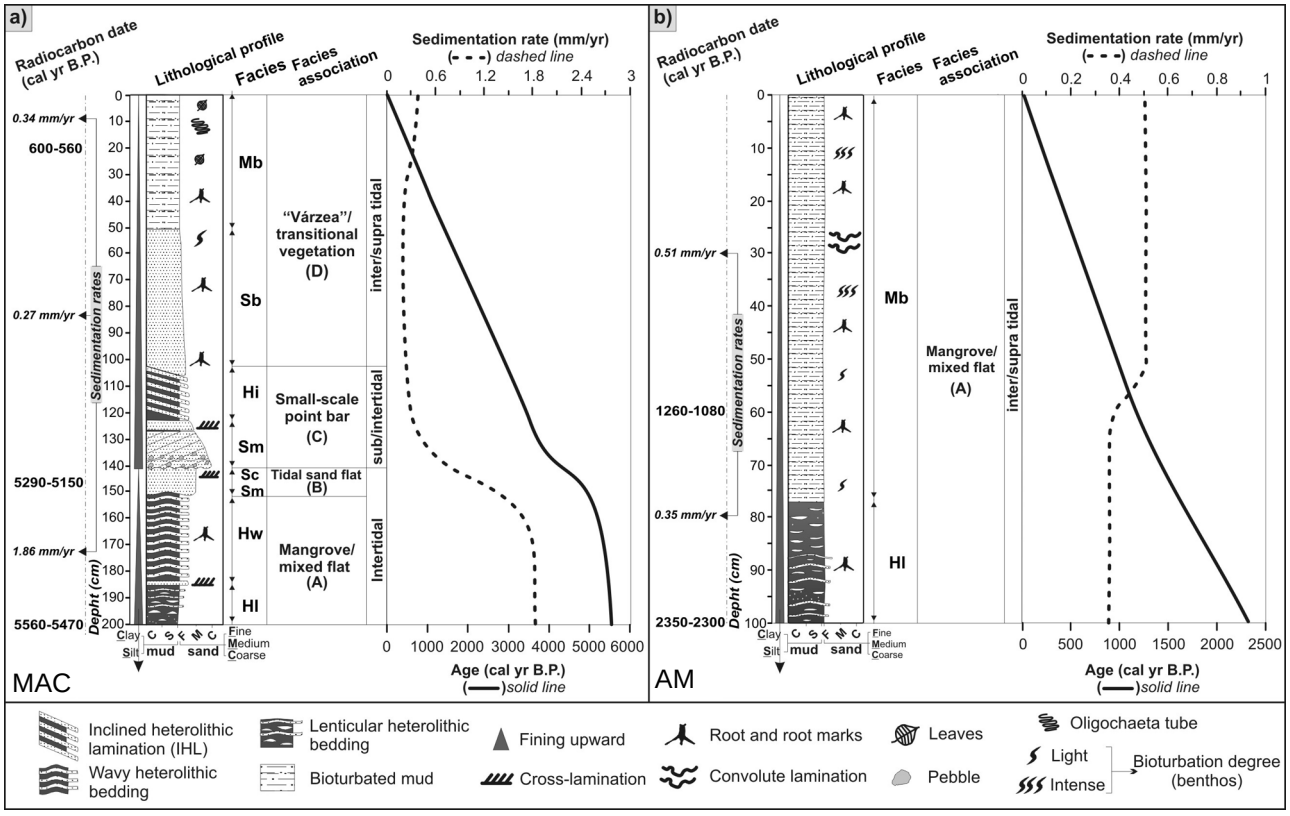

Figure 2. Graphic sedimentary log of the MAC and AM core

(yr BP) normalized to $\delta^{13}C$ of −25‰ VPDB and in cal. yr BP with precision of 2σ (Reimer et al., 2004).

Results and discussion

$\delta^{13}C$ values of vegetation

Within the 15 species collected, which include the most representative vegetation of the study site, the $\delta^{13}C$ values indicated a predominance of C3 plants (Table 2). The contribution of C4 to the $\delta^{13}C$ signal in sediment is restricted to the *Panicum* sp. (Poaceae) and *Paspalum repens* Berg. (Poaceae) and CAM plants to *Sesuvium* sp. (Aizoaceae) (Ramani et al., 2006).

Radiocarbon date and sedimentation rates

Radiocarbon dating of the MAC core at depths of 200 cm, 145 cm, and 20 cm produced ages of 5560–5470 cal. yr BP, 5290–5150 cal. yr BP and 600–560 cal. yr BP, respectively. Based on the ratio between the depth intervals (mm) and the mean time range, the sedimentation rates of MAC core are about 1.86 mm/yr (200–145 cm), 0.27 mm/yr (145–20 cm) and 0.34 mm/yr (20–0 cm). Two radiocarbon dates from AM core at 100 and 60 cm displayed ages of 2350–2300 cal. yr BP and 1260–1080 cal. yr BP, respectively (Table 3). The sedimentation rates are 0.35 mm/yr (100–60 cm) and 0.51 mm/yr (60–0 cm) (Figure 2).

Sediments deposited on vegetated tidal flats of Marajó Island (0.3–1 mm/yr, Behling et al., 2004), Salinopólis and the town of São Caetano (1.7–5.6 mm/yr, Cohen et al., 2009) and Bragança Peninsula (0.6–0.8 mm/yr, Cohen et al., 2005; 0.2–0.4 mm/yr, Vedel et al., 2006) on northern Brazilian coast presented similar sedimentation rates.

Facies descriptions

The sediment cores consist mostly of bioturbated mud and sand, heterolithic deposits, coarse to fine sands with cross-lamination and massive sand (Figure 2, Table 4). These lithologies are partially organized into a fining upward cycle. Pollen and spore records, $\delta^{13}C$, $\delta^{15}N$ and C/N values were added to facies characteristics in order to define four facies associations that represent typical tidal flat settings.

Facies association A (Mangrove/mixed flat). This association occurs in the lowest part of the MAC core from 5560–5470 cal. yr BP until 5290–5150 cal. yr BP, and throughout the AM core from 2350–2300 cal. yr BP until the present (Figure 2). These deposits feature mud with flat lenses of rippled sand (facies Hl and Hw) that indicate low-energy flow with mud deposition from suspension and periodic sand inflows, mostly through migration of isolated ripples (Reineck and Wunderlich, 1968). Besides these structures,

Table 4. Summary of facies descriptions and sedimentary process in the sediment cores

Facies	Description	Process
Lenticular heterolithic (Hl)	Greenish gray mud with single and connected flat lenses of pale olive, rippled fine to very fine sand.	Low-energy flows with mud deposition from suspension, but with periodic sand inflows through migration of isolated ripples.
Wavy heterolithic (Hw)	Greenish gray, wavy mud layers in alternation with pale olive, ripple-bedded fine sand layers.	Equal periods of mud and sand deposition from suspension and bedload transport, respectively.
Bioturbated mud (Mb)	Light yellowish brown and pale olive mud with many roots, root marks, dwelling structures and diffused fine sands following the root traces and benthic tubes.	Diffused mixture of sediments and alternating colors by intense bioturbation and diagenic process, respectively.
Cross-laminated sand (Sc)	Light olive gray, well sorted, fine to medium sand with current ripple cross-lamination.	Migration of small ripples during low-energy, unidirectional flows.
Massive sand (Sm)	Dark reddish brown and light yellowish brown moderately to poorly sorted, medium to coarse sand and locally angular to subangular ferruginous pebbles.	The massive nature may indicate a rapid sedimentation. In the case of the gravel class occurrence, pebbles are left behind, while sands moved as bedload under relatively high-energy flows.
Inclined heterolithic (Hi)	Parallel inclined laminae of light gray fine sand and pale olive mud with dip of ~6°.	Lateral accretion with sand and mud deposited during low-energy flows of a small-scale meandering creak.
Bioturbated sand (Sb)	Pale olive silty sand with light gray mottles, many roots, root traces in growth position and dwelling structures.	Sediment homogenization and mottling by biological activity and diagenic process, respectively.

the AM core presents mud with convolute lamination, many bioturbation features (facies Mb) such as roots, root marks and dwelling structures produced by the benthic fauna. Probably, convolute lamination was produced by localized differential forces acting on a hydroplastic sediment layer, commonly found on mud flats (Collinson et al., 2006).

The pollen assemblages of association A correspond to Zone MAC 1 (Figure 3), AM1 and AM2 (Figure 4). Zone MAC 1 was subdivided in Subzone MAC 1a and MAC 1b. Subzone MAC 1a (5560–5470 cal. yr BP to ~ 5430 cal. yr BP) is characterized by the predominance of mangrove pollen, mainly constituted by *Rhizophora* (20–75%). 'várzea' pollen of Araliaceae, Arecaceae, *Ilex*, *Mauritia* and Mimosoideae appear with very low percentages (<10%). Even profilic producers of windblown pollen such as Poaceae (Colinvaux et al., 1999) show low values (18–40%). However, Poaceae pollen (40–73%) increases in the Subzone MAC 1b (~5430 to 5290–5150 cal. yr BP). *Rhizophora* pollen (0–24%) becomes less frequent. Arecaceae (0–22%), Euphorbiaceae and *Mauritia* (~10%) are the main representatives of 'várzea' pollen.

Zone AM 1 (2350–2300 cal. yr BP to 1260–1080 cal. yr BP) reveals a heterogeneous vegetation assemblage (Figure 4). Inundated field pollen of Poaceae (18–48%), and mangrove pollen of *Rhizophora* (21–36%) and *Avicennia* (3–15%) are prevalent. *Acrostichum* (0–50%) fern is another mangrove indicator (Ng et al., 2002), but presented relatively low values. 'várzea' pollen of Euphorbiaceae (0–22%), *Pseudobombax* (0–10%) and Papilionoideae (2–5%) also showed low values. Subsequently, 'várzea' pollen progressively becomes less abundant. Inundated field pollen represented by Poaceae (20–40%), Amaranthaceae (3–10%) and Malpighiaceae (0–10%), jointly with mangrove pollen of *Rhizophora* (13–49%) and *Avicennia* (2–22%) exhibited high values, but mangrove pollen decreases towards the end of zone AM 1. Nevertheless, in zone AM 2 (1260–1080 cal. yr BP to modern), mangrove pollen is very well represented by *Rhizophora* (20–60%) and *Avicennia* (18–40%). *Acrostichum* (23–98%) fern reached its highest values in this zone.

The sediment $\delta^{13}C$ values ranging between −25‰ and −27.6‰ indicate the dominance of C3 plants (−32‰ to −21‰; Deines, 1980) and/or a mixture of freshwater algae (−26‰ to −30‰, Meyers, 1994; Schidlowski et al., 1983) and perhaps marine DOC (−22‰ to −25‰; Peterson et al., 1994). The $\delta^{15}N$ in the range of 2.1–7.5‰ suggests a mixture of terrestrial plants (~0‰) and aquatic organic matter (>10‰, Meyers, 1997; Thornton and McManus, 1994). The C/N values (11–20) also indicate a mixture of organic matter from vascular plants and algae (< 10 algae dominance and > 12 vascular plants; Meyers, 1994; Tyson, 1995), and the binary diagram between the $\delta^{13}C$ and C/N reveals contribution of marine and freshwater Dissolved Organic Carbon (DOC; Figures 5, 6 and 7).

Facies association B (Tidal sand flat). The association B begins around 5290–5150 cal. yr BP in the MAC core (Figure 2). It consists of massive sands (facies Sm) and cross-laminated sand (facies Sc), which record relatively low and high flow energy with current action shaping the bedform, inducing the migration of small sand ripples (Reineck and Singh, 1980). Pollen was not found in the association B, which corresponds to Subzone MAC 2a1 (Figure 3).

The sediment $\delta^{13}C$ values ranging between −25.8‰ and −26.3‰ suggest the contribution of C3 plants and fluvial Particulate Organic Carbon (POC; −25‰ to −30‰; Barth et al., 1998). The $\delta^{15}N$ values (4.3‰ to 5.4‰) indicate higher aquatic influence than in association A. Furthermore, the C/N values exhibit a reduction to 5.5 and 6.6 (Figure 5), reinforcing the contribution of aquatic materials because of fluvial influence through the relative contribution of phytoplankton (5 to 7; Meyers, 1994; Tyson, 1995). The relationship between $\delta^{13}C$ and C/N indicates freshwater algae as the main source of the organic matter accumulated in this facies association (Figure 7).

Facies association C (Small-scale point-bar). This association only occurs in the MAC core (Figure 2). Given calibrated ages below and above association C (5290–5150 cal. yr BP and ~ 3700 cal. yr BP), a sedimentary gap of 1000 years probably occurred because of the migration of a meandering creek. The association presents erosive base, medium to coarser sands with scattered ferruginous pebbles (facies Sm), which is overlaid by inclined sand and mud (facies Hi). Association C is a product of point-bar lateral accretion within a small-scale meandering creek draining intertidal mudflats, where periodic fluctuations of current

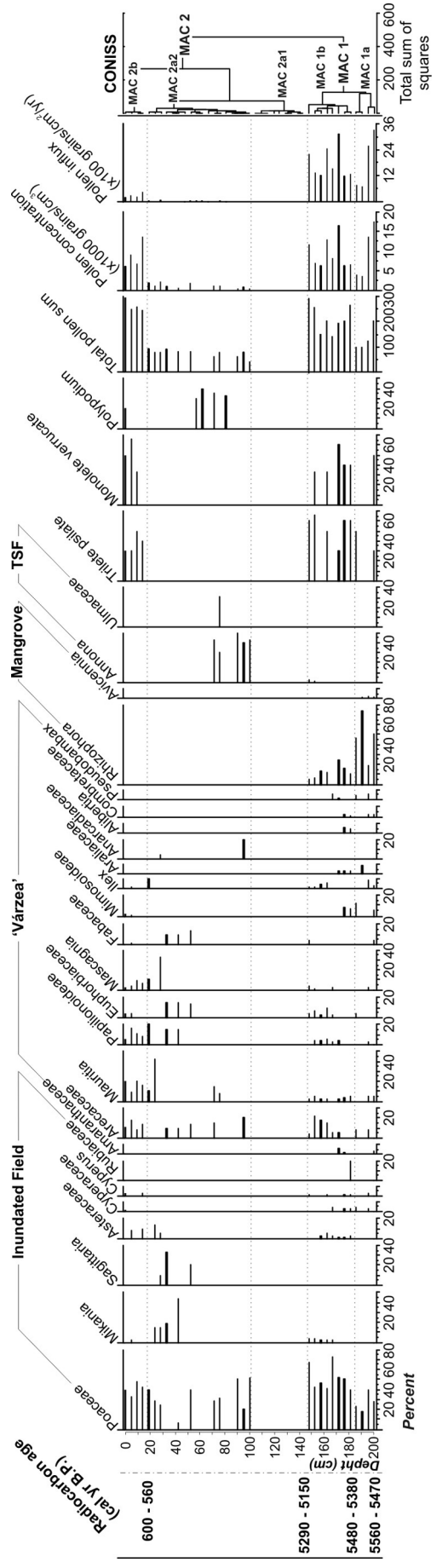

Figure 3. Pollen diagram of the MAC core

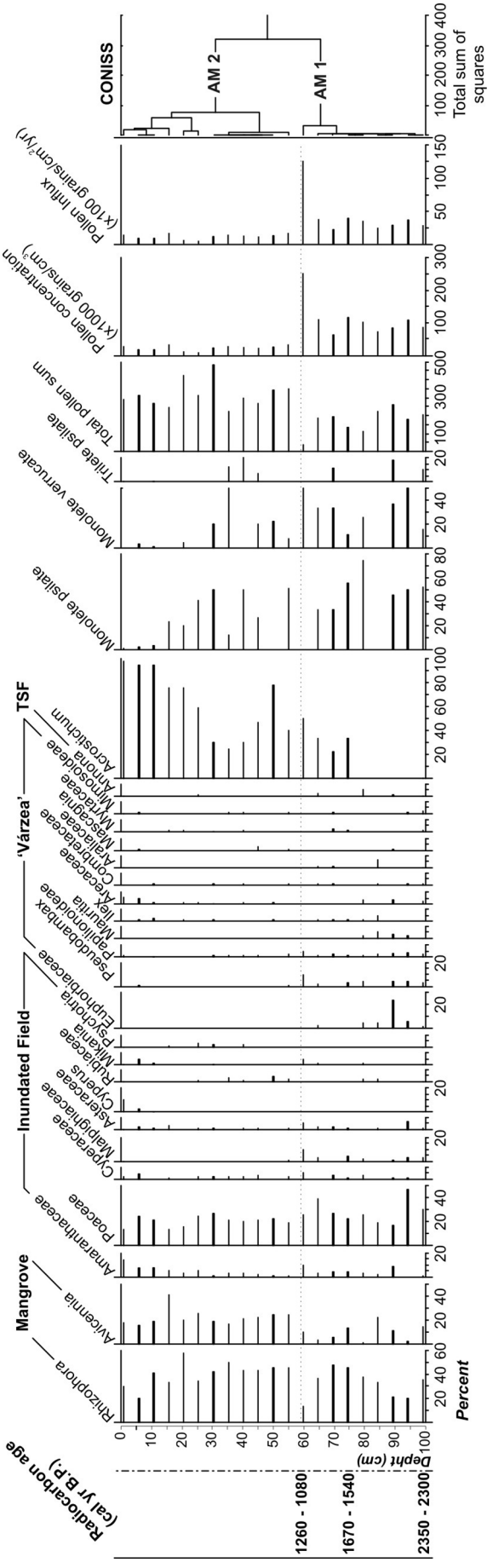

Figure 4. Pollen diagram of the AM core

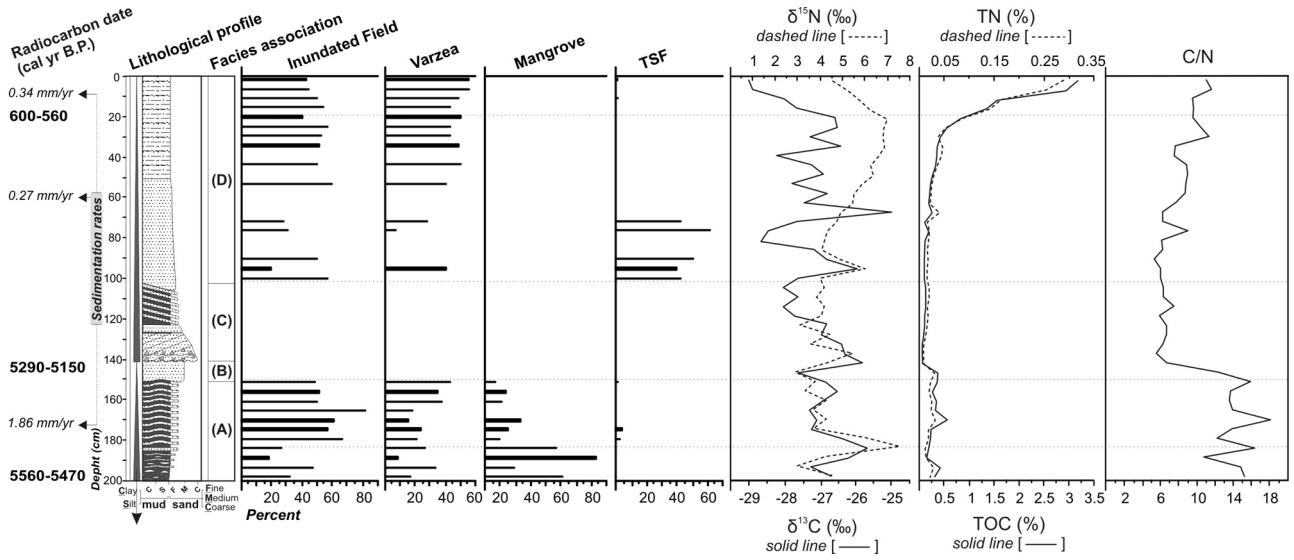

Figure 5. Interproxy records of the MAC core

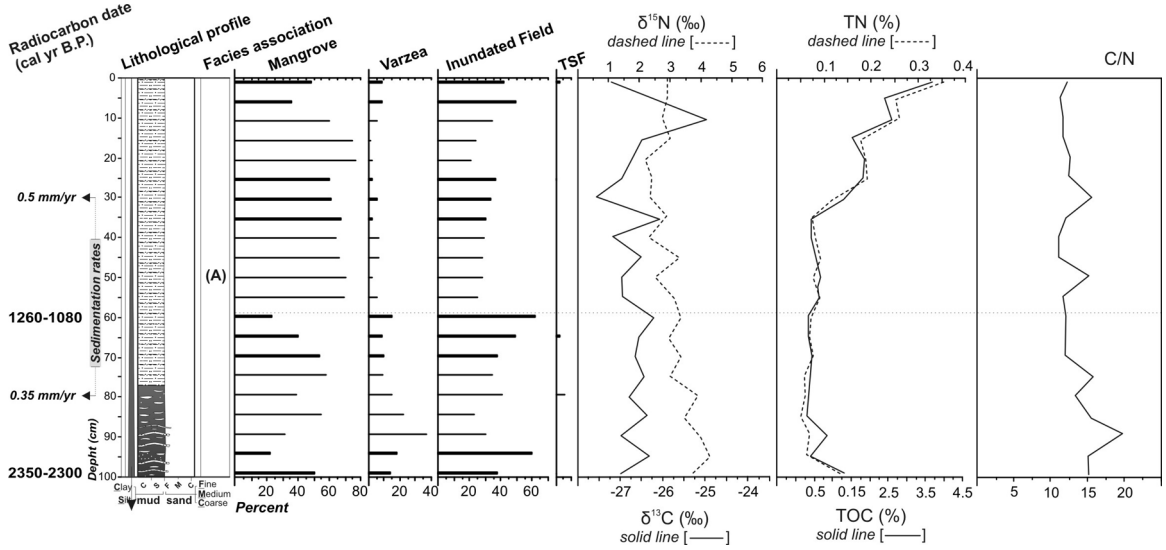

Figure 6. Interproxy records of the AM core

velocity/direction and water levels inherent to the tidal cycles, allowed sand and mud deposition during periods of high (ebb or flood tidal current) and low (slack water) energy flows, respectively (Thomas et al., 1987). The association C also integrates Subzone MAC 2a1 (Figure 3).

Sediment $\delta^{13}C$ values (−26.4‰ to −28‰) were more depleted in ^{13}C than association B, which is indicative of a greater contribution of fluvial POC. The $\delta^{15}N$ values (3‰ to 4.4‰), suggest a mixture of aquatic and terrestrial organic matter. However, the C/N values (5.8 to 6.6) indicate higher contribution of aquatic organic matter (Figure 5), as well as the relationship between $\delta^{13}C$ and C/N also indicates higher contribution of freshwater algae (Figure 7).

Facies association D ('Várzea'/transitional vegetation). The association D only occurs in the MAC core. It presents silty sand (facies Sb) and mud (facies Mb) with many roots, root marks of species with diffuse/fasciculated root systems, fragments of leaves, Oligochaeta tubes and mottling features (Figure 2), which may indicate diagenetic process in a vegetated substrate (e.g. Retallack, 2001).

This association corresponds to Subzone MAC 2a2 and MAC 2b (Figure 3). The Subzone MAC 2a2 (~3700 to 600–560 cal. yr BP) presents TSF and inundated field pollen of *Annona* and Poaceae (0–50%). Inundated field pollen of *Mikania* (0–44%), Poaceae (0–40%), *Sagittaria* (0–35%) and 'várzea' pollen of Euphorbiaceae (0–15%), *Mauritia* (0–43%), *Mascagnia* (0–33%), Papilionoideae (0–20%) increase toward the top. *Polypodium* (0–40%) is the only fern found in MAC 2a2. In the Zone MAC 2b (600–560 cal. yr BP to modern), Arecaceae (10–18%), *Mauritia* (10–20%), Papilionoideae (6–16%), *Mascagnia* (3–10%) and Poaceae (32–47%) pollen are well correlated to the modern vegetation at the sampling site. The incipient pollen results in the Subzone MAC 2a2 of inundated field (0–62%), TSF (0–60%) and 'várzea' (0–50%) suggest that inundated field and other successional vegetation act as pioneers for the stabilization of a new organic horizon for TSF development, until the expansion of 'várzea' forests at 600–560 cal. yr BP.

The sediment $\delta^{13}C$ values varied from −25.9‰ to −29‰, the $\delta^{15}N$ from 3.6‰ to 6.9‰ and the C/N values from 5.2 to 11.6. These are indicative of a mixture of terrestrial and aquatic organic matter (Figure 5). The binary diagram of $\delta^{13}C$ and C/N

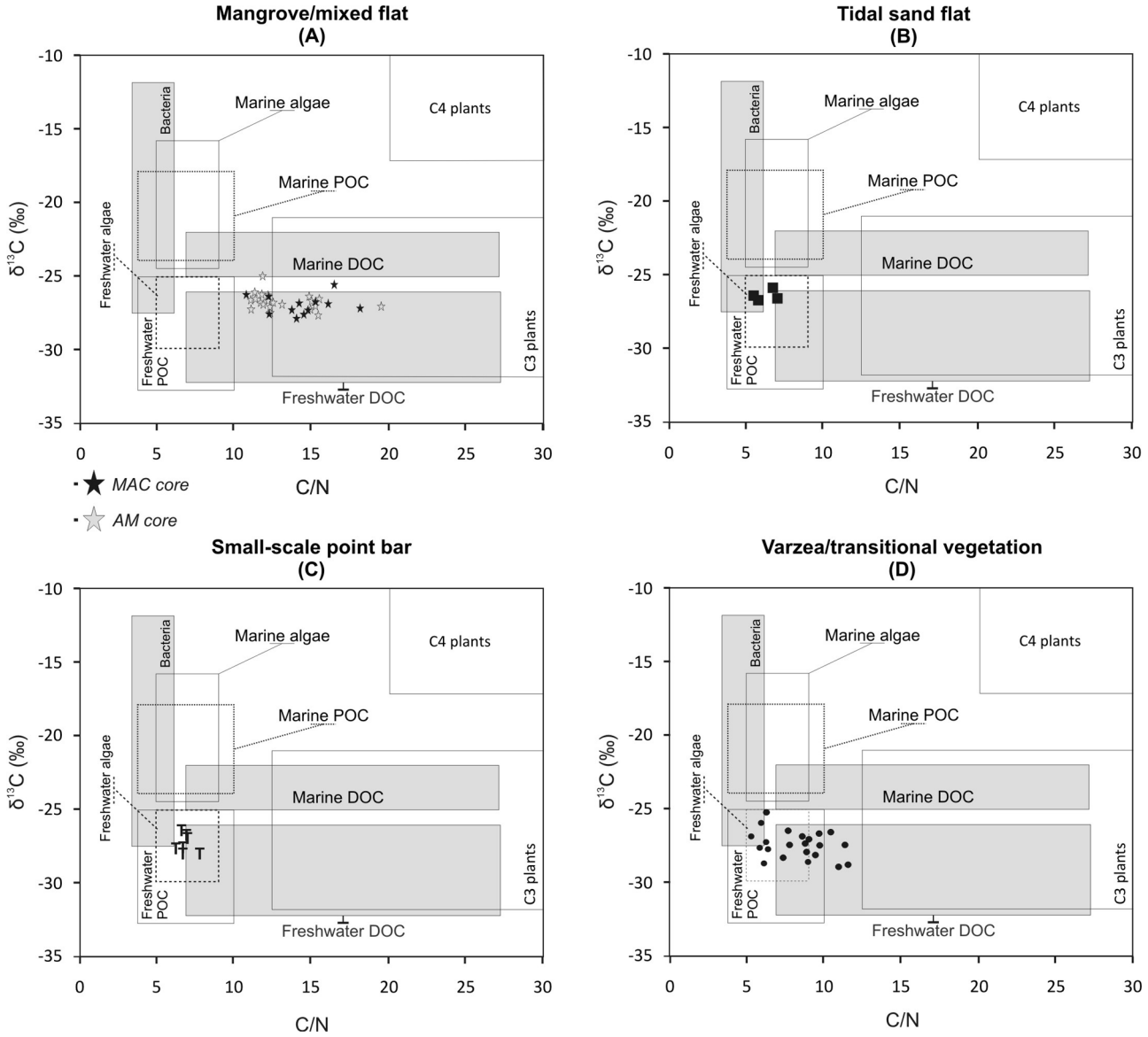

Figure 7. Binary diagram of $\delta^{13}C$ and C/N for each sedimentary facies in the study area with interpretation of carbon sources based on typical ranges recorded in several coastal environments (Deines, 1980; Haines, 1976; Lamb et al., 2006; Meyers, 1994; Middelburg and Nieuwenhuize, 1998; Peterson et al., 1994; Raymond and Bauer, 2001; Schidlowski et al., 1983; Tyson, 1995 and references therein)

values reinforces the influence of freshwater DOC and POC (Figure 7).

Palaeoenviromental interpretation

The data suggest mangrove predominance and the accumulation of brackish water organic matter over a tidal mud flat from Macapá littoral around 5560–5470 cal. yr BP (Figure 5). Between 5560–5470 and 5290–5150 cal. yr BP, the data suggests retraction of mangrove and expansion of Arecaceae and herbaceous vegetation followed by an increase in the contribution of freshwater organic matter (Figure 8). Near the study site (~ 8 km), palaeoecological records from Lake Márcio and Tapera revealed the occurrence of mangrove forests between 8060 and 5840 cal. yr BP, and the replacement of mangrove by freshwater vegetation until 5300 cal. yr BP (Toledo and Bush, 2007).

The point bar sequence found in the Macapá site reveals a common reworking process of the tidal flat through the lateral migration of a meandering creek (e.g. Reineck, 1958; Thomas et al., 1987), with later development of transitional vegetation under freshwater influence. Following the natural vegetation succession under relatively stable climate and hydrological conditions, the expansion of 'várzea' forests occurred since 600–560 cal. yr BP until the present (Figure 8).

Regarding the littoral of the town of Amapá (150 km away from the mouth of the Amazon River, Figure 1), the mangrove forests have colonized tidal mud flats during the last 2350–2300 cal. yr BP. However, the *Acrostichum* sp. (mangrove ferns) has expanded over the last ~1500 cal. yr BP. This fern tends to invade open areas under relatively less salty water and high rainfall conditions (Medina et al., 1990). Furthermore, the current distribution of freshwater vegetation near the town of Amapá (Figure 1) suggests a continuous colonization of 'várzea' vegetation to the detriment of mangrove during the late Holocene.

Despite this fact that this work is restricted to data on depositional environment, palaeovegetation changes and organic matter sources, we consider it appropriate to propose a hypothesis to explain this environmental alteration through palaeoclimate changes affecting the Amazon River inflow during the Holocene. Thus, after the postglacial sea-level rise, the relative sea level along the Northern Brazilian littoral reached the current sea level

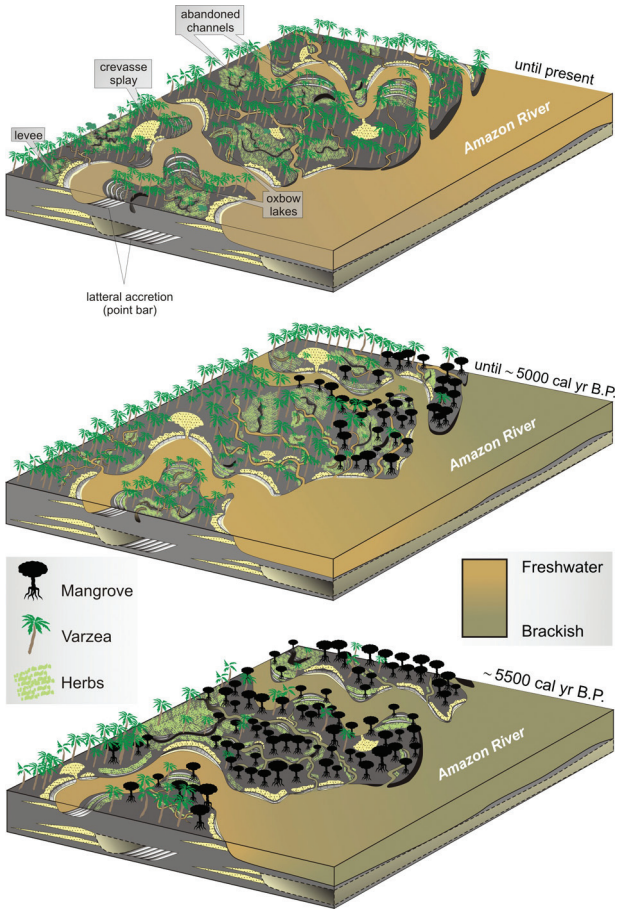

Figure 8. Schematic representation of successive phases of sediment accumulation and vegetation change in the study area according to Amazon River inflow in a stationary littoral

between 7000 and 5000 yr BP, and did not show significant oscillations during the last 5000 years (Cohen et al., 2005; Souza Filho et al., 2006). However, our data show that after the sea-level rise an increase in fluvial influence occurred along the study site. Today, the Amazon River discharge has a great influence on the salinity gradient along the tidal flats, limiting the mangrove vegetation to the northwestern Amapá littoral closer to the Atlantic Ocean (Guimarães et al., 2010).

The northern Brazilian mangroves are part of a wetland system that extends for almost 480 km and holds one of the world's largest mangrove areas (Kjerfve and Lacerda, 1993). The continuity of this mangrove littoral is interrupted by the zone influenced by discharge of the Amazon River, where the 'várzea' vegetation dominates (Cohen et al., 2008). The mangrove zones are the response to the gradients of tidal inundation frequency, waterlogging, nutrient availability and sediment salt concentrations across the intertidal area (Hutchings and Saenger, 1987; Wolanski et al., 1990). The geomorphic setting of mangrove systems also comprises a range of inter-related factors such as substrate types, coastal processes, sediment delivery, and freshwater delivery, all of which influence the occurrence and survivorship of mangroves (Semeniuk, 1994). However, an empirical model based on an ecohydrological approach, which allowed the integration of hydrographical, topographical and physicochemical information with vegetation characteristics of mangroves and marshes, indicates that under the same morphological condition, change in pore water salinity is the main factor displacing the wetlands boundaries on northern Brazil (Cohen and Lara, 2003; Lara and Cohen, 2006). The relations between mangrove and sediment geochemistry have been widely investigated (Alongi et al., 2000; Baltzer, 1970; Clark et al., 1998; Hesse, 1961; Lacerda et al., 1995; Snedaker, 1978; Walsh, 1974; Youssef and Saenger, 1999). The Pará Littoral-Northern Brazil (Behling et al., 2001; Cohen et al., 2005), follows well-known patterns, where salinity excludes certain species (Snedaker, 1978), leading to characteristic patterns of species zonation and predictable types of community structure (Menezes et al., 2003), where the mangroves are more tolerant to sediment salinity than 'várzea' forest (Gonçalves-Alvim et al., 2001).

Regarding the river dynamics affecting the local vegetation and geochemical proxies, only the 105–140 cm interval of the core MAC presented a sedimentary structure that indicates migration of a meandering creek. This interval is a product of point-bar lateral accretion within a small-scale meandering creek (Thomas et al., 1987). Likely, following this dynamic, the organic matter and sediments are products of the reworking of material from the margin along the channel. Indeed, this mechanism may disturb a continuous sequence of pollen and isotopic records. However, as described in the Facies Association C of this work, this process may be identified by the sedimentary facies associated to the pollen and isotopic data (e.g. Miranda et al., 2009). Other sedimentary facies of the studied cores indicate stable tidal sand/mud flats colonized by mangrove and/or 'várzea' vegetation. Thus, this depositional environment accumulated sediment with pollen and organic matter that reflects the main vegetation and organisms colonizing the study site during that time.

Therefore our hypothesis is that, during the mid Holocene, the Amazon River inflow was lower than today, which allowed an increase of marine influence in sector 2 (Figure 1d). Afterward, the retraction of mangrove and expansion of freshwater vegetation during the late Holocene indicates the return of more humid climate conditions and rise of Amazon River inflow.

Along the littoral of the town of Amapá, at least during the last 2350–2300 cal. yr BP, the marine influence allowed the maintenance of mangrove vegetation and the increase in Amazon River inflow during the late Holocene was not strong enough to result in the total replacement of mangrove by 'várzea' and/or inundated field, such as occurred on the Macapá site after 5290–5150 cal. yr BP.

Several palaeoecological studies in the Amazon region also indicate drier climate during the mid Holocene, and a wet period during the late Holocene (e.g. Absy et al., 1991; Behling and Hooghiemstra, 2000; Bush and Colinvaux, 1988; Bush et al., 2007; Desjardins et al., 1996; Gouveia et al., 1997; Pessenda et al., 1998, 2001; Sifeddine et al., 1994, 2001; Weng et al., 2002).

Conclusion

The tidal flat data analyzed indicate significant vegetation changes. The marine influence and resultant mangrove expansion occurred between 5560–5470 cal. yr BP and ~5430 cal. yr BP. Between ~5430 and 5290–5150 cal. yr BP, the mangrove retreated and freshwater vegetation expanded, which suggests a decrease in marine influence. During the late Holocene, freshwater vegetation developed along the tidal flat from Macapá site. However, on the northwestern Amapá littoral, which lies 150 km away from the mouth of Amazon River, the mangrove forests have colonized part of the tidal mud flats during the last 2350–2300 cal. yr BP. This suggests that marine influence allowed the maintenance of this vegetation, and the increase in fluvial inflow did not result in a complete replacement of mangrove by freshwater vegetation.

Acknowledgements

The authors thank the members of the Laboratório de Dinâmica Costeira – Universidade Federal do Pará and the Laboratório de Carbono 14 – Centro de Energia Nuclear na Agricultura, Universidade de São Paulo-USP.

Funding

This work was funded by CNPq (Project 562398/2008-2). The first and second authors hold a scholarship from CNPq (Process 143518/2008-9 and 302943/2008-0).

References

Absy ML, Clief A, Fournier M, Martin L, Servant M, Siffeddine A et al. (1991) Mise en évidence de Quatre phases d'ouverture de la forêt dense dans le sud-estde L'Amazonie au cours des 60,000 dernières années. Première comparaison avec d'autres régions tropicales. *Comptes Rendus Academie des Sciences Paris* 312: 673–678.

Allison MA, Lee MT, Ogston AS and Aller RC (2000) Origin of Amazon mudbanks along the northeastern coast of South America. *Marine Geology* 163: 241–256.

Alongi DM, Tirendi F and Clough BF (2000) Below-ground decomposition of organic matter in forests of the mangrove *Rhizophora stylosa* and *Avicennia marina* along the arid coast of Western Australia. *Aquatic Botany* 68: 97–122.

ANA (2003) *Hydrological Information System*. Brazilian National Water Agency. Online data set, 14.3 MB, http://hidroweb.ana.gov.br/baixar/mapa/Bacia1.zip

Baltzer F (1970) *Etude sédimentologique du marais de Mara (Côte ouest de la Nouvelle Calédonie) et de formations quaternaires voisines*. Mémoires expédition française sur les récifs coralliens de la Nouvelle Calédonie, Foundation Singer-Polignac 4, 146–169.

Barth JAC, Veizer J and Mayer B (1998) Origin of particulate organic carbon in the upper St. Lawrence: Isotopic constraints. *Earth and Planetary Science Letters* 162: 111–121.

Beardsley RC, Candela J, Limeburner R, Geyer WR, Lentz SJ, Castro BM et al. (1995) The M2 tide on the Amazon shelf. *Journal of Geophysical Research* 100: 2283–2319.

Behling H and Costa ML (2000) Holocene environmental changes from the Rio Curuá record in the Caxiuanã region, eastern Amazon Basin. *Quaternary Research* 53: 369–377.

Behling H and Costa ML (2001) Holocene vegetation and coastal environmental changes from Lago Crispim in northeastern Pará State, northern Brazil. *Palaeogeography*, *Palaeoclimatology*, *Palaeoecology* 114: 145–155.

Behling H and Hooghiemstra H (2000) Holocene Amazon rain forest – Savanna dynamics and climatic implications: High resolution pollen record Laguna Loma Linda in eastern Colombia. *Journal of Quaternary Science* 15: 687–695.

Behling H, Cohen MCL and Lara RJ (2001) Studies on Holocene mangroves ecosystem of the Bragança Peninsula in north-eastern Pará, Brazil. *Palaeogeography*, *Palaeoclimatology*, *Palaeoecology* 167: 225–242.

Behling H, Cohen MCL and Lara RJ (2004) Late Holocene mangrove dynamics of Marajó Island in Amazonia, northern Brazil. *Vegetation History and Archaeobotany* 13: 73–80.

Bezerra PEL, Oliveira W, Regis WDE, Brazão JEM, Gavinho J and Coutinho RCP (1990) Amazônia legal: Zoneamento das potencialidades e dos recursos naturais. In: Instituto Brasileiro de Geografia e Estatística, Superintendência de Desenvolvimento da Amazônia. *Projeto zoneamento das potencialidades dos recursos naturais da Amazônia: geologia, solos e vegetação*. Div. 5. Rio de Janeiro, 9–89.

Bush MB and Colinvaux PA (1988) A 7000yr vegetational history from lowland Amazon, Ecuador. *Plant Ecology* 76: 141–154.

Bush MB, Silman MR and Listopad CMCS (2007) A regional study of Holocene climate change and human occupation in Peruvian Amazonia. *Journal of Biogeography* 34: 1342–1356.

Carvalho FP, Costa Neto SV, Costa WJP, Coutinho RS, Figueira ZR, Figueiredo SL et al. (2006) *Atlas Zoneamento Costeiro Estuarino do Estado do Amapá*. Macapá, PNMA/SQA/MMA, 77 pp.

Chivas AR, Garcia A, Van der Kaars S, Couapel MJJ, Holt S, Reeves JM et al. (2001) Sea-level and environmental changes since the last interglacial in the Gulf of Carpentaria, Australia: An overview. *Quaternary International* 83–85: 19–46.

Clark MW, McConchie DM, Lewis DW and Saenger P (1998) Redox stratification and heavy metal partitioning in Avicennia-dominated mangrove sediments: A geochemical model. *Chemistry Geology* 149: 147–171.

Coffin RB, Fry B, Peterson BJ, Wright RT (1989) Carbon isotopic compositions of estuarine bacteria. *Limnology and Oceanography* 34: 1305–1310.

Cohen MCL and Lara RJ (2003) Temporal changes of vegetation boundaries in Amazonia: Application of GIS and Remote sensing techniques. *Wetlands Ecology and Management* 11: 223–231.

Cohen MCL, Souza Filho PWM, Lara RJ, Behling H and Angulo RJ (2005) A model of Holocene mangrove development and relative sea-level changes on the Bragança Peninsula (Northern Brazil). *Wetlands Ecology and Management* 13: 433–443.

Cohen MCL, Lara RJ, Smith CB, Angélica RS, Dias BS and Pequeno T (2008) Wetland dynamics of Marajó Island, northern Brazil, during the last 1000 years. *Catena* 76: 70–77.

Cohen MCL, Lara RJ, Smith CB, Matos HRS and Vedel V (2009).Impact of sea-level and climatic changes on the Amazon coastal wetlands during the late Holocene. *Vegetation History and Archaeobotany* 18: 425–439.

Colinvaux PA, De Oliveira PE and Patiño JEM (1999) *Amazon Pollen Manual and Atlas - Manual e Atlas Palinológico da Amazônia*. Amsterdam: Hardwood Academic, 332 pp.

Collinson J, Mountney N and Thompson D (2006) *Sedimentary Structures*. (Third edition) Terra Publishing, 292 pp.

Costa JB, Hasui Y, Bemerguy RL, Soares-Júnior AV and Villegas J (2002) Tectonics and paleogeography of the Marajó Basin, northern Brazil. *Anais da Academia Brasileira de Ciências* 74: 519–531.

Costa Neto SV (2004) *Relatório de vegetação: Subsídio ao diagnostico sócio ambiental*. Relatório Técnico. Macapá, IEPA/GERCO, 32 pp.

Costa Neto SV and Silva MS (2004) *Vegetação do setor costeiro estuarino do estado do Amapá*. Instituto de Pesquisas Científicas e Tecnológicas do Estado do Amapá. Governo do Estado do Amapá. Cap. 5. Projeto Zoneamento Econômico-Ecológico do setor costeiro estuarino: Diagnóstico sócio ambiental participativo do setor costeiro estuarino, 72–96.

Costa Neto SV, Senna C, Tostes LCL and Silva SRM (2007) Macrófitas aquáticas das Regiões dos Lagos do Amapá, Brasil. *Revista Brasileira de Biociências* 5: 618–620.

CPRM (2010) *Geological Information System*. Brazilian Geological Service. Online data set, Folhas NA/SA-22 23 MB, http://geobank.sa.cprm.gov.br/

Dalrymple RW and Choi K (2007) Morphologic and facies trends through the fluvial-marine transition in tide-dominated systems: A schematic framework for environmental and sequence-stratigraphic interpretation. *Earth-Science Reviews* 81: 135–174.

Deines P (1980) The isotopic composition of reduced organic carbon. In: Fritz P and Fontes JC (eds) *Handbook of Environmental Isotope Geochemistry*. *The Terrestrial Environment, Vol.1*. Amsterdam: Elsevier, 329–406.

Desjardins T, Filho AC, Mariotti A, Chauvel A and Girardin C (1996) Changes of the forest–savanna boundary in Brazilian Amazonia during the Holocene as revealed by soil organic carbon isotope ratios. *Oecologia* 108: 749–756.

Engelhart SE, Horton BP, Roberts DH, Bryant CL and Corbett DR (2007) Mangrove pollen of Indonesia and its suitability as a sea-level indicator. *Marine Geology* 242: 65–68.

Faegri K and Iversen J (1989) *Textbook of Pollen Analyses*. Chichester: John Wiley and Sons LTD, 328 pp.

Freycon V, Krencker M, Schwartz D, Nasi R and Bonal D (2009) The impact of climate changes during the Holocene on vegetation in northern French Guiana. *Quaternary Research* 73: 220–225.

Gallo MN and Vinzon S (2005) Generation of over tides and compound tides in Amazon estuary. *Ocean Dynamics* 55: 441–448.

Gonçalves-Alvim SJ, Vaz dos Santos MCF and Fernandes GW (2001) Leaf gall abundance on *Avicennia germinans* (Avicenniaceae) along an interstitial salinity gradient. *Biotropica* 33: 69–77.

Gouveia SEM, Pessenda LCR, Aravena R, Boulet R, Roveratti R and Gomes BM (1997) Dinâmica de vegetações durante o Quaternário recente no sul do Amazonas indicada pelos isótopos do carbono (^{12}C, ^{13}C e ^{14}C). *Geochimica Brasiliensis* 11: 355–367.

Grimm EC (1987) CONISS: A FORTRAN 77 program for stratigraphically constrained cluster analysis by the method of the incremental sum of square. *Computer and Geosciences* 13: 13–35.

Guimarães JTF, Cohen MCL, França MC, Lara RJ and Behling H (2010) Model of wetland development of the Amapá coast during the late Holocene. *Anais da Academia Brasileira de Ciências* 82: 451–465.

Haines EB (1976) Stable carbon isotope ratios in biota, soils and tidal water of a Georgia salt marsh. *Estuarine and Coastal Marine Science* 4: 609–616.

Hesse M, Halbritter H, Zetter R, Weber M, Buchner R, Frosch-Radivo A et al. (2008) *Pollen Terminology*: *An Illustrated Handbook*. New York: Springer, 264 pp.

Hesse PR (1961) Some differences between the soils of *Rhizophora* and *Avicennia* mangrove swamp in Sierra Leone. *Plant Soil* 14: 335–346.

Horton BP, Gibbard PL, Milne GM, Morley RJ, Purintavaragul C and Stargardt JM (2005) Holocene sea levels and palaeoenvironments of the Malay-Thai Peninsula, southeast Asia. *The Holocene* 15: 1199–1213.

Hutchings P and Saenger P (1987) *Ecology of Mangroves*. Queensland University Press, 388 pp.

Kjerfve B and Lacerda LD (1993) Mangroves of Brazil. In: Lacerda LD (ed.) *Conservation and Sustainable Utilization of mangrove Forests in Latin*

America and Africa Regions. *Part I – Latin America*. Okinawa: ITTO/ International Society for Mangrove Ecosystems, 245–272.

Klein GV (1971) A sedimentary model for determining paleotidal range. Geological Society *of* America *Bulletin* 82: 2585–2592.

Lacerda LD, Ittekkot V, Patchineelam SR (1995) Biogeochemistry of mangrove soil organic matter: A comparison between *Rhizophora*, *Avicennia* soils in south-eastern Brazil. *Estuarine, Coastal and Shelf Science* 40: 713–720.

Lamb AL, Wilson GP and Leng MJ (2006) A review of coastal palaeoclimate and relative sea-level reconstructions using $\delta^{13}C$ and C/N ratios in organic material. *Earth-Science Reviews* 75: 29–57.

Lara JR and Cohen MCL (2006) Sediment porewater salinity, inundation frequency and mangrove vegetation height in Bragança, North Brazil: An ecohydrology-based empirical model. *Wetlands Ecology and Management* 14: 349–358.

Latrubesse EM and Franzinelli E (2002) The Holocene alluvial plain of the middle Amazon River, Brazil. *Geomorphology* 44: 241–257.

Ledru MP (2001) Late Holocene rainforest disturbance in French Guiana. *Review of Palaeobotany and Palynology* 115: 161–176.

Lentz SJ (1995) The Amazon River plume during AMASSEDS: Subtidal current variability and the importance of wind forcing. *Journal of Geophysical Research* 100: 2377–2390.

Lentz SJ and Limeburner R (1995) The Amazon River Plume during AMASSEDS: Spatial characteristics and salinity variability. *Journal of Geophysical Research* 100: 2355–2375.

Lima MIC, Bezerra PE and Araújo HJT (1991) Sistematização da Geologia do Estado do Amapá. In: *Simpósio de geologia da Amazônia*, *vol. 3*. Belém, Anais, SBG, 322–335.

Maslin MA and Burns SJ (2000) Reconstruction of the Amazon Basin effective moisture availability over the past 14,000 years. *Science* 290: 2285–2287.

Medina E, Cuevas E, Popp M and Lugo A (1990) Soil salinity, sun exposure, and growth of *Acrostichum aureum*, the mangrove fern. *Botanical Gazette* 151: 41–49.

Menezes M, Berger U and Worbes M (2003) Annual growth rings and long-term growth patterns of mangrove trees from the Bragança peninsula, North Brazil. *Wetlands Ecology and Management* 11: 233–242.

Meyers PA (1994) Preservation of elemental and isotopic source identification of sedimentary organic matter. *Chemical Geology* 114: 289–302.

Meyers PA (1997) Organic geochemical proxies of paleoceanographic, paleolimnologic and paleoclimatic processes. *Organic Geochemistry* 27: 213–250.

Miall AD (1978) Facies types and vertical profile models in braided river deposits: A summary. In: Miall AD (ed.) *Fluvial Sedimentology*. Calgary: Canadian Society of Petroleum Geologists, 597–604.

Middelburg JJ and Nieuwenhuize J (1998) Carbon and nitrogen stable isotopes in suspended matter and sediments from the Schelde Estuary. *Marine Chemistry* 60: 217–225.

Miranda MCC, Rossetti DF and Pessenda LCR (2009) Quaternary paleoenvironments and relative sea-level changes in Marajó Island (Northern Brazil): Facies, $\delta^{13}C$, $\delta^{>15}N$ and C/N. *Palaeogeography, Palaeoclimatology, Palaeoecology* 282: 19–31.

Ng PKL, Sivasothi N, Morgany T and Murphy DH (2002) *A Guide to the Mangroves of Singapore 1*: *The Ecosystem & Plant Diversity*. Singapore Science Centre, Rev. Edition, 160 pp.

Pessenda LCR, Boulet R, Aravena R, Rosolen V, Gouveia SEM, Ribeiro AS et al. (2001) Origin and dynamics of soil organic matterand vegetation changes during the Holocene in a forest–savanna transition zone, Brazilian Amazon region. *The Holocene* 11: 250–254.

Pessenda LCR, Gouveia SEM, Aravena R, Gomes BM, Boulet R and Ribeiro AS (1998) ^{14}C dating and stable carbon isotopes of soil organic matter in forest–savanna boundary areas in southern Brazilian Amazon region. *Radiocarbon* 40: 1013–1022.

Peterson BJ, Fry B, Hullar M, Saupe S and Wright R (1994) The distribution and stable carbon isotope composition of dissolved organic carbon in estuaries. *Estuaries* 17: 111–121.

Pugh DT (1987) *Tides, Surges and Mean Sea-level*: *A Handbook for Engineers and Scientists*. London: Wiley, 486 pp.

Ramani B, Reeckb T, Debezc A, Stelzerd R, Huchzermeyera B, Schmidta A et al. (2006) *Aster tripolium* L. and *Sesuvium portulacastrum* L.: Two halophytes, two strategies to survive in saline habitats. *Plant Physiology and Biochemistry* 44: 395–408.

Raymond PA and Bauer JE (2001) Use of ^{14}C and ^{13}C natural abundances for evaluating riverine, estuarine, and coastal DOC and POC sources and cycling: A review and synthesis. *Organic Geochemistry* 32: 469–485.

Reimer PJ, Baillie MGL, Bard E, Bayliss A, Beck JW, Bertrand CJH et al. (2004) IntCal04 terrestrial radiocarbon age calibration, 26–0 ka BP. *Radiocarbon* 46: 1029–1058.

Reineck HE (1958) Longitudinale schrägschicht in Watt. *Geologische Rundschau* 47: 73–82.

Reineck HE and Singh IB (1980) *Depositional Sedimentary Environments with Reference to Terrigenous Clastics* (Second edition). Berlin: Springer-Verlag, 542 pp.

Reineck HE and Wunderlich F (1968) Classification and origin of flaser and lenticular bedding. *Sedimentology* 11: 99–104.

Retallack GJ (2001) *Soils of the Past – An Introduction to Paleopedology* (Second edition). Wiley-Blackwell, 512 pp.

Rosario RP, Bezerra MOM and Vinzon SB (2009) Dynamics of the saline front in the Northern Channel of the Amazon River – Influence of fluvial flow and tidal range (Brazil). *Journal of Coastal Research* 2: 503–514.

Roubik DW and Moreno JE (1991) *Pollen and Spores of Barro Colorado Island*. Missouri Botanical Garden, 268 pp.

Schidlowski M, Hayes JM and Kaplan IR (1983) Isotopic inferences of ancient biochemistries: Carbon, sulphur, hydrogen and nitrogen. In: Scholf JW (ed.) *Earth's Earliest Biosphere, Its Origin and Evolution*. Princeton: Princeton University Press, 149–186.

Semeniuk V (1994) Predicting the effect of sea-level rise on mangroves in northwestern Australia. *Journal of Coastal Research* 10: 1050–1076.

Sifeddine A, Fröhlich F, Fournier M, Martin L, Servant M, Soubiés F et al. (1994) La sédimentation lacustre indicateur de changements des paléoenvironnements au cous des 30000 dernières annèes (Carajas, Amazonie, Brésil). *Comptes rendus de l'Académie des sciences* 318: 1645–1652.

Sifeddine A, Martin L, Turcq B, Ribeiro CV, Soubiès F, Cordeiro RC et al. (2001) Variations of the Amazonian rainforest environment: A sedimentological record covering 30,000 years. *Palaeogeography, Palaeoclimatology, Palaeoecology* 168: 221–235.

Snedaker SC (1978) Mangroves: Their value and perpetuation. *Natural Resources* 16: 179–188.

Souza EJ and Pinheiro RVL (2009) *Relações entre as estruturas tectônicas do embasamento e o desenvolvimento da paisagem da região costeira do estado do Amapá uma investigação sobre reativações tectônicas e acumulação de hidrocarbonetos*. Relatório técnico-científico, Brasília: ANP, 105 pp.

Souza Filho PWM, Cohen MCL, Lara RJ, Lessa GC, Koch B and Behling H (2006) Holocene coastal evolution and facies model of the Bragança macrotidal flat on the Amazon mangrove coast, Northern Brazil, *Journal of Coastal Research* SI 39: 306–310.

Szatmari P, Françolin JBL, Zanotto O and Wolff S (1987) Evolução tectônica da margem equatorial brasileira. *Revista Brasileira de Geociências* 17: 180–188.

Thomas RG, Smith DG, Wood JM, Visser J, Calverly-Range EA and Koster EH (1987) Inclined heterolithic stratification: Terminology, description, interpretation and significance. *Sedimentary Geology* 53: 123–179.

Thornton SF and McManus J (1994) Applications of organic carbon and nitrogen stable isotope and C/N ratios as source indicators of organic matter provenance in estuarine systems: Evidence from the Tay Estuary, Scotland. *Estuarine, Coastal and Shelf Science* 38: 219–233.

Toledo MB and Bush MB (2007) A mid-Holocene environmental change in Amazonian savannas. *Journal of Biogeography* 34: 1313–1326.

Tyson RV (1995) *Sedimentary Organic Matter: Organic Facies and Palynofacies*. London: Chapman and Hall, 15 pp.

Vedel V, Behling H, Cohen MCL and Lara RJ (2006) Holocene mangrove dynamics and sea-level changes in Taperebal, northeastern Pará State, northern Brazil. *Vegetation History and Archaeobotany* 15: 115–123.

Van der Hammen T (1974) The Pleistocene changes of vegetation and climate in tropical South America. Journal of Biogeography 1: 3–26.

Vinzon BS, Vilela CPX and Pereira LCC (2008) *Processos fisicos na Plataforma Continental Amazônica. Relatório-Técnico, Potenciais Impactos Ambientais do Transporte de Petróleo e Derivados na Zona Costeira Amazônico*. Petrobrás, Brasil, 31 pp.

Walker RG (1992) Facies, facies models and modern stratigrahic concepts. In: Walker RG and James NP (eds) *Facies Models – Response to Sea Level Change*. Ontario: Geological Association of Canada, 1–14.

Walsh GE (1974) Mangroves, a review. In: Reimold RJ and Queens WH (eds) *Ecology of Halophytes*. Academic Press, 51–174.

Weng C, Bush MB and Athens JS (2002) Two histories of climate change and hydrarch succession in Ecuadorian Amazonia. *Review of Palynology and Paleobotany* 120: 73–90.

Wolanski E, Mazda Y, King B and Gay S (1990) Dynamics, flushing and trapping in Hinchinbrook Channel, a giant mangrove swamp, Australia. *Estuarine, Coastal and Shelf Science* 31: 555–579.

Youssef T and Saenger P (1999) Mangrove zonation in Mobbs Bay, Australia. *Estuarine, Coastal and Shelf Science* 49: 43–50.

3 EL NIÑO AND LA NIÑA EFFECTS ON TIDAL FLATS NEAR THE MOUTH OF THE AMAZON RIVER*

José Tasso Felix Guimarães[1], Marcelo Cancela Lisboa Cohen[1,2], Marlon Carlos França[1], Yuri Souza Friaes[1]

[1]Programa de Pós-Graduação em Geologia e Geoquímica, Universidade Federal do Pará. Rua Augusto Corrêa 1, Guamá, 66075-110 Belém, PA, Brasil
[2]Faculdade de Oceanografia, Universidade Federal do Pará. Rua Augusto Corrêa 1, Guamá, 66075-110 Belém, PA, Brasil

* Submitted to Earth Surface Process and Landscape

ABSTRACT

The goal of this work was to understand the main processes acting on the tidal flats of the coast of Amapá near the mouth of the Amazon River, and how they change over the short-term (~ 30 years). The analysis of morphological and geobotanical units was carried out using processing and interpretation methods in optical and synthetic aperture radar (SAR) images, as well as water salinity, maximum flood height, historical rain series and sedimentary facies data. The coastal plateau presents a flat to gently undulated surface shaped by erosive processes. Plateau vegetation is represented by "várzea" (flooded freshwater forests) and savannah. Avulsion of alluvial channels and birdfoot features possibly related to six deltaic lobes were also identified in this region. The coastal plain measures on average 10 km in length, and it consists of the tidal-fluvial channel, paleochannels, lakes, "várzea", inundated fields, mangroves, chenier ridges, elongated tidal mud bars (ETMB), tidal mud and non-vegetated mixed flats. The sedimentary facies indicate tide and wave-dominated environments. The temporal analysis of morphological and geobotanical units suggests the relative stabilization of savannah (+1.4%), "várzea" (+0.2%) and mangrove (+2.2%) areas, with the formation of extensive tidal mud flats (+1800%) during drier periods under the influence of El Niño events. La Niña events are characterized by wetter periods that led to an increase in the area of "várzea" (+2.9%) and lakes (+426%) over savannah (-9.6%), and the expansion of mangroves (+14.7%) mainly over the inundated field (-2.6%). Thus, the decrease in rainfall index during El Niño may have reduced the inflow of the Calçoene River and favored an increase in tide propagation and transport and deposition of mud along the

tidal-fluvial channel and its secondary channels. The development of mangroves on muddy substrates near the coastline followed during La Niña.

KEYWORDS: coastal Amazonia; remote sensing; sedimentary facies; mangrove; chenier ridges.

Introduction

Sedimentary models commonly propose to subdivide modern tidal flats into supra, inter and subtidal environments based on the flat zonation related to different tidal water levels with singular facies distribution (e.g. Klein, 1977; Reineck and Singh 1980; Weimer *et al.*, 1982; Dalrymple, 1992). These models are very well applied to tidal flats of the North Sea coast of Europe (e.g. Van Straaten, 1961; Evans, 1965; Reineck, 1975), Georgia coast (Howard and Frey, 1975; Basan and Frey, 1978), Gulf of California (Thompson, 1975), Bay of Fundy - Canada (Klein, 1970; Knight and Dalrymple, 1975; Dalrymple *et al.*, 1978) and those associated to tide-dominated estuaries such as the Cobequid and Salmon - Canada (Dalrymple *et al.*, 1990), Ord, South Alligator, Mary and Louisa - Australia (Woodroffe *et al.*, 1989; Chappell and Woodroffe, 1994), Severn - Britain (Harris and Collins, 1985; Allen, 1990), Gironde and Seine - France (Allen, 1991; Lesourd *et al.*, 2003).

Morphostratigraphic studies of the northern Brazilian coast have resulted in alternative models being proposed. Such models consider tidal flat development during the Holocene and reflect the post-glacial sea level rise that invaded the coast, embayed by rather shallow and broad valleys that were subsequently filled with muddy sediments under stable conditions. Modern tidal flats are then the product of the filling process of coastal valleys (Cohen *et al.*, 2005; Souza Filho *et al.*, 2006), and supratidal environments possibly correspond to the topographically highest ancient zones (Souza Filho *et al.*, 2006).

Few studies have been conducted on the most extensive tidal flats of Brazil near the mouth of the Amazon River, on the coast of Amapá (e.g. Silveira, 1998; Santos, 2006). These tidal flats are dominated by a macrotidal regime and are strongly influenced by the Amazon River's discharge (Meade *et al.*, 1985; ANA, 2003). About 20% of the particulate flow reaches the coast in the form of mud flats (Allison *et al.*, 1995) colonized by mangroves near the coastline, and inundated fields in the inner zone of the coastal plain (Guimarães *et al.*, 2010). However, the deposition of muddy sediments may not have been constant during the Holocene, which allowed the development of several chenier ridges (Silveira, 1998). Furthermore, the short-term development of mudflats which involves the activity of waves,

coastal currents, tides, sediment transport and balance, interactions with physico-chemical parameters and climatic event cycles still remain poorly understood.

Regarding climatic event cycles, the decadal variation in the rainfall regime and river inflow produced by El Niño-Southern Oscillation (ENSO) may also influence the morphological and geobotanical setting of costal zones. Effects can include the defoliation and mortality of emergent trees, replacement of trees by herbaceous strata and increased rates of erosion and deposition (e.g. Viles and Goudie, 2003; Holmgren *et al.*, 2001). All of these interrelated processes may act on different time and spatial scales and the lack of accurate geomorphological data makes subsurface interpretations difficult for the coast of Amapá.

Therefore, this study aimed to analyze morphological and geobotanical units as they changed over the short term (~ 30 yr), based on processing and interpretation methods in optical and synthetic aperture radar (SAR) images, historical rain series, and water salinity, maximum spring tide height and sedimentary facies data to understand the main processes acting on tidal flats near the mouth of the Amazon River.

Study Area

Geological and physiographic setting

The study area is located in the Amapá Platform, which corresponds to emerged and submerged continental areas continuously stable during several episodes of distensional tectonics followed by the Gondwana break up and Equatorial Atlantic opening during the Jurassic/early Cretaceous (Szatmari *et al.*, 1987).

The regional geology includes Mesoarchean-Devonian Crystaline and Metassedimentary rocks in the western region, and Pleistocene sandstone and conglomerates in the eastern region interpreted as tidal depositional systems (Souza, 2010). Erosional and depositional processes due to late Pleistocene and Holocene climatic and sea-level changes, jointly with tectonic processes, shaped the relief of the coast of Amapá, resulting in its current configuration (Lima *et al.*, 1991). Indeed, along the coastal plain adjacent to the Amazon River, extensive north-south trending Holocene terraces composed of sand and mud have developed (Figure 1a).

Geomorphological units are represented by Amapá Hills and Coastal Plateau in the hinterland, fluviolacustrine and marine plains (unconsolidated sedimentary deposits) along the coast (Figure 1b). Soil types are derived from geological features of the coast of Amapá and can be classified as Oxisols, Ultisols and Entisols following Soil Taxonomy (USDA, 1999).

Floristic studies of Costa Neto and Silva (2004) and Carvalho *et al.* (2006) described geobotanical and land use units. At the study site, a vegetation survey based on qualitative descriptions was carried out. Modern vegetation is thus characterized by savannah in the hinterland, "várzea" (flooded freshwater forests) in tidal flats, alluvial and lacustrine plains, inundated fields in the upper intertidal flat and well-developed mangrove forests near the coastline (Table 1).

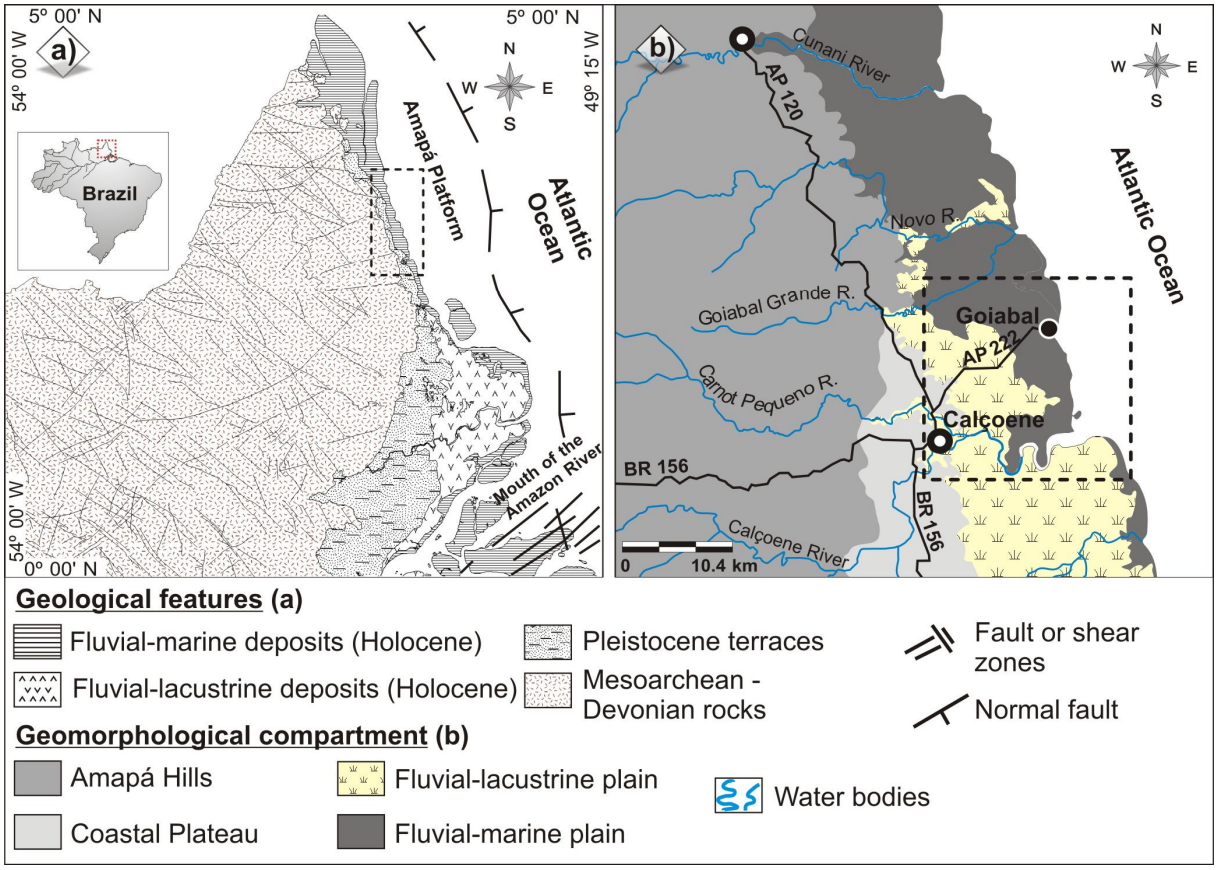

Figure 1. Study area: a) Regional geology (modified from CPRM, 2010 and Costa *et al.*, 2002), b) Regional geomorphology (modified from IBGE, 2008).

Table 1. Main plant species identified at the study site. Geobotanical units: AG/CB: agriculture and cattle breeding; SV: savannah; V: "várzea"; IF: inundated field; MG: Mangrove.

Family and species	**Biological form**	**Geobotanical units**
Aizoaceae		
Sesuvium sp.	Herb	IF
Anarcadiaceae		
Spondias mombin L.	Tree	V
Tapirira guianensis Aubl.	Tree	V
Aquifoliaceae		
Ilex sp.	Tree	V
Araceae		

Montrichardia arborescens L.	Herb	V
Pistia stratioites L.	Herb	V, IF
Arecaceae		
Euterpe oleracea Mart.	Tree	V
Mauritia flexuosa L.f.	Tree	V
Avicenniaceae		
Avicennia germinans L.	Tree	MG
Cabombaceae		
Cabomba aquatica DC.	Herb	V, IF
Ceratopteridaceae		
Acrostichum sp	Herb	MG
Cobretaceae		
Laguncularia racemosa Gaertn.	Tree	MG
Cyperaceae		
Cyperus giganteus Vahl.	Herb	IF
Cyperus luzulae (L.) Retz.	Herb	IF
Eleocharis emarginata Ness	Herb	IF
Eleocharis mutata L.	Herb	IF
Fimbristylis annua All.	Herb	IF
Rhynchospora barbata Vahl	Herb	SV
Scleria sp.	Herb	IF
Euphorbiaceae		
Alchornea sp.	Tree	V
Hevea guianensis Aubl.	Tree	V
Hura crepitans L.	Tree	V
Manihot esculenta Crantz.	Shrub	AG/CB
Fabaceae		
Campsiandra laurifolia Benth.	Tree	V
Chamaecrista sp.	Herb	SV
Machaerium lunatum SP.	Tree	V
Macrolobium sp.	Tree	V
Parkia nitida Miq.	Tree	V
Pentaclethra sp.	Tree	V
Vatairea guianensis Aubl.	Tree	V
Helioconiaceae		
Heliconia sp.	Herb	IF
Malpighiaceae		
Byrsonima crassifolia L.	Tree	AG/CB, SV
Byrsonima verbascifolia L.	Tree	AG/CB, SV
Mascagnia sp.	Climber	FV
Malvaceae		
Pachira aquatica Aubl.	Tree	V
Pseudobombax sp.	Tree	V
Nymphaeceae		
Nymphaea sp.	Herb	V, IF
Poaceae		
Hymenachne amplexicaule Nees	Herb	SV, IF
Olyra latifolia L.	Herb	V, IF
Paspalum sp.	Herb	SV
Panicum laxum Sw.	Herb	IF

Paspalum repens Berg.	Herb	IF
Zea sp.	Herb	AG/CB
Ponteridaceae		
Eichhornia azurea (Sw.) Kunth	Herb	IF
Eichhornia crassipes Mart.	Herb	IF
Rubiaceae	Herb	
Alibertia sp.	Tree	FV
Borreria sp.	Herb	SV, AG/CB
Psychotria	Herb	IF
Sapotaceae		
Pouteria sp.	Tree	V
Rhizophoraceae		
Rhizophora harrisonii Leechman	Tree	MG
Rhizophora mangle L.	Tree	MG
Rhizophora racemosa G. Mey.	Tree	MG

Climate and hydrology

The regional climate is humid tropical characterized by well-defined dry (September to December) and wet (January to July) seasons, with annual average precipitation and temperature around 3,000 mm and 27.5ºC, respectively (Bezerra *et al.*, 1990). The mean discharge of the Amazon River is approximately 170,000 m^3/s (at the town of Óbidos), with maximum and minimum outflow of 270,000 and 60,000 m^3/s (ANA, 2003). This discharge contributes ~1.2 x 10^9 tons/yr of sediment (Meade *et al.*, 1985). The Amazon's estuary is classified as semidiurnal macrotidal (Pugh, 1987), with a tidal range of ~6 m (Gallo and Vinzon, 2005). The plume of the Amazon River is a seasonal feature extending ~3,000 km into the Atlantic Ocean, and covers approximately 2 x 10^6 km^2 (Cooley *et al.*, 2007). The structure of the plume is controlled by the North Brazilian Current, which induces a northwestern flow with speeds of 40 - 80 cm/s over the continental shelf (Lentz, 1995), strong tidal currents (Beardsley *et al.*, 1995), trade winds and the Intertropical Convergence Zone - ITCZ (Lentz and Limeburner, 1995). Consequently, river discharge and hydrodynamic conditions allow a strong reduction of water salinity along the Amazon River and adjacent coast (Rosario *et al.*, 2009).

Materials and Methods

Remote sensing data and image processing

The mapping, temporal and spatial analyses of morphological and geobotanical units were carried out by processing and interpretation methods in optical and SAR images, jointly with field surveys related to geomorphology and sedimentology. A set of six Landsat/TM images from 1987, 1997 and 2008 (225_58 and 225_68), one SAR/SRTM V2 image from 2000 and

two SLAR/GEMS 1000 images from 1971 corresponding to the NA22VD and NA22XC sheets of the RADAM project (DNPM, 1971) were used for the remote sensing analysis (Table 2).

The Landsat/TM images, obtained from the National Institute for Space Research - Brazil (INPE), were processed using the Spring 4.3 software (Câmara *et al.*, 1996) and geometrically corrected using another, previously corrected ETM+ image. The mean squared error was less than one and data resampling followed the nearest neighbor method. Radiometric correction was based on the minimum histogram pixel approach (Chaves, 1988). Image enhancements were applied based on linear and equalization stretches. Three bands for a red-green-blue (RGB) color composite (TM 4-5-6) were selected based on the optimum index factor scheme (Chavez *et al.*, 1982), and chosen for visual interpretation. These data were subsequently exported in shapefile vector format for spatial analysis in the ArcMap 9.2 (ESRI, 2006) software. Validation was conducted with 50 ground control points obtained from a GPSMAP 60CSx GPS receiver, throughout the study site.

The SRTM data (C band, $\lambda = 5.6$ cm) were acquired from the National Aeronautics and Space Administration (NASA), the National Imagery and Mapping Agency (NIMA), the German Space Agency (DLR) and the Italian Space Agency (ASI). The wavelength of the C band interacts with canopy trees, resulting in elevations which reflect the combination of morphology and tree height (e.g. Hofton *et al.*, 2006). Data were processed to improve their potential usefulness for geomorphological descriptions, including the customization of shading schemes and palettes using Global Mapper 8 (Global Mapper LLC, 2009). Development of such palettes was achieved through an interactive approach using display tools, which allowed highlighting the morphological features of interest for this research according to on-screen observations (e.g. Hayakawa *et al.*, 2010). Morphometric analysis based on topographic profiles was applied to enhance the potential of feature visualization.

SLAR/GEMS1000 data were purchased from the twin-jet Caravelle flying at an altitude of 12 km with approximate speeds of 690 km/h. The on board side-looking Goodyear Mapping System 1000 (GEMS) radar was operating in the X band ($\lambda = 3$ cm and frequency between 8 and 12.5 GHz). The flight was conducted along N-S lines with spacing of 27.5 km between lines. The altitude was controlled by Stewart-Warner radar altimeter (precision of 50 m). Aircraft positioning was obtained by Litton Inertial Navigator Platform supported by Transit tracking (precision of 15 m) and Shoran ground stations (400 km ranges) related to geodesic data of “Córrego Alegre” (DNPM, 1971). The NA22VD and NA22XC sheets were

scanned at high resolution and stored in digital matrix format, which allowed data enhancements by the application of a gamma filter and the interpretation of ground features.

Table 2. Main characteristics of the remotely sensed data.

Platform	**Sensor**	**Acquisition date**	**Angle of incidence**	**Spatial resolution (m)**	**Tidal condition**
Twin-jet	GEMS 1000	1972 20/09/1987	45-77º	16	-
Landsat-5	TM	15/09/1997 28/08/2008	Nadir	30	Low
SRTM	InSAR	Fev. 2000	*off*-nadir	90	-

Sampling and facies description

Fieldwork was conducted during May 2009 (rainy season) and December 2010 (drier season) to validate the remote sensing data and indentify the main sedimentary processes acting at the study site. Hydrotopographic and water salinity measurements (e.g. Cohen, 2003), were carried out at 30 stations distributed along Goiabal road (AP 222) and that intercept the main morphological and geobotanical units. These measurements use graduated rulers, where acrylic cylinders fixed at 10 cm intervals recorded the maximum height of spring tide in 2009 (DHN, 2009). The salinity of tidal water was measured with portable instruments in situ, without filtration. Monthly rainfall data between January 1987 and December 2008 were acquired from HidroWeb (ANA, 2010). Distinct seasonal patterns were identified based on these data, including a rainy season from January to June and drier season from June to November. The mean seasonal rainfall (monthly average during the rainy and drier seasons) and annual rainfall (sum of seasonal means) were compared to positive (El Niño) and negative (La Niña) anomalies from the Oceanic Niño Index between 1986 and 2008 (CPC/NOAA, 2010), to recognize the influence of ENSO events in the rainfall regime, morphological and geobotanical settings of the studied coast.

Sedimentary records consist of surface features, exposed terraces, trenches and cores (using a Russian Sampler). Following the proposal of Walker (1992), facies analysis included descriptions of color, lithology, texture and structures. X-ray radiographs aided the identification of sedimentary structures. The interpretation of the sedimentological data in this work is also based on clastic tidalite process-response models (after Klein, 1971). The sedimentary facies was codified following Miall (1978).

Results and Discussion

Geomorphological setting

Coastal plateau

This compartment is bordered to the west by crystalline basement rocks related to the Amapá Hills, and to the east by the coastal plain. It has an elevation of approximately 10 m (Figure 2) and presents a flat to slightly undulated surface shaped by erosive processes. Significant protuberance of an ancient shoreline in the form of a delta was identified at the study area. The feature covers an area of ~ 100 km^2 and likely preserves the main fluvial channel with SW-NE direction ("Goiabal Grande" River) that displays confined flow over the coastal plain. Additionally, another fluvial channel with NW-SE orientation was delineated, but river flow is interrupted near inundated fields of the Goiabal site (Figure 3).

An elongated feature of birdfoot type, likely correlated to six paleodeltaic lobes, and avulsion of the main fluvial channel from the deltaic system were also observed in this compartment. The lack of roads prevented a detailed stratigraphic study to demonstrate the presence of such a depositional system.

The avulsion process may also have been responsible for the partial or complete abandonment of several channels, which allowed the development of elongated lakes with SW-NE and SE-NW direction. These lakes represent parts of or complete channels, abandoned or filled due to rapid sedimentation rates, depth reduction and/or tectonic uplift (e.g. Rossetti *et al.*, 2010).

The base of the coastal plain may partially correspond to these deposits, and contact between the coastal plateau and plain is marked by abrupt lithological (sand and mud) and vegetation (savannah/"várzea" and inundated field) changes (Figure 4c and 4d). Paleochannels are common in this transitional sector, which consists of a thick peat layer (facies Pt), laminated mud, kaolinitic in nature (facies Ml), and cross-laminated sand (facies Sc) (Figure 4e; Table 3).

The predominant vegetation units are "várzea" with a total area of 190.9 km^2, and savannah with total area of 103.2 km2. The "várzea" also colonizes transitional sectors between the coastal plateau and plain.

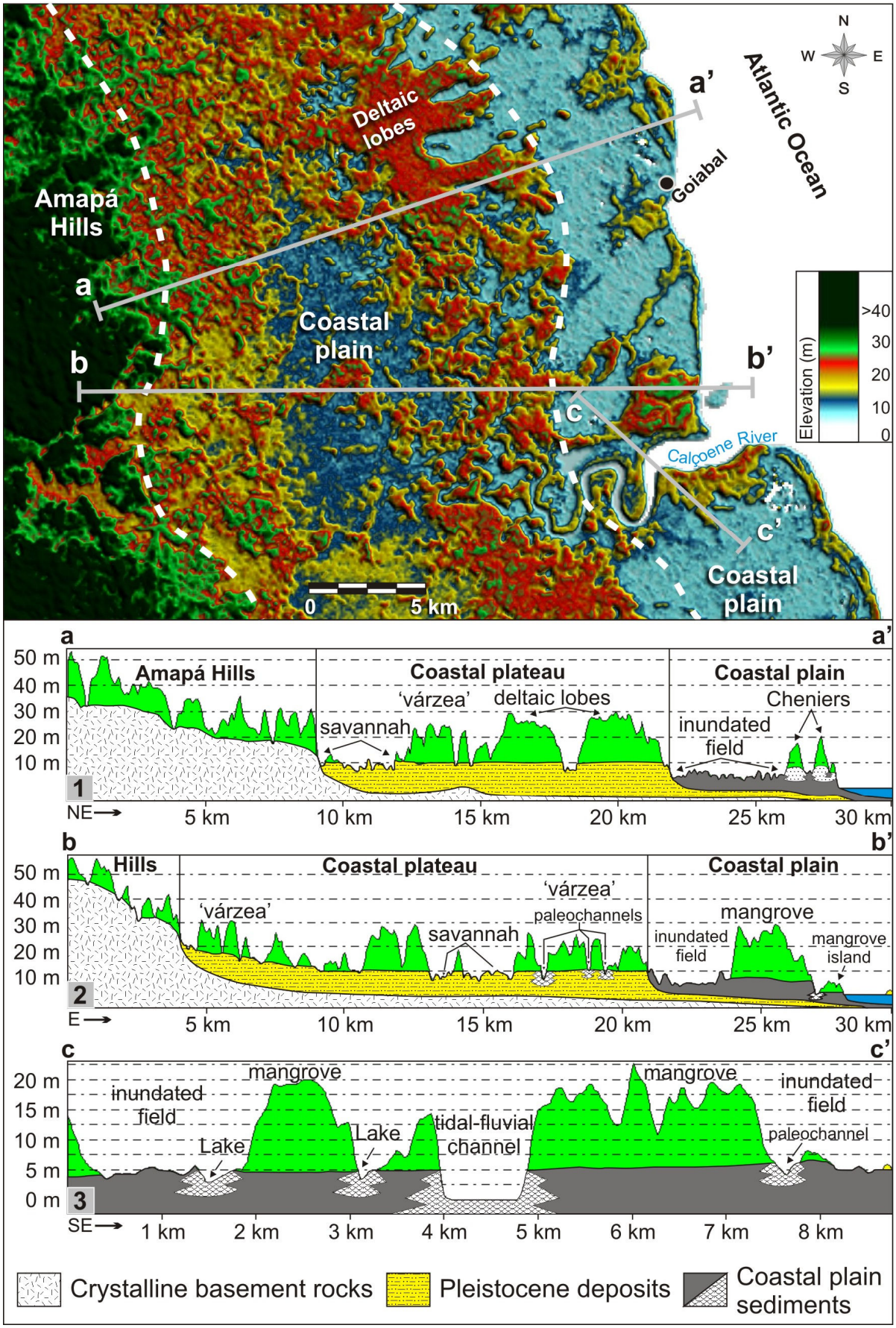

Figure 2. Digital elevation model of the Amapá Coast based on SRTM data with morphometric profiles along the morphological and geobotanical units.

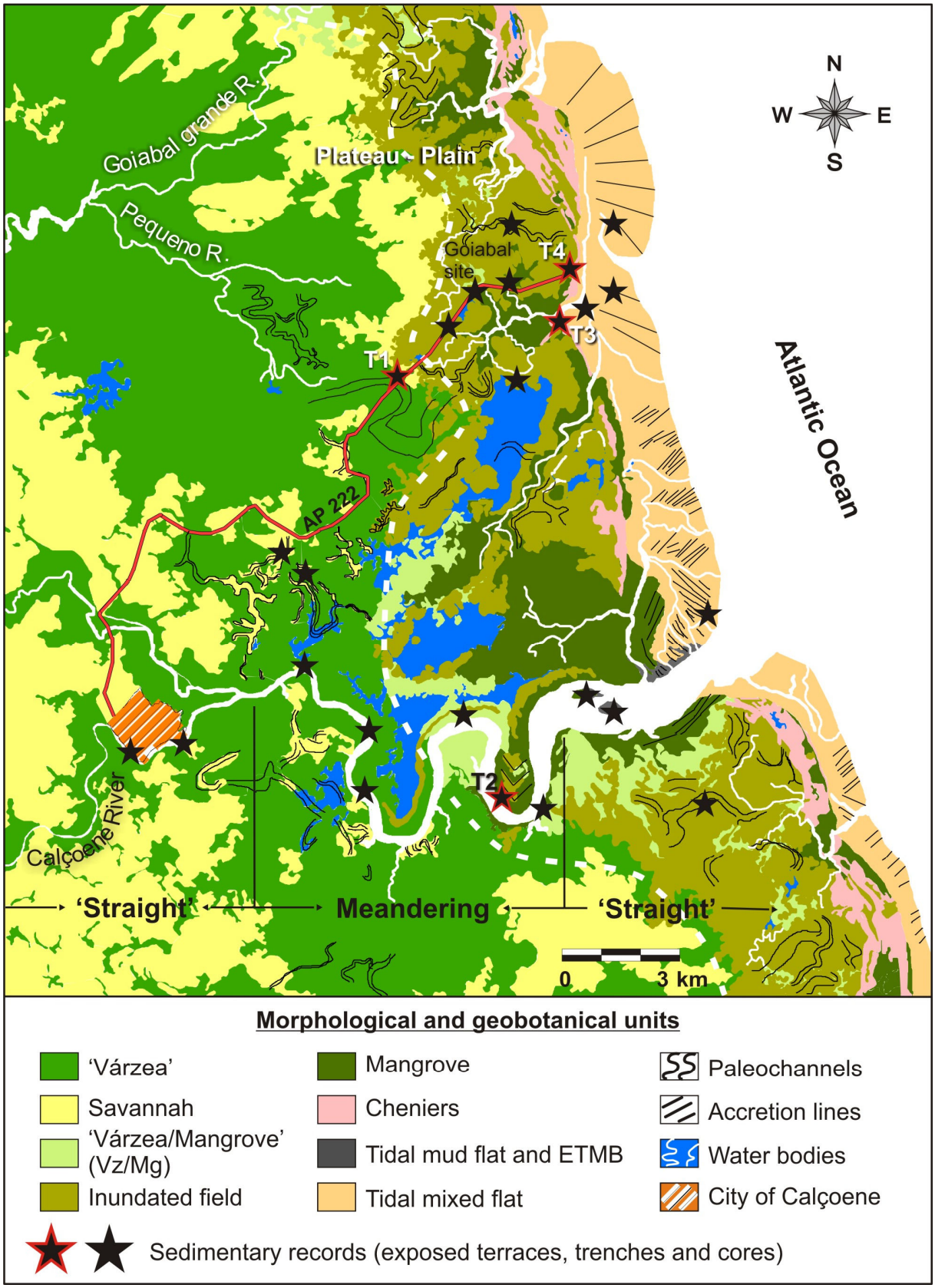

Figure 3. Geomorphological map of the Calçoene Coast with the location of sedimentary records consisting of exposed terraces, trenches and cores. Stars with a red outline correspond to the following lithological columns and figures described in the text: T1, Figure 4e; T2, Figure 5d; T3, Figure 7d; T4, Figure 7f.

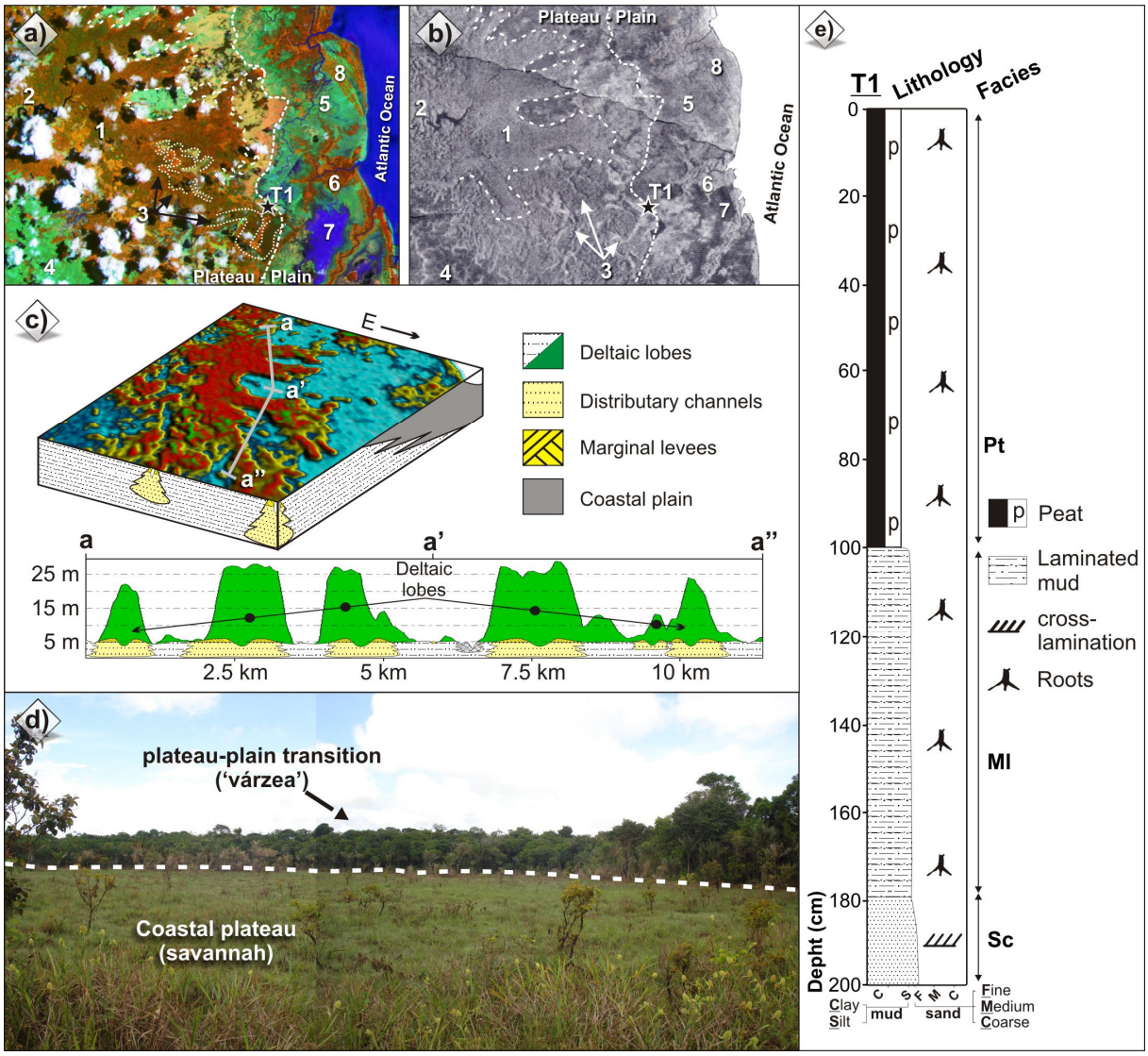

Figure 4. Features of the coastal plateau and plain: a) Landsat and b) GEMS 1000 images, 1: deltaic lobes, 2: fluvial channel avulsion corresponding to the Goiabal Grande River, 3: paleochannels, 4: savannah, 5: inundated field, 6: mangrove, 7: lakes, 8: chenier ridges; b) Digital elevation model based on SRTM data and cross-sectional profiles of deltaic lobes; d) the coastal plateau and plain transition; e) Graphic sedimentary log of a paleochannels near the coastal plateau and plain transition.

Table 3. Summary of facies descriptions and sedimentary processes at the study site.

Facies	Description	Process
Peat (Pt)	Very dark gray organic deposit with decomposed and intact vegetable fibers.	Deposition and accumulation of vegetable debris indicating autochthonous source and reducing condition.

Bioturbated mud (Mb)	Greenish gray mud with many roots, root marks and vegetable debris. Herbaceous roots and root marks can also be locally observed.	Intense mixture of fine sediments by bioturbation.
Laminated mud (Ml)	Very light gray and greenish gray mud with plane-parallel lamination.	Alternation of flocculated and non flocculated laminae deposited from suspension, and variations in the organic colloid content. Lighter tones may correspond to the presence of kaulinite.
Lenticular bedding (Hl)	Gray and greenish gray mud with single and connected flat lenses of fine to very fine sand.	Low energy flows with mud deposition from suspension, but with periodic sand inflows through migration of isolated ripples.
Wavy bedding (Hw)	Greenish gray, wavy mud laminae in alternation with ripple-bedded fine sand layers.	Equal periods of mud and sand deposition from suspension and bed-load transport, respectively.
Flaser bedding (Hf)	Light gray fine sand with dark gray, thin laminae of mud on bottomset.	Predominance of sand deposition from traction currents and mud during slack water periods.
Inclined mud (Mi)	Inclined laminae of dark gray mud bounded by thin films of organic matter.	Lateral accretion with predominance of mud deposition from suspension.
Inclined heterolithic (Hi)	Parallel inclined thin laminae of fine sand and gray mud with dip of ~15º. Granules can be locally observed.	Lateral accretion with sand and mud deposited during low energy flows of a small-scale point bar.
Massive mud (Mm)	Greenish gray mud and locally subangular quartz granules.	The massive nature indicates channel waters with high suspended load. Considering the gravel class occurrence, granules are left behind, while mud moved as suspension clouds.

Cross-laminated sand (Sc)	Olive gray, well sorted, fine to very fine sand with ripple cross-lamination.	Migration of small ripples during low energy flows.
Bioturbated sand (Sb)	Pale olive fine sand with reddish and yellowish mottles, many herbaceous roots in growth position.	Sediment homogenization and mottling by biological activity and diagenic process, respectively.
Planar sand (Sp)	Alternation of dark gray (heavy minerals) and brown (light minerals) fine to very fine sand with plane-parallel lamination or low-angle cross-lamination.	Deposition of sand by *swash* and *backwash* on gently sloping surface.

Coastal plain

Tidal sedimentary facies predominate in this compartment that is approximately 10 km long and contains a tidal-fluvial channel, paleochannels, lakes, "várzea", inundated fields, mangroves, elongated tidal mud bars (ETMB), chenier ridges, tidal mud and mixed (non-vegetated) flats (Figures 2 and 3). The main plant species are described in Table 1.

Tidal-fluvial channel

This channel is represented by the Calçoene River that shows a "straight" to meandering pattern, and water flow on basement crystalline rocks in its proximal portion, contrasting with high sinuosity and a funnel shape in the distal portion (Figures 3, 5a and 5b). River discharge increases down the fluvial system as a result of the addition of precipitation and runoff from tributary drainage basins, producing a "straight" channel pattern. However, the river channel becomes more sinuous as one moves from steeper inland areas toward low-gradient coastal areas, with the occurrence of the tightest meander bends at the location of bedload convergence at the location with lowest hydraulic energy. This high sinuosity setting was also allowed by the cohesive nature of muddy sediments and vegetation development along channel margins (e.g. Miall, 1992). In the fluvial-marine transition, the tidal prism exerts the strongest control on the magnitude of water flux, and it tends to increase seaward as a result of the progressive enlargement in the area to be flooded and drained on each tide. Consequently, all tidal channels present a "straight" style and seaward increase in cross-sectional area, namely funnel-shaped geometry (Dalymple and Choi, 2007).

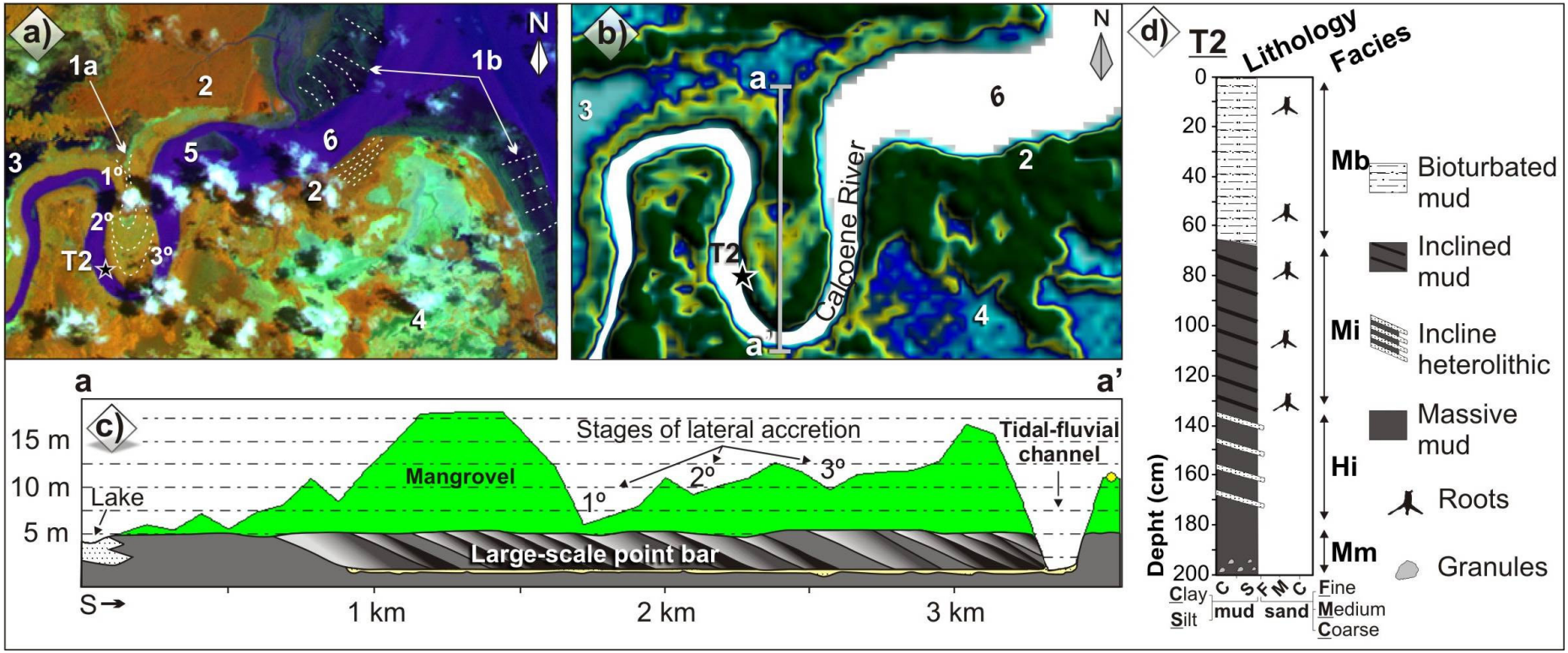

Figure 5. Distal portion of the tidal-fluvial channel with meandering and "straight" segments: a) landsat and b) GEMS 1000 images, 1a: lateral accretion lines, 1b: longitudinal accretion lines, 2: mangrove, 3: lakes, 4: inundated field, 5: elongated tidal mud bars - ETMB, 6: funnel-shaped morphology; b) digital elevation model based on SRTM data, 2: mangrove, 3: lakes, 6: funnel-shaped morphology and cross-sectional profile of the large-scale point bar, showing associated lakes with paleochannels, mangrove, stages of lateral accretion and tidal-fluvial channel; d) Graphic sedimentary log of convex margin.

This "straight"-meandering-"straight" channel pattern is typical within tide-dominated estuaries (Dalrymple *et al.*, 1992), when only channel patterns are considered. However, estuaries are restricted to incised-valley systems and abandoned portions of delta plains that are undergoing transgression (Dalrymple, 2006). Furthermore, the study area is located on the Amapá Platform, which remained stable during several episodes of distensional tectonics, followed by the Gondwana break up and Equatorial Atlantic opening during the Jurassic/early Cretaceous (e.g. Szatmari *et al.*, 1987). Despite the scarcity of local geophysical studies looking at small subsiding basins and the presence of several outcrops of crystalline basement rocks along the Calçoene River (e.g. in the fluvial-marine transition), we considered it most suitable to suggest a tide-dominated river considering the geological data available in the scientific literature.

The reversal flow of the Calçoene River by tidal flood currents may be effective up to ~ 20 km upstream from the mouth, during the drier season. Water salinity is low, with maximum values of 5‰ near the mouth. There are only a few secondary channels along this river which remain active, and they represent a short extension. Large and small-scale point-bars and cut banks are frequent in the convex and concave margins of the river channel, respectively (Figure 5c). The small-scale point-bar deposits display inclined heterolithic lamination (facies Hi) with local residual granules, inclined (facies Mi) and bioturbated mud (facies Mb) (Figure 5d; Table 3).

Paleochannels and lakes

An extensive paleochannel network was indentified in the coastal plain. The paleochannels maintain the shape and typical concavity of the original channel, resulting in the formation of lakes and lake belts (Figures 6a, 6b and 6c). The lakes show SW-NE orientation, elevation between 1 and 3 m, around 1 m in depth, water salinity of ~ 0‰ and ephemeral behavior due to the seasonality of climate and hydrology. The deposits consist of thick peat layers (facies Pt), laminated mud (facies Ml) and bioturbated mud (facies Mb).

"Várzea"

"Várzea" is located on narrow tidal flats in the proximal portion of the tide-dominated river, and it has an elevation of approximately 4 m and maximum water salinity ~ 2‰. Additionally, several elements of this unit may be recognized surrounding paleochannels and lakes of the coastal plain (Table 1). The deposits present lenticular bedding (facies Hl) and bioturbated mud (facies Mb).

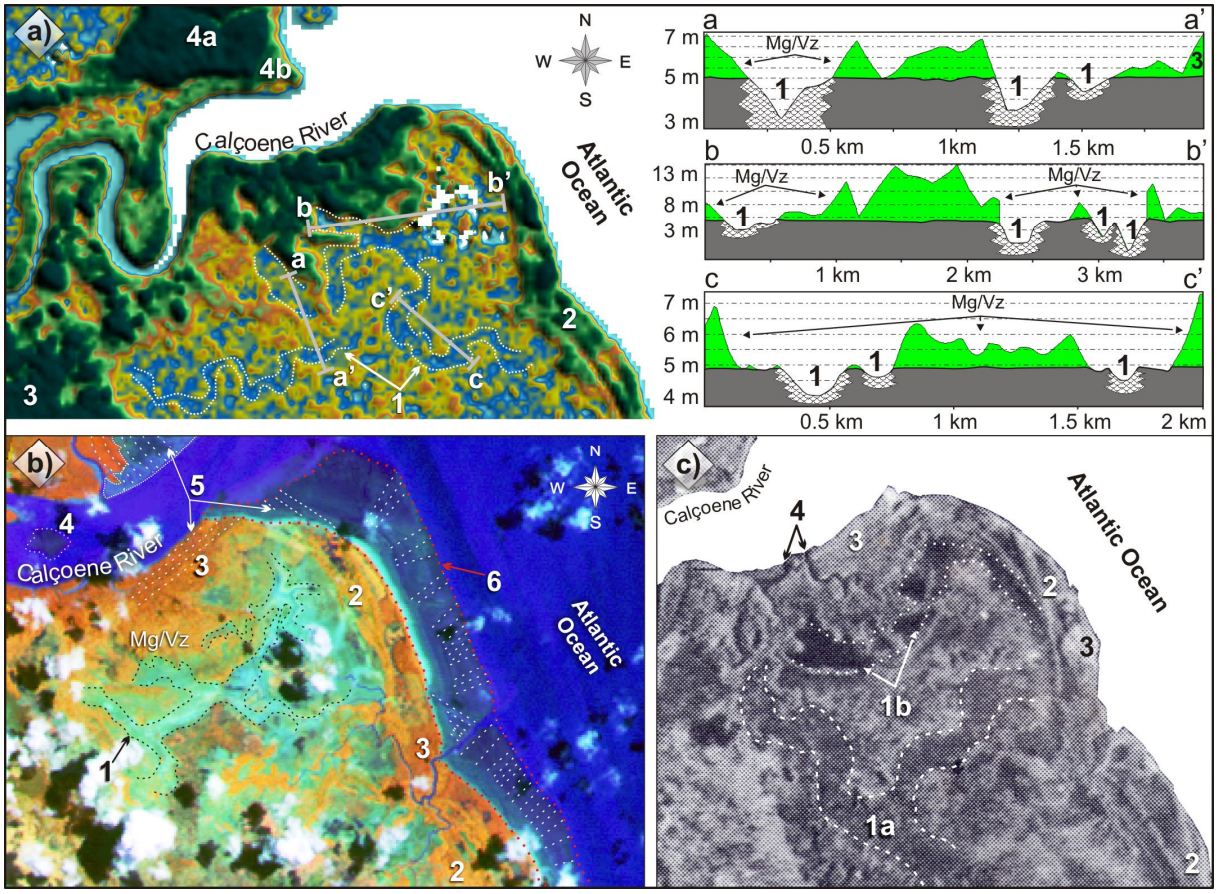

Figure 6. Digital elevation model based on SRTM data showing paleochannels (1) of the coastal plain and adjacent units such as chenier ridges (2), "várzea" (3), mangrove (4), accretion lines (5) and morphometric profiles of paleochannels.

Inundated field

The inundated field covers an area of 67.4 km^2, with predominantly herbaceous vegetation (Table 1). It is only flooded by a water column of 10 cm during overbank flow at high spring tides in the rainy season, and is characterized by an elevation between approximately 2 and 4 m and low drainage density due to the silting of the tidal channels. Tidal channels have maximum width and depth of 4 and 2 m, respectively, and water salinity ~2‰. Several paleochannels were identified in this unit (Figure 7a). Fallen blocks can be observed in the concave margin of the tidal channels indicating the development of listric faults and subsequent washout of the muddy terrace by tidal currents. The deposits consist of bioturbated mud (facies Mb) with the predominance of herbaceous roots and root channels. Well-developed mud cracks are frequent during the drier season.

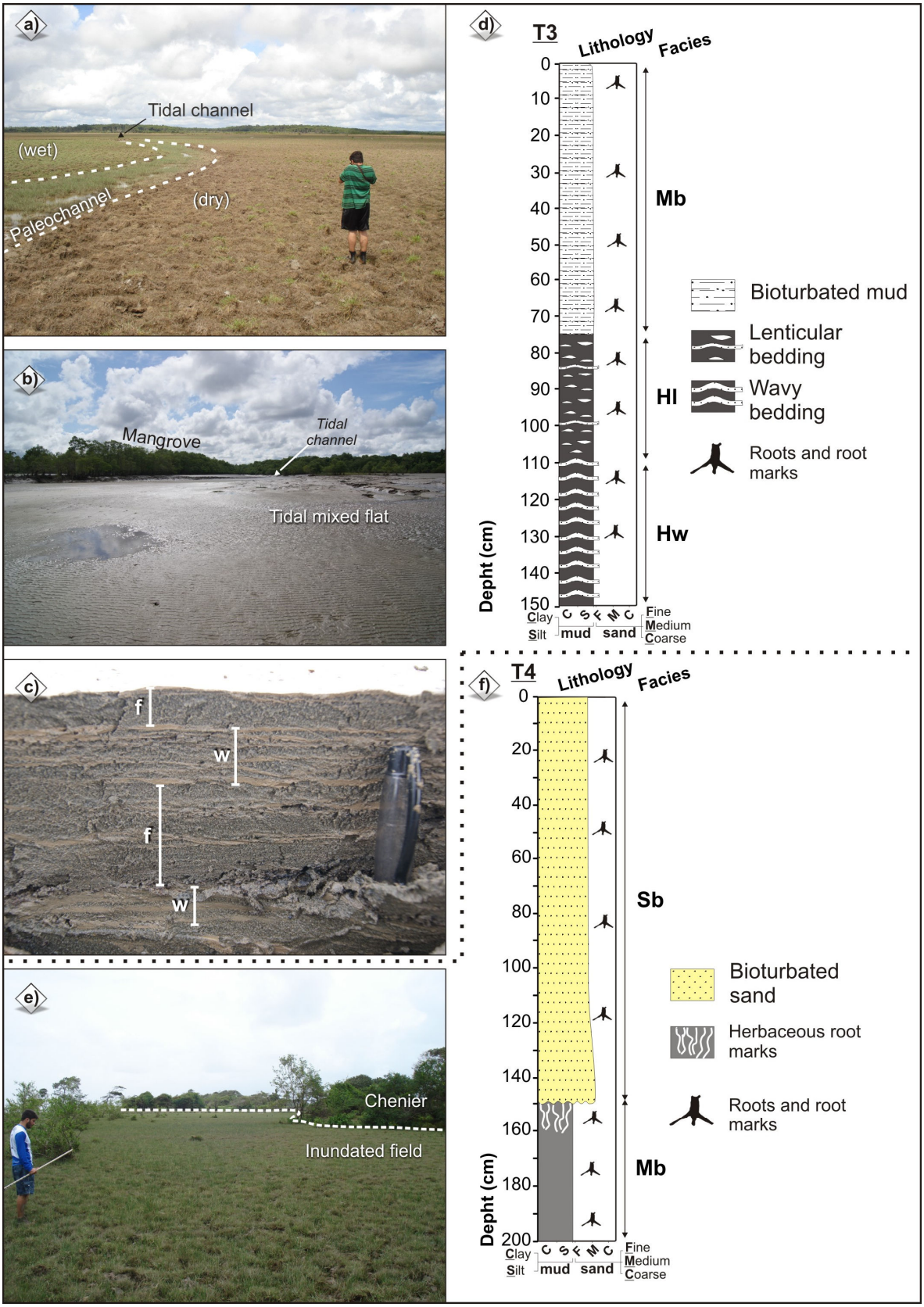

Figure 7. a) Inundated field with dry and wet sectors due to the abandonment of a tidal channel, b) surface relationship between mangrove, tidal mixed flat and tidal channel in advanced stages of silting, c) detail of typical facies of tidal flats, d) Graphic sedimentary log of vegetated tidal flats, e) and f) surface and vertical relationship of chenier and inundated field.

Considering that the accommodation space may be very small (see discussion in subsection *Tidal-fluvial channel)*, we suggest that the formation of this extensive inundated field was supported by high rates of vertical accretion with large concentration of muddy sediments continuously supplied by the Amazon River, which limited tidal flat drainage by the silting of tidal channels. This process may be responsible for herbaceous strata expansion over the tidal flat, since herbs are more adapted to hydric stress than arboreal vegetation (e.g. Long, 1999).

Other studies focused in the coexistence of arboreal and herbaceous strata in the Amazonia also indicate a dynamic history of channel abandonment, which controlled a set of interrelated parameters (soil type, topography and hydrology) that determined species location (e.g. Rossetti *et al.*, 2010; Horbe *et al.*, 2011). In the Marajó Island, as the channels became progressively abandoned and filled with sandy sediments, the sand bodies acted as freshwater reservoirs, and also stood slightly higher in the landscape due the positive topography of marginal levees, eventually remaining above water level even during rainy seasons, configuring substrates favourable for tree growth (Rossetti *et al.*, 2010). However, the tidal flat of the study site are mud-rich in nature and it did not present marginal levees. Thus, we propose that the restriction of the drainage system by the silting of the tidal channels with muddy sediments prevented the formation of water reservoirs and it favored the development of stressful conditions to colonization of arboreal strata such as mangrove and "várzea".

Mangroves

Mangroves cover an area of 36.7 km^2 and are restricted to the coastline, colonizing tidal flats of the distal portion of the tide-dominated river and wider tidal channels of the coastal plain (Figure 7b). However, this unit shows limited lateral continuity likely due to the silting and rapid narrowing of the channels, which limit tidal flat drainage. Mangroves have an elevation similar to that of the inundated field and their upper intertidal portion is flooded by a water column of ~ 20 cm (water salinity between 2 and 4‰) during high spring tides in the rainy season. The sediment is composed of wavy (facies Hw) and lenticular bedding (facies Hl), and bioturbated mud (facies Mb) with abundant plant debris (Figures 7c and 7d; Table 3).

Elongated tidal mud bars (ETMB)

ETMB were identified near the mouth of the Calçoene River, consisting of muddy bodies with E-W orientation and 600 to 800 m in length. The advanced stage of mud bar stabilization

is recognized by mangrove development (Figures 3 and 5a). The sediments consist of lenticular bedding (facies Hl) and bioturbated mud (facies Mb) (Table 3).

Chenier ridges

Chenier ridges cover an area of 10.1 km^2 at the study site, and represent extensive, straight to slightly curved sand bodies overlaid on mangrove and inundated field deposits, indicating an interruption of mud flat progradation (e.g. Augustinus, 1989). This feature has N-S and NW-SE orientation, elevation of about 4 m, measures 2 to 4 km in length with interridge spacing between 20 and 200 m and inner chenier ridges ~ 2 km from the modern coastline (Figures 6 and 7e). Additionally, some ridges occur at an angle of 25º to 30º to the normal orientation of the coastline. The deposits show bioturbated sand (facies Sb, Figure 7f). The intense bioturbation and mottling features prevented the identification of synsedimentary structures, possibly related to large-scale cross-bedding, as described by Augustinus (1989) and Augustinus *et al.* (1989) in others chenier ridges in the northern coast of South America.

Tidal mud flats

Tidal mud flats (non-vegetated) were only observed near the mouth of the Calçoene River, where the substrate was not yet stabilized by pioneer mangrove and/or "várzea" vegetation. They comprise a small area of 0.7 km^2. The sediments are represented by laminated mud (facies Ml) and lenticular bedding (facies Hl).

Tidal mixed flats

Tidal mixed flats (non-vegetated) encompass an area of 37.1 km^2, with SE-NW orientation and a relatively flat surface 0.5 to 2.5 km wide near the mouth of the Calçoene River. Longitudinal accretion lines were also observed. On this feature, plane beds with parting lineation produced by wave activity (Figures 8a and 8b), ripples with multidirectional (Figure 8c) and continuous crests (Figure 8d), isolated ripples, mud clasts related to reworking of the flat during tidal channel dynamics (Figure 8e), obstacle and moving tool marks, and beyond rill marks with braided style (Figure 8f) are commonly identified. Tidal channels and mangroves undergoing silting and burial processes, respectively, can also be recognized (Figures 8g and 8h). Mixed flat deposits are represented by planar to quasi-planar fine to very fine sand (facies Sp), flaser, wavy and lenticular bedding (facies Hf, Hw and Hl, respectively; Table 3).

Figure 8: Tidal mixed flat with plane beds produced by swash and backwash, b) subsurface detail of fine sands with plane and low-angle cross-lamination, and parting lineation; dashed arrows are heavy minerals and straight arrow are light minerals, c) ripple marks with multidirectional crests, d) straight crests, e) mud clasts, f) isolated ripples and rill marks with braided style, arrows showing small-scale bars, g) mangrove and tidal channel undergoing burial and silting process, respectively and, h) detail of trench revealing the upper part of the sedimentary deposit of tidal channel abandonment and filling with associated mangrove.

The sedimentary structures of tidal mixed flats are typically found in wave-dominated environments, while the predominance of tidal sedimentary facies is restricted to sites near tidal channels.

The definition of a beach environment generally includes sandy deposits located between the mean low tides and dune fields or sea cliffs, which are entirely conditioned by a wave regime (e.g. Komar, 1976; Davis Jr, 1978, Hoefel, 1998). According to the analysis of laterally adjacent environments such as mangroves, the inundated field, chenier ridges and tidal mud flats, and considering their migration and superposition through time based on Walther's law, we cannot report the presence of a beach environment at the study site (e.g. Reinson, 1992).

Short-term changes in morphological and geobotanical units

The main changes in the coastal plain occurred in "várzea" and savannah areas with a complex network of meandering paleochannels. The "várzea" covered an area of approximately 185 km^2 between 1987 and 1997, which had increased by 5.3 km^2 in 2008. Savannah areas showed a slight net increase of 1.6 km^2 between 1987 and 1997. This increase is likely related to the abandonment of small tidal channels along the Calçoene River. However, savannah lost an area of 10.9 km^2 between 1997 and 2008 (Table 4), concomitant to the development of lakes on existing paleochannels, previously occupied by savannah. The progressive growth of the town of Calçoene apparently did not influence in this process, since "várzea" expanded over savannah after 1997 (Figures 9a, 9b and 9c). Furthermore, the irregular and multiple shapes of savannah areas, with meandering features are not consistent with anthropic intervention (e.g. Soares Filho *et al.*, 2006). In this sector, the tidal-fluvial channel shows high lateral migration, typical of low-gradient rivers with elevated suspension load (e.g. Leopold and Wolman, 1957; Allen, 1965; Schumm, 1977). The maximum rates of erosion and lateral accretion are ~ 9 m/yr (Figure 9d).

Inundated fields predominate in the coastal plain, but suffered a reduction in area of 2.6 km^2 between 1987 and 1997, and 1.8 km^2 between 1997 and 2008 (Table 4). Flooded forests with "várzea" and mangrove species (Vz/Mg) were relatively stable during 1987-1997 interval, but they presented a net loss area of about 3.8 km^2 between 1997 and 2008. Mangroves, on the other hand, expanded over the inundated field in the northern sectors of the Calçoene River, with migration rates near 21 m/yr (Figures 10a, 10b and 10c). Additionally, mangrove expansion over mixed flats near the mouth of the Calçoene River occurred at rates of 20 to 110 m/yr between 1987 and 1997, and 30 to 130 m/yr between 1997 to 2008 (Figure

10d). ETMB and tidal mud flats were also substrates for the development of mangroves between 1997 and 2008 (Figure 10d). However, mangrove erosion at a rate of approximately 14 m/yr between 1987 and 2008, and its replacement by an inundated field can be observed in the southern sectors of the mouth of the Calçoene River (Figures 10d and 10e).

The expansion and accretion profiles may be related to the formation of secondary channels and muddy substrates suitable for colonization by pioneer species of mangrove, and the contractive and erosion profiles to abandonment and silting of tidal channels and tidal-fluvial channel migration, followed by the development of extensive cut banks.

Chenier ridges are characterized by a generally erosive trend with a reduction in area of 0.2 km^2 between 1987 and 1997, and 0.6 km^2 between 1997 and 2008, mainly in the northern and southern limits of the study site (Figures 10b and 10e). This unit displays ancient coastlines and the interruption of mud flat progradation (e.g. Silveira, 1998). During the time interval analyzed, both chenier ridge erosion and formation were recognized. Some existing chenier ridges were reworked by wave action and some ridges were formed and isolated by mud flat accretion. Such processes were also observed in the Guiana and Suriname coasts, where the northwestern migration of shoreface-attached mud banks and interbanks allowed the evolution of accretion and erosive profiles, respectively (Prost, 1989; Augustinus *et al.*, 1989).

The shoreface-attached mud banks undergo migration over decadal time frames, related to the supply of sediment from the Amazon River and wind patterns and intensity, which affect the wave regime on the coast of Amapá. The littoral is thus easily eroded when mud banks migrate (e.g. Allison *et al.*, 2000; Augustinus, 2004). However, Silveira (1998) suggested that sedimentation and erosive processes operated at larger temporal and spatial scales on chenier ridges developed approximately 5,000 and 3,000 cal yr BP between the Cunani and Cassiporé Rivers, north of the Calçoene River. Therefore, morphostratigraphic studies are required to better understand the process of chenier ridges formation in the coast of Amapá.

Geobotanical and morphological units	1987		1997		2008		Changes between 1987 e 1997		Changes between 1997 e 2008	
	km^2	%	km^2	%	km^2	%	km^2	%	km^2	%
"Várzea"	185.2	39	185.5	39	190.9	40	+0.3	+0.2	+5.3	+2.9
Savannah	112.5	24	114.1	24	103.2	21	+1.6	+1.4	-10.9	-9.6
Inundated field	71.8	15	69.2	15	67.4	14	-2.6	-3.6	-1.8	-2.6
Tidal mixed flat	31.2	6.6	35.7	7.5	37.1	7.7	+4.6	+14.4	+1.4	+3.9
Mangrove	31.3	6.6	32.0	6.7	36.7	7.6	+0.7	+2.2	+4.7	+14.7
Flooded forests with mangrove and "várzea" species (Vz/Mg)	21.5	3.7	21.7	4.5	17.9	4.6	+0.2	+0.9	-3.8	-17.5
Chenier	10.9	2.3	10.7	2.2	10.1	2.1	-0.2	-1.8	-0.6	-5.6
Lakes	3.1	0.7	3.1	0.6	16.3	3.4	0.0	0.0	+13.2	+426
Tidal mud flat	0.1	0.0	1.9	0.4	0.7	0.1	+1.8	+1800	-1.2	-75

Table 4. Changes in morphological and geobotanical units between 1987, 1997 and 2008.

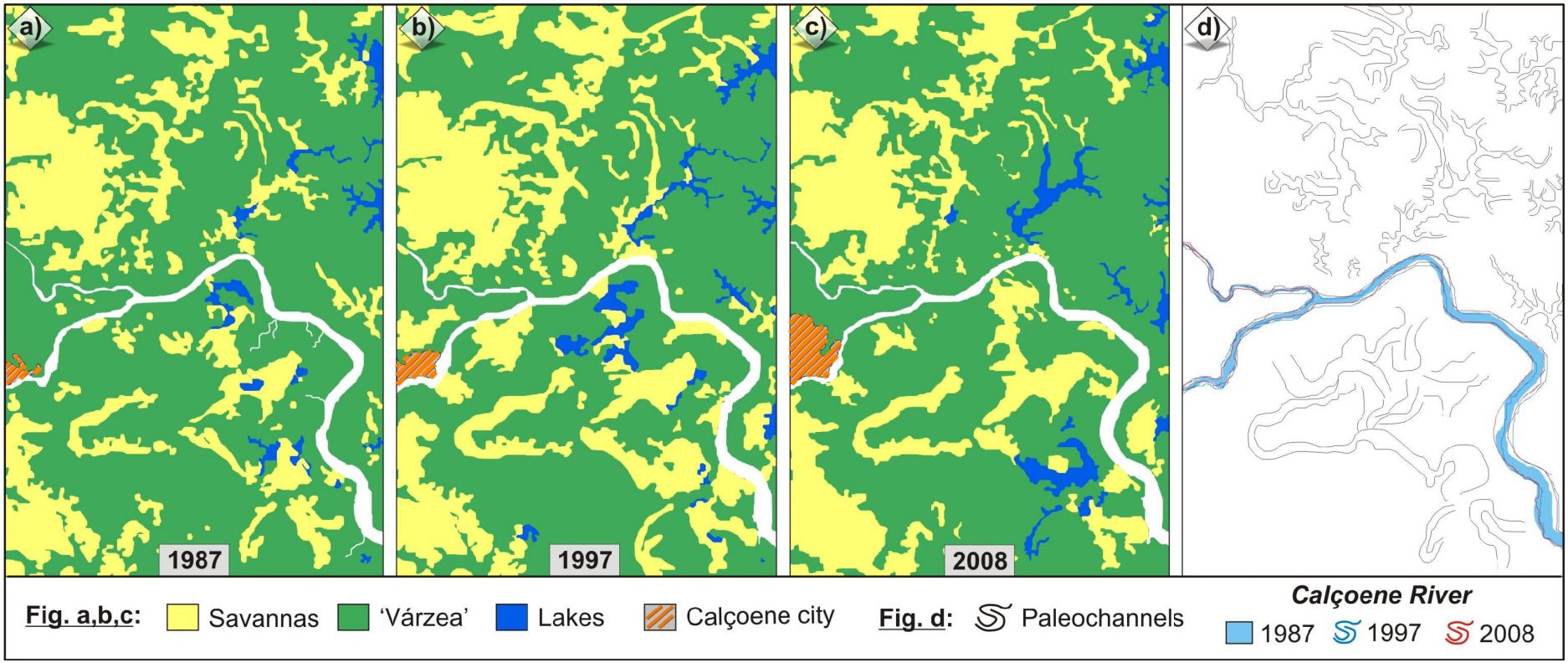

Figure 9. a), b) and c) Changes in savannah, "várzea" and lake areas and, d) relationship with paleochannels of the coastal plain, beyond lateral migration of the tidal-fluvial channel between 1987, 1997 and 2008.

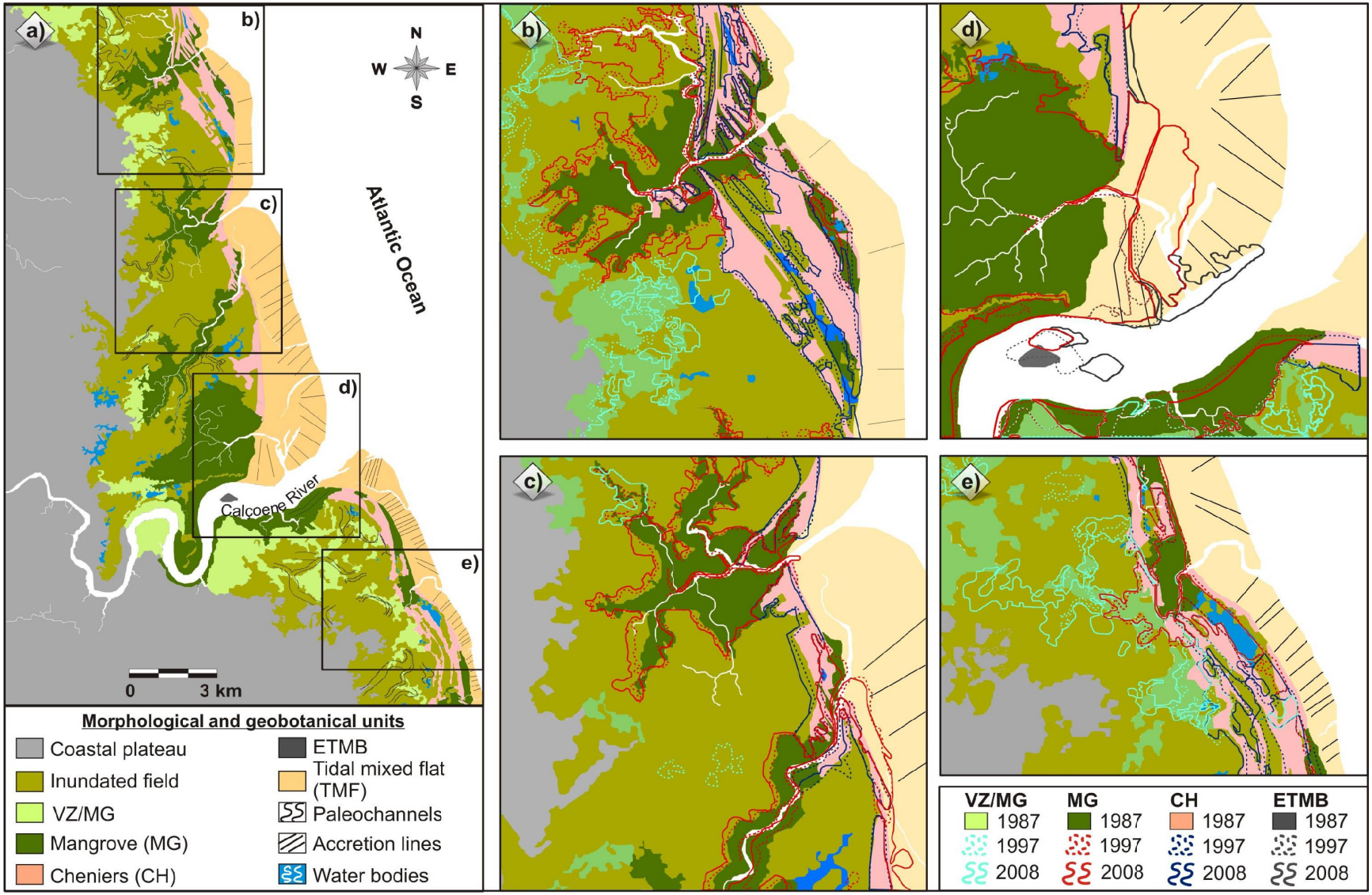

Figure 10. a) Geomorphology of the Calçoene coastal plain in 1987, b), c), d) and e) changes in the morphological and geobotanical units between 1987, 1997 and 2008.

Influence of climate variability on the coastal setting

El Niño and La Niña events significantly affected the rainfall regime on the Calçoene coast, with intense positive anomalies between 1987 and 1997 resulting in low rates of mean annual rainfall ($\bar{x}$ = 605 mm), as well as low rates during the rainy ($\bar{x}$ = 494 mm) and drier ($\bar{x}$ = 112 mm) seasons. Conversely, small-scale positive oscillations and intense negative anomalies between 1997 and 2008 corresponded to high rates of mean annual rainfall ($\bar{x}$ = 781 mm), as well as higher rates in the rainy ($\bar{x}$ = 653 mm) and drier ($\bar{x}$ = 127 mm) seasons (Figure 11).

During the most intense El Niño events, between 1986 and 1998, a shrinking in the area of the inundated field (-3.6%) took place. The area covered by freshwater wetlands was relatively stable, while "várzea" and flooded forests with mangrove and "várzea" species (Vz/Mg) changed by approximately +0.2% and +0.9%, respectively (Table 4). The brackish water wetland represented by the mangrove underwent a relatively small expansion of 2.2%. This relatively dry period also resulted in the expansion of the savannah by approximately 1.4%. Furthermore, tidal mud flats were formed during this period. Subsequently, the most intense La Niña events between 1998 and 2008 likely contributed to the increase in size of the "várzea" (+2.9%) and lakes (+426%) to the detriment of savannah (-9.5%), and mangrove expanded (+14.7%) over the inundated field (-2.6%). Therefore, the lowest rainfall rates during El Niño events may have reduced the inflow of the Calçoene River, which lead to an intensification of tide propagation, transport and deposition of muddy sediments along the tidal-fluvial channel and its secondary channels, followed by mangrove development and stabilization of muddy substrate near the coastline.

The relationship between mangroves and "várzea" in morphostratigraphic and paleoecological studies can be used to identify marine and fluvial influence over time. Indeed the "várzea" occupies the coastal plateau and tidal flats in the proximal portion of the tidal-fluvial channel, is topographically higher than the coastal plain and is influenced by freshwater. On the other hand, mangroves colonize tidal flats of the distal portion of the Calçoene River and wider tidal channels of the coastal plain influenced by brackish tidal water.

This segregation of vegetation types and its relationship to wetland expansion and high rainfall rates suggests, in the case of the coastal plain, an increase in the flooded area, secondary channel development, changes in salinity, and the transport of mangrove seeds into more elevated areas. The wetter period also allowed the "várzea" to migrate into areas covered by savannah in the coastal plateau compartment.

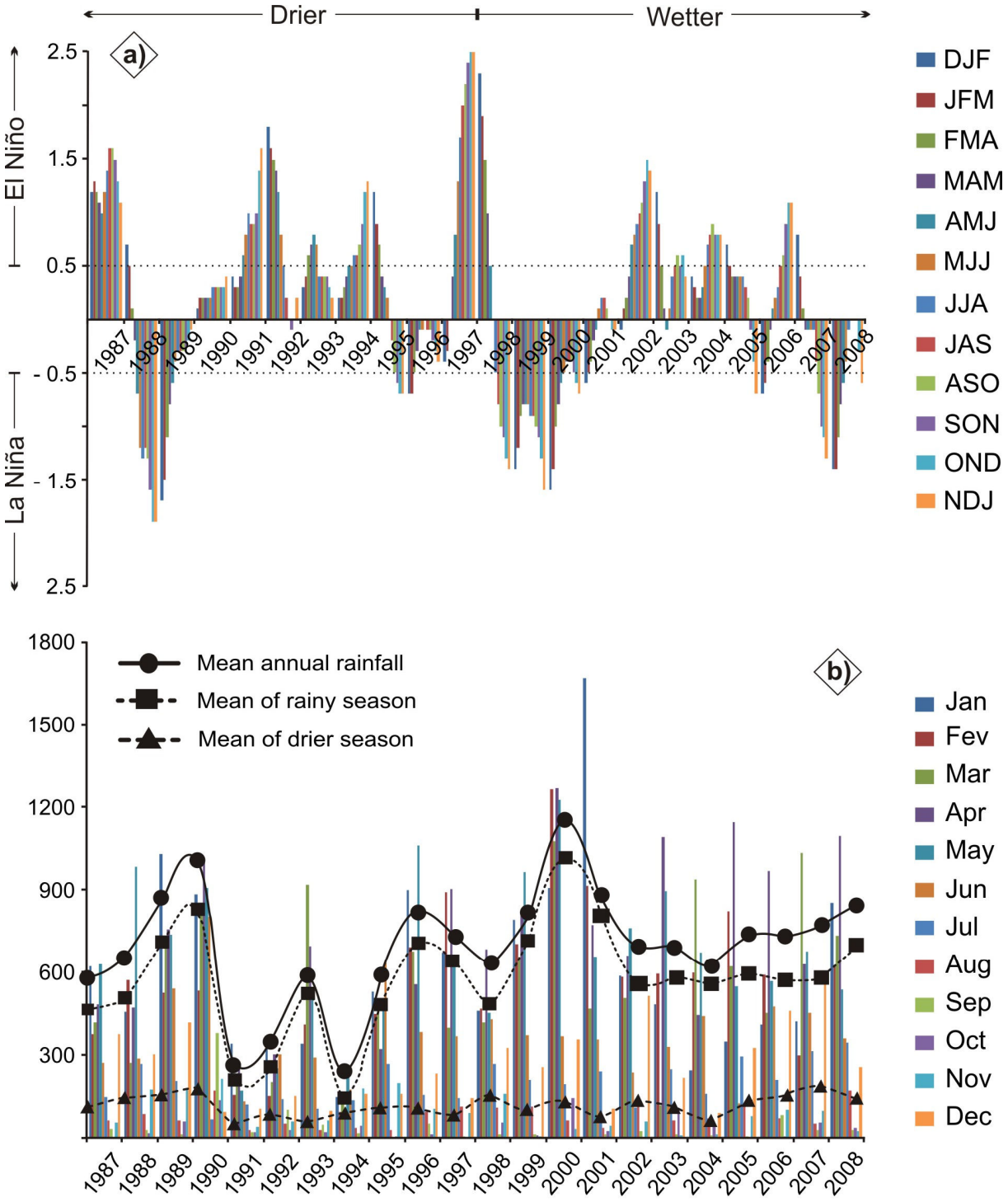

Figure 11. a) Warm (+) and cold (-) episodes based on the thershold of ± 5ºC for the Oceanic Niño Index (three months running mean of sea surface temperature anomalies, based on the 1987-2008 period. For historical purposes cold and warm episodes are defined when the threshold is met for a minimum of five consecutive overlapping seasons (modified from CPC/NOAA, 2010); b) montly rainfall index superimposed by mean seasonal (monthly mean of rainy and drier season) and annual (sum of mean seasonal) rainfall.

Conclusions

The integrated analysis allowed the identification of two distinct compartments on the Calçoene coast: the coastal plateau and plain. The costal plateau is bordered to the west by the Amapá Hills and to the east by the coastal plain. It has elevations near 10 m, with the predominance of "várzea" and savannah vegetation that laterally coexist near extensive meandering paleochannels. The coastal plain contains a tidal-fluvial channel, paleochannels, lakes, "várzea", an inundated field, mangroves, chenier ridges, elongated tidal mudbars (ETMB), tidal mud and mixed flats (non-vegetated). The temporal analysis of morphological and geobotanical units suggests the relative stabilization of savannah (+1.4%), "várzea" (+0.2%) and mangrove (+2.2%) areas, with the formation of extensive tidal mud flats (+1800%) during drier periods under the influence of El Niño events. La Niña events are characterized by wetter periods that led to an increase in the area of "várzea" (+2.9%) and lakes (+426%) over savannah (-9.6%), and the expansion of mangroves (+14.7%) mainly over the inundated field (-2.6%). Therefore, the decrease in rainfall regime during El Niño may have reduced the inflow of the Calçoene River and favored an intensification of tide propagation, transport and deposition of mud along the tidal-fluvial channel and its secondary channels with subsequent development of mangroves on muddy substrate near the coastline during La Niña.

Acknowledgements

This work was funded by CNPq (Project 562398/2008-2). The first and second authors hold a scholarship from CNPq (Process 143518/2008-9 and 302943/2008-0). The authors thank members of the "Laboratório de Dinâmica Costeira" and "Grupo de Análises de Bacias Sedimentares da Amazônia" of the "Universidade Federal do Pará", especially Prof. Dr. Afonso César Rodrigues Nogueira and sedimentologist Luiz Saturnino de Andrade for numerous comments and suggestions that helped to significantly improve this manuscript.

References

Allen JRL. 1965. A review of the origin and characteristics of recent alluvial sediments. *Sedimentology* **5**: 98-191.

Allen JRL. 1990. The Severn Estuary in southwest Britain: its retreat under marine transgression and fine sediment regime. *Sedimentary Geology* **66**: 13–28.

Allen GP. 1991. Sedimentary processes and facies in the Gironde estuary: a recent model for macrotidal estuarine systems. In: Smith DG, Reinson GE, Zaitlin BA, Rahmani RA (Eds),

Clastic Tidal Sedimentology, vol. 16. Canadian Society of Petroleum Geologists Memoir, Canada, p. 29–40.

Allison MA, Nittrouer CA and Kineke GC. 1995. Seasonal sediment storage on mudflats adjacent to the Amazon River. *Marine Geology* **125**: 303–328.

Allison MA, Lee MT, Ogston AS and Aller RC. 2000. Origin of Amazon mudbanks along the northeastern coast of South America. *Marine Geology* ***163***: 241-256.

ANA. 2003. Agência Nacional de Águas. Sistema de Informações Hidrológicas. On line dataset, 14.3 MB, http://hidroweb.ana.gov.br/baixar/mapa/Bacia1.zip.

ANA. 2010. Agência Nacional de Águas. Sistema de Informações Hidrológicas. On line dataset, 216 KB, http://hidroweb.ana.gov.br/Estacao.asp?Codigo=8250002.

Augustinus PGEF. 1989. Cheniers and chenier plains: a general introduction. *Marine Geology* **90**: 219-229.

Augustinus PGEF, Hazelhoff L, Kroon A. 1989. The chenier coast of Suriname: modern and geological development. *Marine Geology* **90**: 269-281.

Augustinus PGEF. 2004. The influence of the trade winds on the coastal development of the Guianas at various scale levels: a synthesis. *Marine Geology* **208**: 145-151.

Basan PB and Frey RW. 1978. Actual-paleontology and neoichnology of salt marches near Sapelo Island, Georgia. In: Crimes TP and Harper JC (Eds), *Trace fossils* 2. Geol Jour Spec Pub 9, p. 41-70.

Beardsley RC, Candela J, Limeburner R, Geyer WR, Lentz SJ, Castro BM, Cacchione D and Carneiro N. 1995. The M2 tide on the Amazon shelf. *Journal of Geophysical Research* **100**: 2283-2319.

Bezerra PEL, Oliveira W, Regis WDE, Brazão JEM, Gavinho J, Coutinho RCP. 1990. Amazônia legal: zoneamento das potencialidades e dos recursos naturais. In: Instituto Brasileiro de Geografia e Estatística, Superintendência de Desenvolvimento da Amazônia. Projeto zoneamento das potencialidades dos recursos naturais da Amazônia: geologia, solos e vegetação. Div. 5. Rio de Janeiro, p. 9-89.

Câmara G, Souza RCM, Freitas UM, Garrido J. 1996. SPRING: Integrating remote sensing and GIS by object-oriented data modeling. *Computers & Graphics* **20**: 395-403.

Carvalho FP, Costa Neto SV, Costa WJP, Coutinho RS, Figueira ZR, Figueiredo SL, Martins MHA, Santos VF, Silva AQ, Silva LMA, Silva MS, Silveira OFM and Takyiama LR. 2006. Atlas Zoneamento Costeiro Estuarino do Estado do Amapá. Macapá, PNMA/SQA/MMA. 77 p.

Chappell JMA and Woodroffe CD. 1994. Macrotidal estuaries. In: Carter RWG and Woodroffe CD (Eds), Coastal Evolution: Late Quaternary Shoreline Morpho-dynamics .Cambridge University Press, Canberra, 539 p.

Chavez PS, Berlin GL, Sowers LB. 1982. Statistical method for selecting Landsat MSS ratios. *Journal of Applied Photographic Engineering* **8**: 23-30.

Chavez PS. 1988. An improved dark-object subtraction technique for atmospheric scattering correction of multispectral data. *Remote Sensing of Environment* **24**: 450-479.

Cohen MCL. 2003. Past and current mangrove dynamics on the Bragança peninsula, northern Brazil. Ph.D. Thesis. Bremen, University of Bremen. Center for Tropical Marine Ecology. 110 p.

Cohen MCL, Souza Filho PWM, Lara RJ, Behling H and Angulo RJ. 2005. A model of Holocene mangrove development and relative sea-level changes on the Bragança Peninsula (Northern Brazil). *Wetlands Ecology and Management* **13**: 433-443.

Cooley SR, Coles VJ, Subramaniam A and Yager PL. 2007. Seasonal variations in the Amazon plume-related atmospheric carbon sink. *Global Biogeochemical Cycles* **21**: GB3014.

Costa JB, Hasui Y, Bemerguy RL, Soares-Júnior AV, Villegas J. 2002. Tectonics and paleogeography of the Marajó Basin, northern Brazil. *Anais da Academia Brasileira de Ciências* **74**: 519-531.

Costa Neto SV and Silva MS. 2004. Vegetação do setor costeiro estuarino do estado do Amapá. Instituto de Pesquisas Científicas e Tecnológicas do Estado do Amapá. Governo do Estado do Amapá. Cap. 5. Projeto Zoneamento Econômico-Ecológico do setor costeiro estuarino: diagnóstico sócio ambiental participativo do setor costeiro estuarino, p.72-96.

CPC/NOAA, (2010). Cold & Warm Episodes by Season. Climate Prediction Center. On line dataset, http://www.cpc.ncep.noaa.gov/products/analysis_monitoring/ensostuff/ensoyears.

CPRM. 2010. Serviço Geológico do Brasil. Sistema de Informação Geológica. On line dataset, Folhas NA-22, 10MB, http://geobank.sa.cprm.gov.br/.

Dalrymple RW, Knight RJ and Lambiase JJ. 1978. Bedforms and their hydraulic stability relationships in a tidal environment, Bay of Fundy, Canada. *Nature* **275**: 293-307.

Dalrymple RW, Knight RJ, Zaitlin BA, Middleton GV. 1990. Dynamics and facies model of a macrotidal sand-bar complex, Cobequid Bay - Salmon River estuary (Bay of Fundy). *Sedimentology* **37**: 577–612.

Dalrymple RW, Zaitlin BA and Boyd R. 1992. Estuarine facies models: Conceptual basis and stratigraphic implications. *Journal of Sedimentary Petrology* **62**: 1130–1146.

Dalrymple RW. 2006. Incised valleys in time and space: introduction to the volume and an examination of the controls on valley formation and filling. In: Dalrymple RW, Leckie DA, Tillman R (Eds), *Incised Valleys in Time and Space*. SEPM Special Publication, vol. 85, p. 5–12.

Dalrymple RW and Choi K. 2007. Morphologic and facies trends through the fluvial-marine transition in tide-dominated systems: A schematic framework for environmental and sequence-stratigraphic interpretation. *Earth-Science Reviews* **81**: 135-174.

Davis Jr RA. 1978. Coastal sedimentary environments. Springer Verlag, New York. 420 p.

DHN, 2009. Diretoria de Hidrografia e Navegacão, Tábuas de Marés do ano de 2009. On line dataset, http://www.mar.mil.br/dhn/chm/tabuas/index.htm.

DNPM. 1971. Projeto RadamBrasil. Levantamento de recursos naturais, v. 21, 23 e 24. Folhas: NA22, MACAPA. Rio de Janeiro, MME/DNPM.

ESRI 2006. ArcGIS Version 9.0 Software. Redland, California.

Evans G. 1965. Intertidal flat sediments and their environments of deposition in the Wash. *Geol Soc London Quart Jour*. **121**: 209-245.

Gallo MN and Vinzon S. 2005. Generation of over tides and compound tides in Amazon estuary. *Ocean Dynamics* **55**: 441-448.

Global Mapper LLC. 2009. Global Mapper Version 9.0 Software. Colorado, Parker.

Guimarães JTF, Cohen MCL, França MC, Lara RJ and Behling H. 2010. Model of wetland development of the Amapá coast during the late Holocene. *Anais da Academia Brasileira de Ciências* **82**: 451-465.

Harris PT and Collins MB. 1985. Bedform distributions and sediment transport paths in the Bristol Channel and Severn Estuary, UK. *Marine Geology* **62**: 153–166.

Hayakawa EH, Rossetti DF and Valeriano MM. 2010. Applying DEM-SRTM for reconstructing a late Quaternary paleodrainage in Amazonia. *Earth and Planetary Science Letters* **297**: 262-270.

Hofton M, Dubayah R, Blair JB and Rabine D. 2006. Validation of SRTM elevations over vegetated and non-vegetared terrain using medium footprint Lidar. *Photogrammetric Engineering & Remote Sensing* **72**: 279–285.

Hoefel FG. 1998. Morfodinâmica de praias arenosas oceânicas: uma revisão bibliográfica. Editora da Univali. Itajaí. 92 p.

Holmgren M, Scheffer M, Ezcurra E, Gutiérrez JR, Mohren GMJ. 2001. El Niño effects on the dynamics of terrestrial ecosystems. *Trends in Ecology & Evolution* **16**: 89-94.

Horbe AMC, Behling H, Nogueira ACR, Mapes R. 2011. Environmental changes in the western Amazônia: morphological framework, geochemistry, palynology and radiocarbon dating data. *Anais da Academia Brasileira de Ciências* **83**: 863-874.

Howard JD and Frey RW. 1975. Estuaries of the Georgia coast, USA: Sedimentology and Biology. II. Regional animal-sediment characteristics of Georgia estuaries: *Senchenberiana merti.* **7**: 33-103.

IBGE. 2008. Mapa Geomorfológico do Estado do Amapá. Instituto Brasileiro de Geografia e Estatística – Coordenação de Pesquisas Naturais e Estudos Ambientais. On line dataset, 10MB, ftp://geoftp.ibge.gov.br/mapas/tematicos/tematico_estadual/AP_geomorfologia.pdf

Klein GV. 1970. Deposition and dispersal dynamics of intertidal sandbars. *Journal of Sedimentary Petrology* **40**: 1095-1127.

Klein GV. 1971. A sedimentary model for determining paleotidal range. *Geological Society* of *America* Bulletin **82**: 2585-2592.

Klein GV. 1977. *Clastic tidal facies*. Continuing Education Publication Company, Champaign, Illinois, 149 p.

Knight RJ and Dalrymple RW. 1975. Intertidal sediments from the south shore of Cobequid Bay, Bay of Fundy, Nova Scotia, Canada. In: Ginsburg RN (Ed) *Tidal deposits: a casebook of recent examples and fossil counterparts*. Springer-Verlag, New-York, p. 47-55.

Komar PD. 1976. *Beach process and sedimentation*. Prentice Hall Editors, New Jersey, 429 p.

Lesourd S, Lesueur P, Brun-Cottan JC, Garnaud S and Poupinet N. 2003. Seasonal variations in the characteristics of superficial sediments in a macrotidal estuary (the Seine inlet, France). *Estuarine, Coastal and Shelf Science* **58**: 3-16.

Lentz SJ. 1995. The Amazon River plume during AMASSEDS: subtidal current variability and the importance of wind forcing. *Journal of Geophysical Research* **100**: 2377-2390.

Lentz SJ and Limeburner R. 1995. The Amazon River Plume during AMASSEDS: Spatial characteristics and salinity variability. *Journal of Geophysical Research* **100**: 2355-2375.

Leopold LB and Wolman MG. 1957. *River channel patterns: braided, meandering and straight*. Physiographic and hydraulic studies of rivers. US Geological Survey Professional Paper, 282B: 39-85.

Lima MIC, Bezerra PE and Araújo HJT. 1991. Sistematização da Geologia do Estado do Amapá. In: Simpósio de geologia da Amazônia, vol. 3, Belém. Anais. SBG. p. 322-335.

Long SP.1999. Environmental responses. In: Sage RF and Monson RK (Eds), *C4 plant biology*. Academic Press, San Diego, p 215-249.

Meade RH, Dunee T, Richey JE, Santos UM and Salati E. 1985. Storage and remobilization of suspended sediment in the lower Amazon River of Brazil. *Science* **228**: 488-490.

Miall AD. 1978. Facies types and vertical profile models in braided river deposits: a summary. In: Miall AD (Ed), *Fluvial sedimentology*. Canadian Society of Petroleum Geologists, Calgary, p 597-604.

Miall AD. 1992. Alluvial Models. In: Walker RG and James NP (Eds) *Facies Models - Response to sea-level change*. Geological Association of Canada, Newfoundland, p 119-142.

Prost MT. 1989. Coastal dynamics and chenier sands in French Guiana. *Marine Geology* **90**: 259-267.

Pugh DT. 1987. *Tides, surges and mean sea-level: a Handbook for Engineers and Scientists*. Wiley, London. 486 p.

Reineck HE. 1975. German North Sea tidal flats. In: Ginsburg RN (Ed.), *Tidal deposits: a casebook of recent examples and fossil counterparts*. Springer-Verlag, New York, p. 5-12.

Reineck HE and Singh IB. 1980. *Depositional Sedimentary Environments with Reference to Terrigenous Clastics* 2nd ed. Springer-Verlag, Berlin, Germany. 542 p.

Reinson GE. 1992. Transgressive Barrier Island and estuarine systems. In: Walker RG and James NP (Eds), *Facies Models - Response to Sea Level Change*. Ontario, Geological Association of Canada, p. 179-194.

Rosario RP, Bezerra MOM and Vinzon SB. 2009. Dynamics of the saline front in the Northern Channel of the Amazon River - influence of fluvial flow and tidal range (Brazil). *Journal of Coastal Research* **2**: 503-514.

Rossetti DF, Almeida S, Amaral DD, Lima CM and Pessenda LCR. 2010. Coexistence of forest and savanna in an Amazonian area from a geological perspective. *Journal of Vegetation Science* **21**: 120-132.

Santos VF. 2006. *Ambientes Costeiros Amazônicos: avaliação de Modificações por Sensoriamento Remoto. Curso de Pós-Graduação em Geologia e Geofísica Marinha, Universidade Federal Fluminense*. PhD Thesis. 306 p.

Schumm SA. 1977. *The Fluvial System*. John Wiley 7 Sons, New York, 338 p.

Silveira OFM. 1998. *A Planície costeira do Amapá: dinâmica de ambiente costeiro influenciado por grandes fontes fluviais quaternárias. Programa de Pós-Graduação em Geologia e Geoquímica, Universidade Federal do Pará*. PhD Thesis. 215 p.

Soares-Filho BS, Nepstad D, Curran L, Voll E, Cerqueira G, Garcia RA, Ramos CA, Mcdonald A, Lefebvre P and Schlesinger P. 2006. Modeling conservation in the Amazon basin. *Nature* **440**: 520-523.

Souza Filho PWM, Cohen MCL, Lara RJ, Lessa GC, Koch B and Behling H. 2006. Holocene coastal evolution and facies model of the Bragança macrotidal flat on the Amazon Mangrove Coast, Northern Brazil. *Journal of Coastal Research* **SI 39**: 306–310.

Souza EJ. 2010. *Geologia da região costeira do Amapá com ênfase na estratigrafia, morfotectônica e geomorfologia*. Faculdade de Geologia, Universidade Federal do Pará. Monografia de Conclusão de Curso. 118 p.

Szatmari P, Françolin JBL, Zanotto O and Wolff S. 1987. Evolução tectônica da margem equatorial brasileira. *Revista Brasileira de Geociências* **17**: 180-188.

Thompson RW. 1975. Tidal flat sediments of the Colorado delta, northwestern Gulf of California. In: Ginsburg RN (Ed) *Tidal deposits: a casebook of recent examples and fossil counterparts*, Springer-Verlag, New-York, p. 57-65.

USDA, 1999. *Soil Taxonomy: a basic system of soil classification for making and interpreting soil surveys*. United State Department of Agriculture. Natural Resources Conservation Service. Soil Survey Staff. 2ed. Washington. 169 p.

Van Straaten LMJU. 1961. Sedimentation in tidal flat areas. *Alberta Soc Petrol Jour*. 9: 203-226.

Viles HA and Goudie AS. 2003. Interannual, decadal and multidecadal scale climatic variability and geomorphology. *Earth-Science Reviews* **61**: 105-131.

Walker RG. 1992. Facies, facies models and modern stratigrahic concepts. In: Walker, R.G. and James N.P. (Eds.), *Facies Models - Response to Sea Level Change*. Ontario, Geological Association of Canada, p. 1-14.

Weimer RJ, Howard JD and Lindasay DR. 1982. Tidal flats and associated tidal channels. In: Scholle PA and Spearing D (Eds.), *Sandstone Depositional Environments*. The American Association of Petroleum Geologists, Wisconsin, p 191-245.

Woodroffe CD, Chappell JMA, Thom BG and Wolanski E. 1989. Depositional model of a macrotidal estuary and floodplain, South Alligator River, Northern Australia. *Sedimentology* **36**: 737–756.

4 MORPHOLOGICAL CHANGES AND WETLAND DEVELOPMENT ON TIDAL FLATS NEAR THE MOUTH OF THE AMAZON RIVER DURING LAST 5000 YR CAL. YR B.P.*

[a,*] José Tasso Felix Guimarães, [a] Marcelo Cancela Lisboa Cohen, [b] Marlon Carlos França, [b] Luiz Carlos Ruiz Pessenda, [c] Hermann Behling

[a] *Programa de Pós-Graduação em Geologia e Geoquímica, Instituto de Geociências, Universidade Federal do Pará (UFPA). Rua Augusto Correa 01, 66075-110, Belém/PA, Brasil.*

[b] *Centro de Energia Nuclear na Agricultura (CENA), 13400-000, Piracicaba/SP, Brasil.*

[c] *Department of Palynology and Climate Dynamics, Albrecht-von-Haller-Institute for Plant Sciences, University of Göttingen, Untere Karspüle 2, 37073 Göttingen – Germany).*

* Submitted to The Holocene

Abstract

The analysis of morphology, sedimentary facies, palynological, carbon and nitrogen isotopes, C/N ratio and radiocarbon data from tidal flats sediments near the mouth of the Amazon River indicate that vegetation development during the mid and late Holocene occurred according to the aquatic influence and chenier dynamic. The data suggest a mud-rich tidal flat that presents alternations between supra and intertidal environments. The proximal portion of the tidal flat is related to the transitional sector between the costal plateau and plain and represents the final filling stage of the concave-up feature formed by the abandoned channel that contributed to water accumulation under very low energy flows, and the presence of fern and other terrestrial vegetation surrounding the formed lake since 5280 - 5160 cal. yr BP. During the last 2840 - 2750 cal. yr BP, the source of mud ceased and autochthonous organic material became prevalent as well as the increase in contribution of terrestrial organic matter (C3 plants), mainly represented by "várzea" vegetation. Herbaceous field already colonized the tidal flat at least during the last 3170 - 2970 cal. yr BP. However, part of distal portion of the tidal flat related to the herbaceous field was covered by chenier ridges between 3170-2970 and 220-140 cal. yr BP. The mangrove establishment, characterized mainly by estuarine organic matter, *Rhizophora* and *Avicennia* pollen, occurred after 1350-1290 cal. yr B.P and 220-140

cal. yr B.P. on G3 and G2 sites, respectively. This stacking pattern of sediments indicates a retrogradation, with distal facies over proximal facies, and gradual transition of herbaceous to mangrove sediment (e.g. G3 site). Thus, the creation of an accommodation space was produced during an increase of wave action, tidal inundation frequency and evolution of secondary channels in the study site, with possible influence of relative sea-level rise.

Key Words: Amazonia, Facies analysis, Palynology, C and N Isotopes, Coastal plain, Holocene.

Introduction

The development of the most extensive tidal flats of Brazil, located downdrift of the mouth of the Amazon River, are characterized by the interaction of morphological, hydrological and climatic process operating on different time and spatial scale during the Holocene (e.g. Allison et al., 1995; 2004). Consequently, widespread shoreface-attached mudflats alternating with sandy cheniers dominate the coast with its vegetation history characterized by mangrove (brackish water forest) and "várzea" (freshwater forests) expansion/contraction phases and coexistence of arboreal and herbaceous strata (Guimarães et al., 2010; Guimarães et al., in press).

The mangroves near the mouth of the Amazon River are part of a wetland system that extends for almost 480 km and holds one of the world's largest mangrove areas (Kjerve and Lacerda, 1993). The continuity of this mangrove is interrupted by the zone influenced by discharge of the Amazon River, where the "várzea" vegetation dominates (Cohen et al., 2008; Guimarães et al., 2010). The mangrove zones are the response to the morphology, gradients of tidal inundation frequency, waterlogging, nutrient availability and sediment salt concentrations across the intertidal area (Semeniuk, 1994; Duke et al., 1998; Kao et al., 2004; Stuart et al., 2007; Krauss et al., 2008).

Changes in wetlands distribution may be interpreted as a reflex of the coastal geomorphology (e.g. Lara and Cohen, 2009; Fromard et al., 2004; Souza Filho et al., 2006; Souza Filho et al., 2007), since its development and expansion is determinate by the continent-ocean interaction, morphology, tidal regime (Gornitz, 1991; Cohen and Lara, 2003) and the flow energy (Woodroffe, 1982). Therefore, coastal vegetation may be eroded and migrate landward due to higher inundation frequency. Similarly, internal vegetation domains on elevated mudflats will be subject to boundary adjustments, since mangroves would migrate to higher locations and could invade these areas, resulting in a stacking pattern of distal over

proximal sedimentary facies (Cohen and Lara, 2003). The conjunction of those factors allows to the mangroves be considered highly susceptible to climatic and hydrological changes (e.g. Alongi, 2008; Cohen et al., 2008; Lara and Cohen, 2009), and regarding the influence of precipitation regime, which strongly influences run-off and river discharge, on tidal amplitude, significant local sea-level oscillations may be caused by century or millennium-scale regional dry/wet events (e.g. Mörner, 1996; Mörner, 1999).

Considering large-scale hydrological and climatic process on Amazon region and its effects on vegetation patterns, several palaeoecological studies indicate a drier climate during the early and mid Holocene (e.g. Absy et al., 1991; Desjardins et al., 1996; Ledru, 2001; Behling and Costa, 2000; Freitas et al., 2001; Pessenda et al., 2001) and probably a decrease in the Amazon River discharge (e.g. Maslin and Burns, 2000; Latrubesse and Franzinelli, 2002; Eisma et al., 1991). In this period, mangrove established instead of the current "várzea" forest on tidal flats located in the mouth of Amazon River. After this drier event, occurred a return to more humid climate conditions and increase of the Amazon River inflow most likely similar to those prevailing today (e.g. Behling and Hooghiemstra, 2000; Weng et al., 2002; Bush et al., 2007; Mayle and Power, 2008; Guimarães et al., in press). Consequently, the mangroves were replaced by "várzea" (Toledo and Bush, 2007; Mayle and Power, 2008; Guimarães et al., in press, Smith et al., in press).

The alternations between mangrove and "várzea" phases are probably related to changes in the river water discharge that affect the salinity gradients along the estuarine environments such as tidal flats (Guimarães et al., 2010) and mangroves are more tolerant to porewater salinity than "várzea" (e.g. Cohen and Lara, 2003). However, data interpretation must primarily consider that vegetation changes occur on a variety of scales, both temporal and spatial, and such changes are due to allochtonous and authochnous processes (e.g. Bradley, 1999). Therefore, morphostratigraphic, $\delta^{13}C$, $\delta^{15}N$ and C/N records must be used in conjunction with pollen and spore data since they provide powerful information relating to sedimentary processes, lateral relationship between sedimentary deposits, organic matter sources and vegetation patterns which is required to isolate the climatic signal from the nonclimatic noise and better interpret the main process acting on vegetation changes (e.g. Dalrymple, 1992; Marzo and Puigdefabregas, 1993; Boutton et al., 1998). Thus, this work presents a detailed description of morphological and vegetation changes on tidal flats near the mouth of the Amazon River during the last 5000 cal. yr B.P. using geomorphology, sedimentary facies, palynological, $\delta^{13}C$, $\delta^{15}N$, C/N and radiocarbon data. The goal is to

identify and discuss the relationship between the main morphological processes and its influence on vegetation patterns.

Study area

Geological and physiographic setting

The study area is located in the Amapá Platform that correspond to emerged and submerged continental areas continuously stable during several episodes of distensional tectonics followed by the Gondwana break up and Equatorial Atlantic opening during Jurassic/early Cretaceous (Szatmari et al., 1987; Azevedo, 1991). The regional geology includes Mesoarchean-Devonian Crystaline and Metassedimentary rocks to western part, and Pleistocene sandstone and conglomerates in the eastern part interpreted as tidal depositional systems (Souza and Pinheiro, 2009), which are geomorphologically related to the Amapá Hills and costal plateau, respectively.

The coastal plateau presents a flat surface, gently undulating and strongly shaped by erosive process. Avulsion of alluvial channels and birdfoot features related to paleodeltaic lobes were also identified in this compartment (Guimarães et al., submitted). From the Late Pleistocene to Holocene, erosional and depositional processes due climatic and sea-level changes, with tectonic processes, shaped the relief of the Amapá coast, resulting in its current configuration (Lima et al., 1991). Therefore, extensive north-south trending Holocene terraces composed of sand and mud have developed along the coastal plain adjacent to the mouth of Amazon River (Figure 1a, b).

The main sedimentary systems of the coastal plain are tidal flats, which present tide-dominated rivers, paleochannels, lakes, lake belts, “várzea” (flooded freshwater forests on inter and supratidal flat), herbaceous fields (freshwater herbs located on supratidal flat), mangroves (flooded brackish water forest located on intertidal flat), cheniers, elongated tidal mud bars (ETMB), tidal mud and mixed flat (Figure 1c). The presence of lakes and lake belts, jointly with the coexistence of mangrove and herbaceous fields may be related to natural abandonment and silting of tidal channels. Furthermore, the main lithologies and sedimentary structures observed in the coastal plain are flaser, wavy, lenticular and inclined heterolithic, inclined and bioturbated muds, cross-laminated and low-angle cross-laminated sand, which represent tidal and wave-dominated environments strongly influenced by the Amazon River discharge and macrotidal regime (Guimarães et al., submitted).

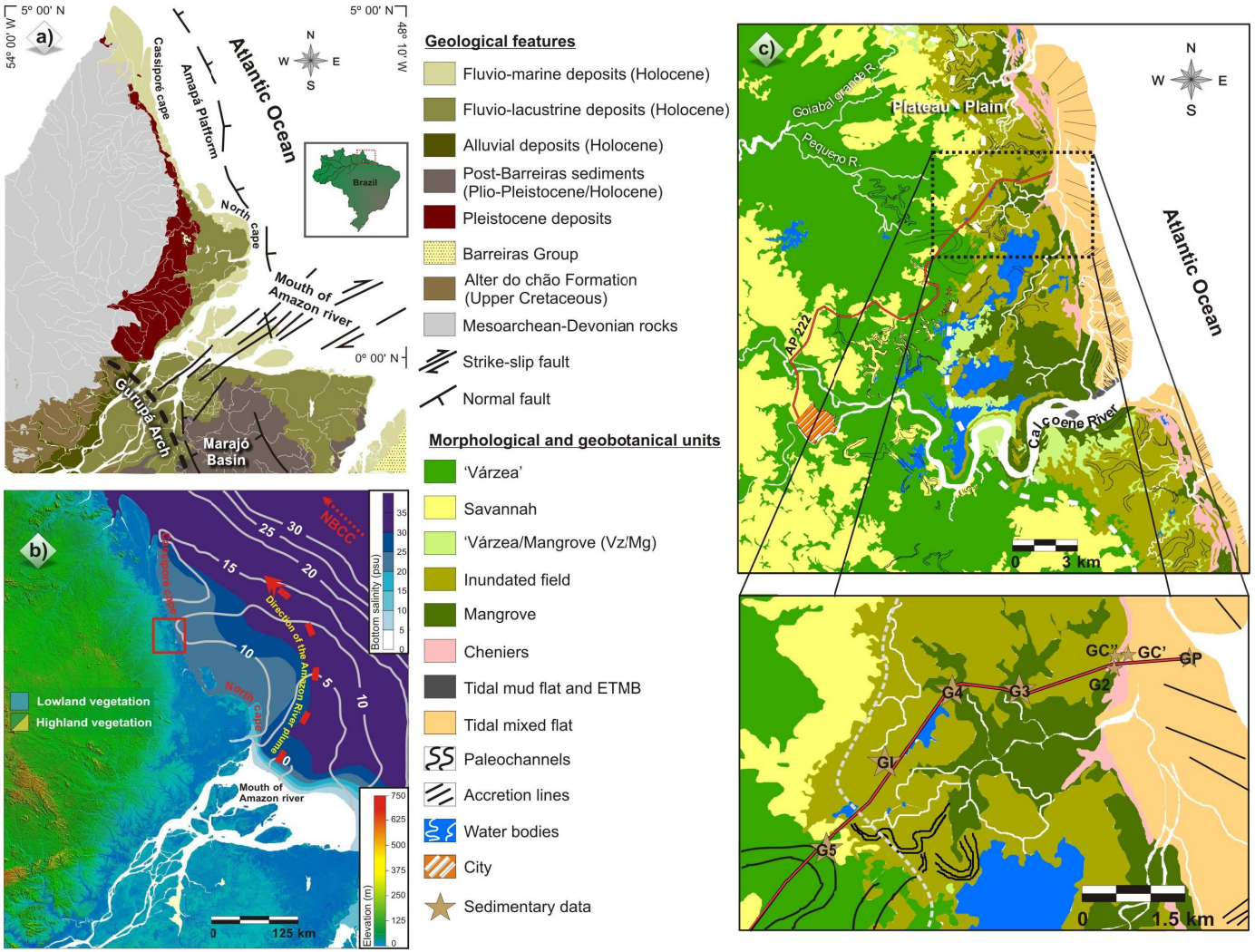

Figure 1. Study site: a) Regional geology of the study area in the Marajó basin (modified from CPRM 2010 and Costa et al, 2002), b) Elevation map with bottom and surface water salinity, direction of the Amazon River plume and North Brazilian Coastal Current (NBCC) near the Amapá littoral (modified from Vinzon et al, 2008 and Rosario et al, 2009) and c) geomorphological map of the study site (Guimarães et al., submitted).

Floristic studies of Costa Neto (2004), Costa Neto and Silva (2004), Carvalho et al. (2006) and Costa Neto et al. (2007) described geobotanical and land use units. For the study site (Figure 1c and Table 1), a vegetation survey based on qualitative descriptions was carried out. Therefore, the modern vegetation is characterized by well-developed mangrove forests near the coastline, herbs vegetation (supratidal zone) and "várzea" (flooded freshwater forests).

Table 1. Main plant species identified in the study site. Vegetation units: WF: Woody Field; VF: "Várzea" (flooded freshwater forest); IF: Inundated Field; MG: Mangrove.

Family and species	Biological form	Vegetation units
Aizoaceae		
Sesuvium sp.	Herb	IF
Anarcadiaceae		
Tapirira guianensis Aubl.	Tree	VF
Apocynaceae		
Himatanthus articulata Vahl.	Tree	WF
Araceae		
Montrichardia arborescens (L.) Schott.	Herb	VF
Arecaceae		
Euterpe oleracea Mart.	Tree	VF
Mauritia flexuosa L.f.	Tree	VF
Avicenniaceae		
Avicennia germinans (L.) Stearn	Tree	MG
Cabombaceae		
Cabomba aquatica DC.	Herb	VF, IF
Ceratopteridaceae		
Acrostichum sp.	Herb	MG
Cyperaceae		
Cyperus sp.	Herb	IF
Eleocharis sp.	Herb	IF
Euphorbiaceae		
Alchornea sp.	Tree	VF
Hura crepitans L.	Tree	VF
Fabaceae		
Macrolobium sp.	Tree	VF
Parkia sp.	Tree	VF
Malpighiaceae		
Byrsonima sp.	Tree	WF
Mascagnia sp.	Climber	FV
Malvaceae		
Pachira aquatica Aubl.	Tree	VF
Pseudobombax munguba (Mart. et Zucc.)	Tree	VF
Nymphaeceae		
Nymphaea sp.	Herb	VF, IF
Poaceae		

Olyra latifolia L.	Herb	VF, IF
Panicum laxum Sw.	Herb	IF
Paspalum repens Berg.	Herb	IF
Ponteridaceae		
Eichhornia sp.	Herb	IF
Rubiaceae	Herb	
Borreria sp.	Herb	WF
Psychotria	Herb	IF
Sapotaceae		
Pouteria sp.	Tree	VF
Rhizophoraceae		
Rhizophora sp.	Tree	MG

Climate and hydrology

The regional climate is humid tropical characterized by well-defined dry (September to December) and wet (January to July) seasons, with annual average precipitation and temperature around 3000 mm and 27.5ºC, respectively (Bezerra et al., 1990). The mean Amazon River discharge is about 170.000 m^3/s (at Óbidos city), with maximum and minimum outflow of 270.000 and 60.000 m^3/s (ANA, 2003). The Amazon estuary is classified as semidiurnal macrotidal (Pugh, 1987), with a tidal range of 4 to 6 m (Gallo and Vinzon, 2005). The structure of the plume is controlled by the North Brazilian Current, which induces a northwestern flow with speeds of 40 - 80 cm/s over the continental shelf (Figure 1b; Lentz, 1995), strong tidal currents (Beardsley et al., 1995), trade winds and the Intertropical Convergence Zone - ITCZ (Lentz and Limeburner, 1995). Consequently, the river discharge and hydrodynamic conditions allow a strong reduction of water salinity along the Amazon River and adjacent coast (Figure 1b; Vinzon et al., 2008; Rosario et al., 2009).

Materials and methods

Sampling and facies description

Sedimentary records consists of exposed terraces, trenches and cores described and sampled from the town of Calçoene (Figure 1c) using a Russian Sampler with the geographical and topographical position of the transection obtained from the digital elevation model based on SRTM and Landsat/TM data analysis presented by Guimarães et al. (submitted). Following the proposal of Walker (1992), facies analysis included descriptions of color, lithology, texture and structures. X-ray radiographs aided the identification of sedimentary structures. The interpretation of the sedimentological data is also based on clastic tidalite process-response models (after Klein, 1971). The sedimentary facies was codified following Miall

(1978). Morphostratigraphic concepts such as the organization and correlation of sediment strata based on their surface morphology, lateral coexistence and superposition through time were applied following the geomorphological analysis developed in the same study site (Guimarães et al., submitted).

The sedimentary records were acquired from a transitional sector between the coastal plateau and plain related to paleochannels setting colonized by "várzea" (G5 core to 1.5m meter depth, 02º34'42''N, 50º53'11'W), tidal flat colonized by herbaceous field (GI exposed terrace and core to 2m depth, 02º35'30''N, 50º52'37'') and mangrove (G4 core to 1m depth, 02º36'00''N, 50º52'06''W; G3 core to 1.5m depth, 02º35'59''N, 50º51'29''W; G2 core to 1.5m depth, 02º36'07''N, 50º50'48''W) and chenier ridge (GC's trenchs and cores to 2m depth, 02º36'10''N, 50º50'50''W). Additionally, leaves of the most abundant genera were collected to heights of up to 2 meters, to identify the carbon isotopic signatures.

Pollen and spore analyses

Throughout the sedimentary facies, 1 cm^3 of sediments were picked in 5 cm intervals. One tablet of exotic *Lycopodium* spores was added to each sample for the calculation of pollen concentration (grains/cm^3). All samples were prepared using standard techniques of pollen analysis including acetolysis (Faegri and Iversen, 1989). Handbooks of pollen and spores morphology were consulted (Roubik and Moreno, 1991; Colinvaux et al., 1999; Hesse et al., 2008) jointly with the reference collection of the "Laboratório de Dinâmica Costeira - UFPa" to identify of pollen grains and spores. Samples were counted to a minimum of about 300 pollen grains. The total pollen sum only considers pollen grains and excludes algae, micro-foraminifers, fungal and fern spores. Thirty pollen taxa were identified (Figure 3, 4 and 5). Pollen and spore data are presented in pollen diagrams as percentages of the total pollen amount. Taxa were grouped into Mangrove, Herbaceous field, "Várzea" and Transitional/Secondary Forest (TSF). The softwares Tilia and Tilia Graph were used to the calculation and plotting of pollen diagrams. The pollen diagrams were statistically subdivided into zones of pollen and spores assemblages based on square-root-transformation of the percentage data and stratigraphically constrained cluster analysis by the method of total sum of squares (Grimm, 1987).

C/N, Carbon and Nitrogen isotopes

The $\delta^{13}C$, $\delta^{15}N$ and elemental C and N (C/N) amounts were analyzed from sediment samples (6-50 mg) taken at 5 cm intervals along the sedimentary facies. The stable carbon and

nitrogen isotopes as well as the total organic carbon (TOC) and nitrogen (TN) were determined at the Stable Isotopes Laboratory of Center for Nuclear Energy in Agriculture (CENA), University of Sao Paulo (USP), using a Continuous Flow Isotopic Ratio Mass Spectrometer (CF-IRMS). Organic carbon and nitrogen are expressed as percentage of dry weight and ^{13}C and ^{15}N results are given with respect to VPDB standard and atmospheric N_2, respectively, using the conventional δ (‰) notation. Analytical precision is ± 0.1 % and ±0.2‰, respectively.

Radiocarbon dating

Nine bulk samples of ~ 2g each were used for radiocarbon dating. The sediment samples were checked and physically cleaned under the microscope. The residual material was then extracted with 2 % HCl at 60°C during 4 hours, washed with distilled water until neutral pH and dried (50 ºC). The sediment organic matter was analyzed by Accelerator Mass Spectrometry (AMS) at the Center for Applied Isotope Studies (Athens, Georgia, USA) and Physikalisches Institut, University of Erlangen (Nürnberg, GER). Radiocarbon ages are reported in years before AD 1950 (yr BP) normalized to $\delta^{13}C$ of -25‰VPDB and in cal. yr BP with precision of 2σ (Reimer et al., 2004).

Results and discussion

$\delta^{13}C$ values of vegetation

From the fifteen most representative species collected in the study site, the $\delta^{13}C$ values indicate the predominance of C3 plants (Table 2). The contribution of C4 plants in the sediment is restricted to the *Panicum* sp. (Poaceae) and *Paspalum repens* Berg. (Poaceae), and CAM plants as *Sesuvium* sp. (Aizoaceae).

Table 2. Carbon Isotopic ($\delta^{13}C$) signature of leaves from main genres of the study site showing C3 plant dominance (more depleted values ranging from -26.6 to -34.4).

Family	**Species**	**$\delta^{13}C$ (‰) VPDB**
Aizoaceae	*Sesuvium* sp.	-13.9
Arecaceae	*Euterpe oleracea* Mart.	-34.4
Araceae	*Montrichardia*	-27.6
	Pistia stratioides L.	-26.6
Avicenniaceae	*Avicennia germinans* (L.)	-31
Cyperaceae	*Cyperus* sp.	-29.8
Heliconiaceae	*Heliconia* sp.	-29.7
Strelitziaceae	*Phenakospermum* sp.	-34.3

Nymphaeaceae	*Nymphaea* sp.	-27
Poaceae	*Panicum* sp.	-12
	Hymenachne amplexicaule	-29.2
	Olyra latifolia L.	-32
	Paspalum repens Berg.	-11
Pteridaceae	*Acrostichum* L.	-32
	Ceratopteris sp.	-27.8
Rhizophoraceae	*Rhizophora mangle L.*	-33.5
Rubiaceae	*Borreria* sp.	-30.1

Radiocarbon date and sedimentation rates

The respective radiocarbon ages and sedimentation rates of the sediment samples are described in Table 3 and Figure 2. The sedimentation rates are based on the ratio between the depth intervals (mm) and the mean time range. The calculated sedimentation rates to the studied cores are between 0.14 and 2.7 mm/yr. The G1 presents 0.14 (100-30 cm) and 0.67 mm/yr (30-0 cm), while the G2 shows 0.22 (130-65 cm) and 2.7 mm/yr (65-0 cm). The G3 exhibits rates of 0.35 mm/yr (150-100 cm) and 0.72 mm/yr (100-0 cm), and the G5 presents 0.32 mm/yr (150-70 cm) and 0.25 mm/yr (70-0 cm).

Table 3. Radiocarbon dates (AMS) of the samples

Sample ID	**Lab. number**	**Depth (cm)**	**Radiocarbon age (yr B.P)**	**2σ Calibration (cal yr B.P.)**
G5 70	UGAMS 8198	70	2680 ± 30	2840 - 2750
G5 150	UGAMS 8197	150	4460 ± 30	5280 - 5160
G3 100	UGAMS 8199	100	1410 ± 25	1350 - 1290
G3 150	UGAMS 8202	150	2600 ± 30	2770-2710
G2 65	UGAMS 8203	65	210 ± 30	220 - 140
G2 130	UGAMS 8200	130	2930 ± 30	3170 - 2970
G1 30	UGAMS 8201	30	320 ± 30	470 - 310
G1 100	UGAMS 8196	100	4810 ± 40	5610 - 5470

Sediments deposited on vegetated tidal flats of Marajó Island (0.3-1 mm/yr, Behling et al., 2004), Salinopólis and the town of São Caetano (1.7-5.6 mm/yr, Cohen et al., 2009) and Bragança Peninsula (0.6-0.8 mm/yr, Cohen et al., 2005; 0.2-0.4 mm/yr, Vedel et al., 2006) on northern Brazilian coast presented similar sedimentation rates.

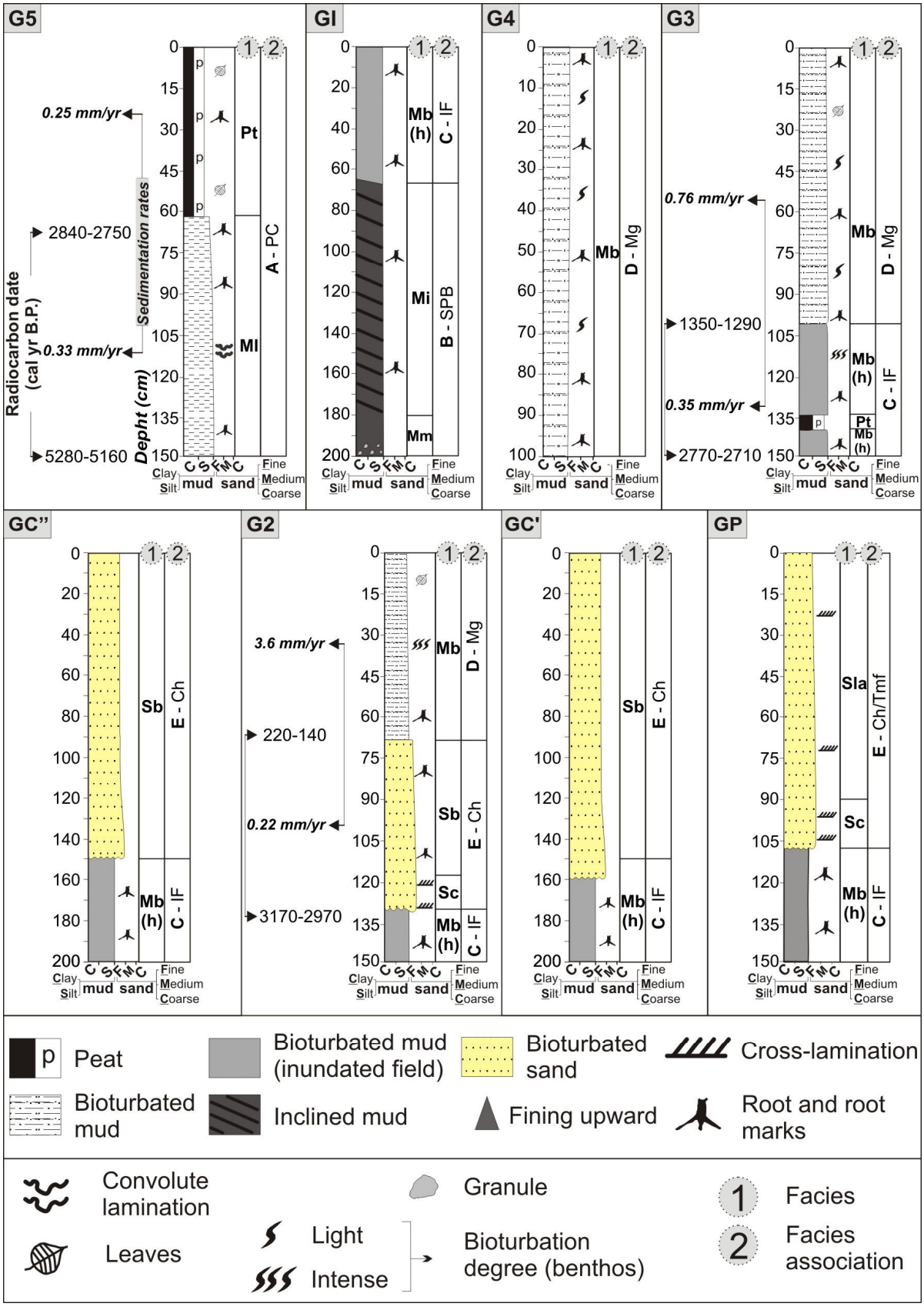

Figure 2. Graphic sedimentary logs of the sedimentary data from the study site.

Facies descriptions

The sediment records consist mostly of peat, massive mud, laminated, inclined mud, bioturbated mud and sand, and fine sands with cross-lamination (Figure 2, Table 4). Pollen and spore records, $\delta^{13}C$, $\delta^{15}N$ and C/N values were added to facies characteristics in order to define five facies associations that represent typical tidal flat setting with chenier development (Figure 3, 4, 5 and 6).

Table 4. Summary of facies descriptions and sedimentary process (interpreted following descriptions after Klein, 1971).

Facies	**Description**	**Process**
Laminated mud (Mb)	Very light gray and greenish gray mud with plane-parallel lamination, fine root marks and plant debris.	Alternation of flocculated and non flocculated laminae deposited from suspension, and variations in the organic colloid content. Lighter tones may correspond to the presence of kaulinite.
Peat (Pt)	Dark greenish gray and very dark brown organic material with decomposed and intact vegetable fibers.	Stagnant and reduced conditions with vegetable tissues as the main source of the deposit, indicating autochthonous source.
Massive mud (Mm)	Greenish gray mud and locally subangular quartz granules.	The massive nature indicates creek waters with high suspended load. Considering the gravel class occurrence, granules are left behind, while mud moved as suspension clouds.
Inclined mud (Li)	Parallel inclined mud laminae of greenish gray mud and organic matter – OM films with dip ~ 25º.	Lateral accretion with mud and OM films deposited during low energy flows of a small-scale meandering creak.
Bioturbated mud (Mbh) and Mb)	Pale olive and light olive gray mud with many woody and herbaceous roots (facies Mb (h)), root marks, leaves and dwelling structures.	Diffused mixture of sediments and alternating colors by intense bioturbation and diagenic process, respectively.

Low-angle cross-laminated sand (Sla)	Alternation of dark gray (heavy minerals) and brown (light minerals) fine sand with low-angle cross-stratification.	Deposition of sand by swash and backwash on gently sloping surface.
Cross-laminated sand (Sc)	Olive gray, well sorted, fine to very fine sand with ripple cross-lamination.	Migration of small ripples during low energy flows.
Bioturbated sand (Sb)	Pale olive sand with reddish and yellowish mottles, many herbaceous roots in growth position.	Sediment homogenization and mottling by biological activity and diagenic process, respectively.

Facies association A (Paleochannel-upper deposit). This association only occurs in the G5 core from 5280 - 5160 cal. yr BP until the present (Figure 2, 3a, b). These deposits feature laminated mud with convolute lamination, and fine root marks (facies Ml), deposited from suspension with differential compaction and hydroplastic readjustment (Dott and Howard, 1962). These sediments were overlaid by peat material (facies Pt) indicating predominantly autochthonous conditions from 2840 - 2750 cal. yr BP until the present.

The pollen assemblages of association A correspond to Zone G5A and G5B, related to facies Ml and Pt, respectively (Figure 3a). Zone G5A (5280 - 5160 to 2840 - 2759 cal. yr BP) is characterized by the predominance of Trilete psilate (77-95%) and Polypodiaceae (3-25%) ferns. In Zone G5B (2840 - 2759 cal. yr BP until the present), Poaceae pollen (0-95%) appears with very high values. Papilionoideae (0-20%), Euphorbiaceae (0-14%) and *Montrichardia* (0-7%) are the main representative of "várzea" pollen. Polypodiaceae and Trilete psilate ferns (0-100%) are also present.

The $\delta^{13}C$ values ranging between -14.9‰ and -28.6‰ indicate contribution of C3 and C4 plants (-32‰ to -21‰ for C3 plants and -17‰ to -9‰ for C4 plants; Deines, 1980) and/or a mixture of freshwater aquatic plants (-50‰ to -11‰; Osmond et al., 1981; Keeley and Sandquist, 1992). The $\delta^{15}N$ in the range of -1.4 and 3.5‰ suggests a mixture of terrestrial plants and aquatic organic matter (~0‰ to >10‰, respectively; Thornton and McManus, 1994; Meyers, 1997). The C/N values (8-41) also indicate a mixture of organic matter from vascular plants and algae (Figure 3b; < 10 algae dominance and > 12 vascular plants; Meyers, 1994; Tyson, 1995).

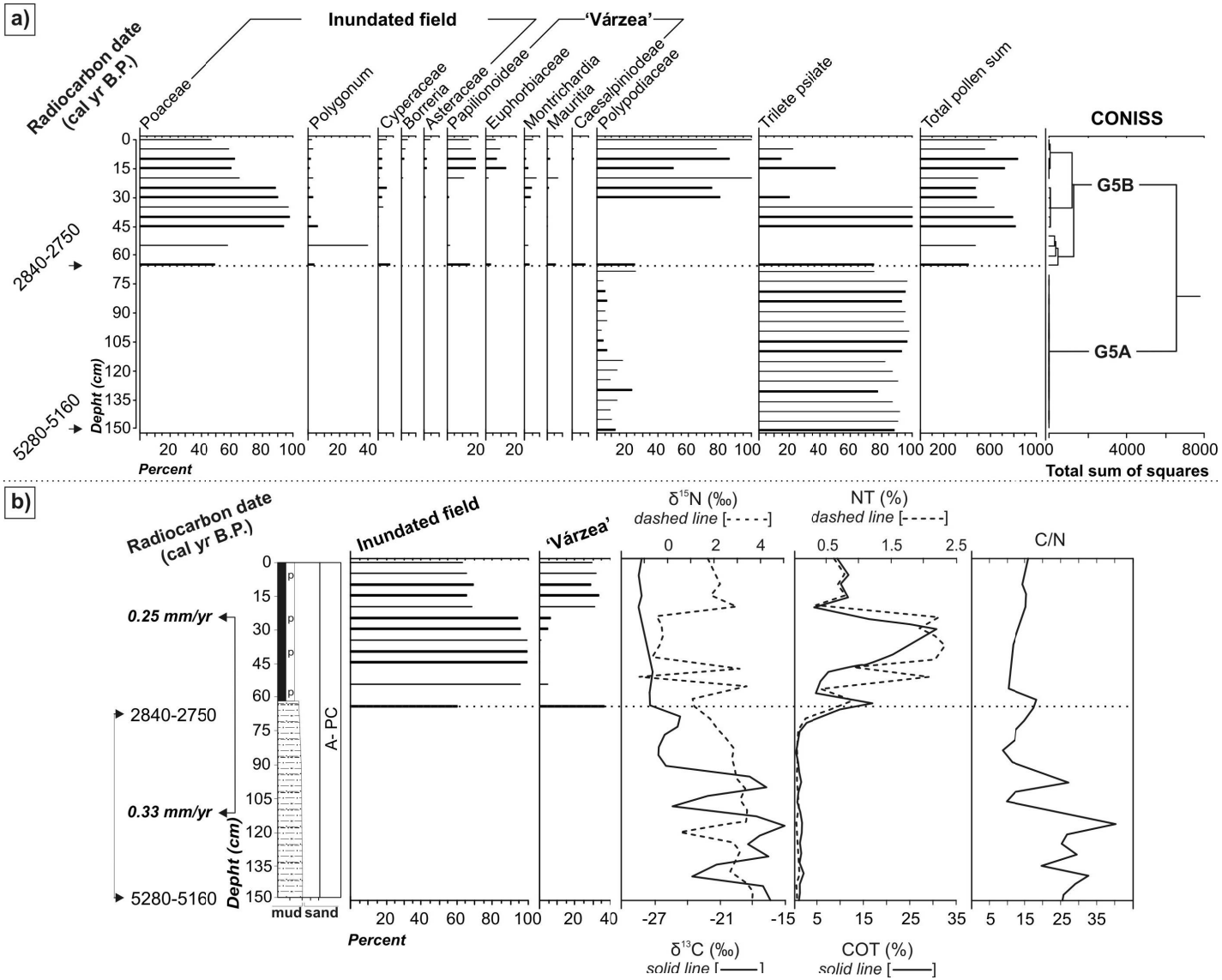

Figure 3. Integrated graphics, a) pollen diagram and b) interproxy records of G5 core.

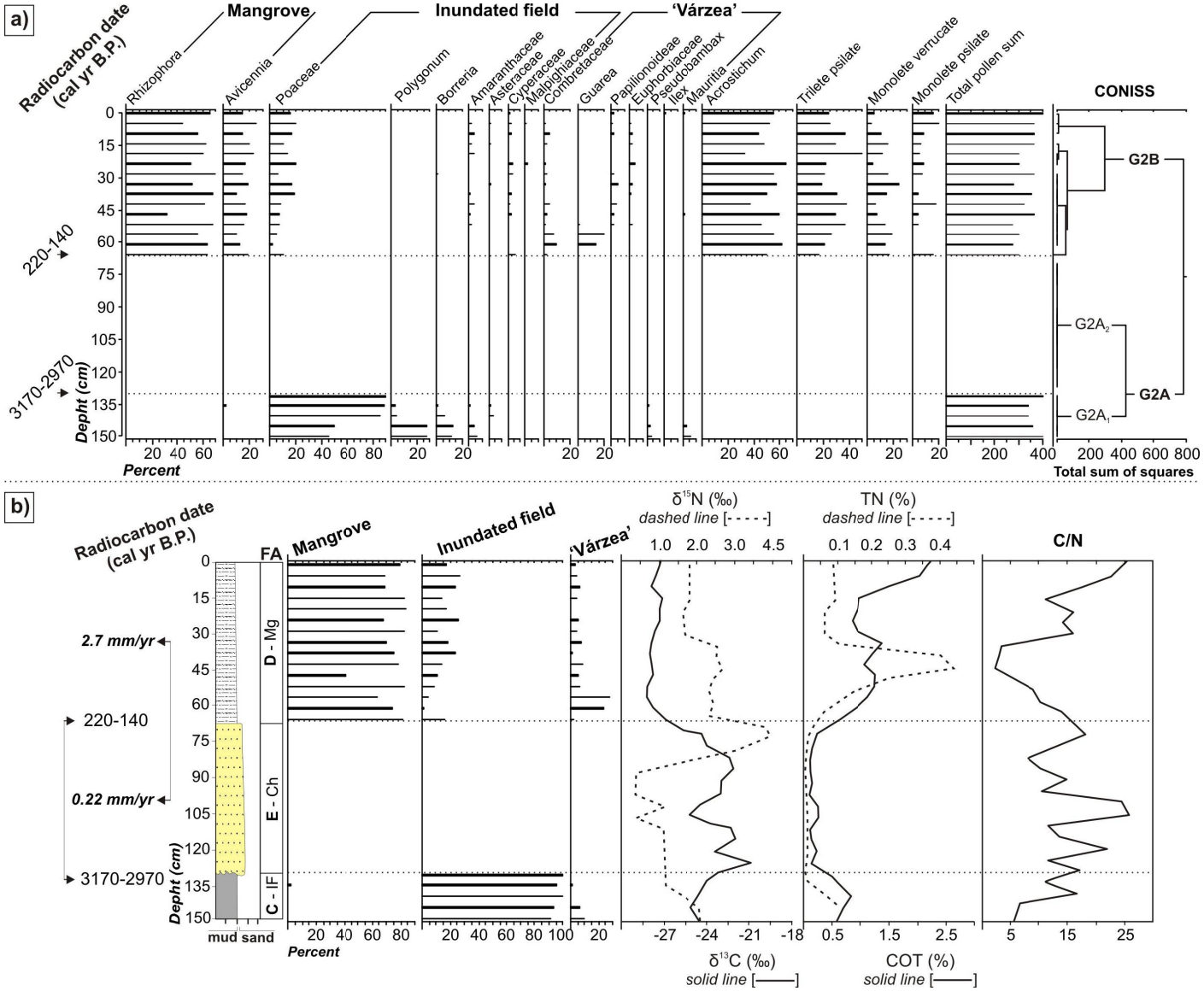

Figure 4. Integrated graphics, a) pollen diagram and b) interproxy records of G2 core.

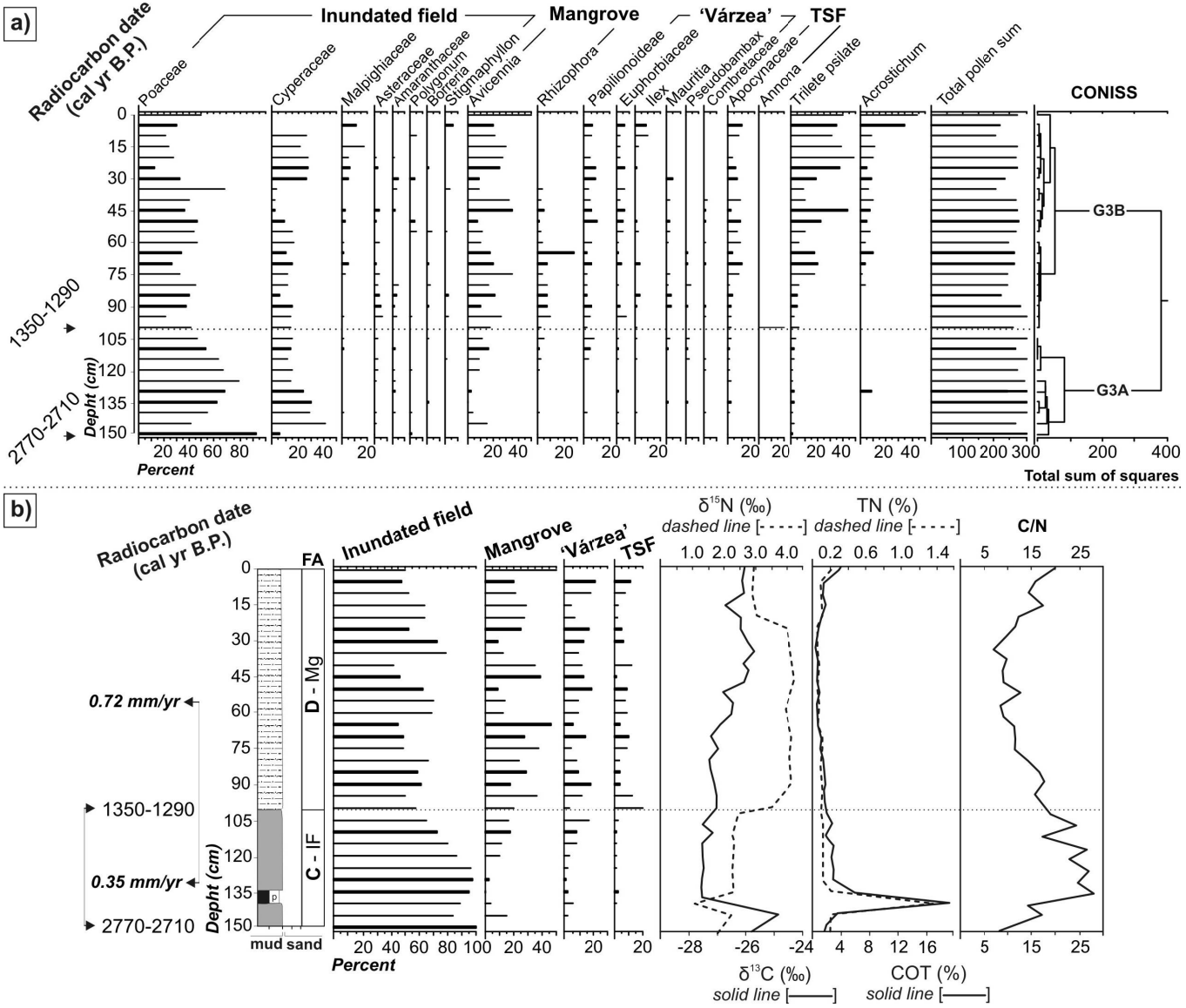

Figure 5. Integrated graphics, a) pollen diagram and b) interproxy records of G3 core.

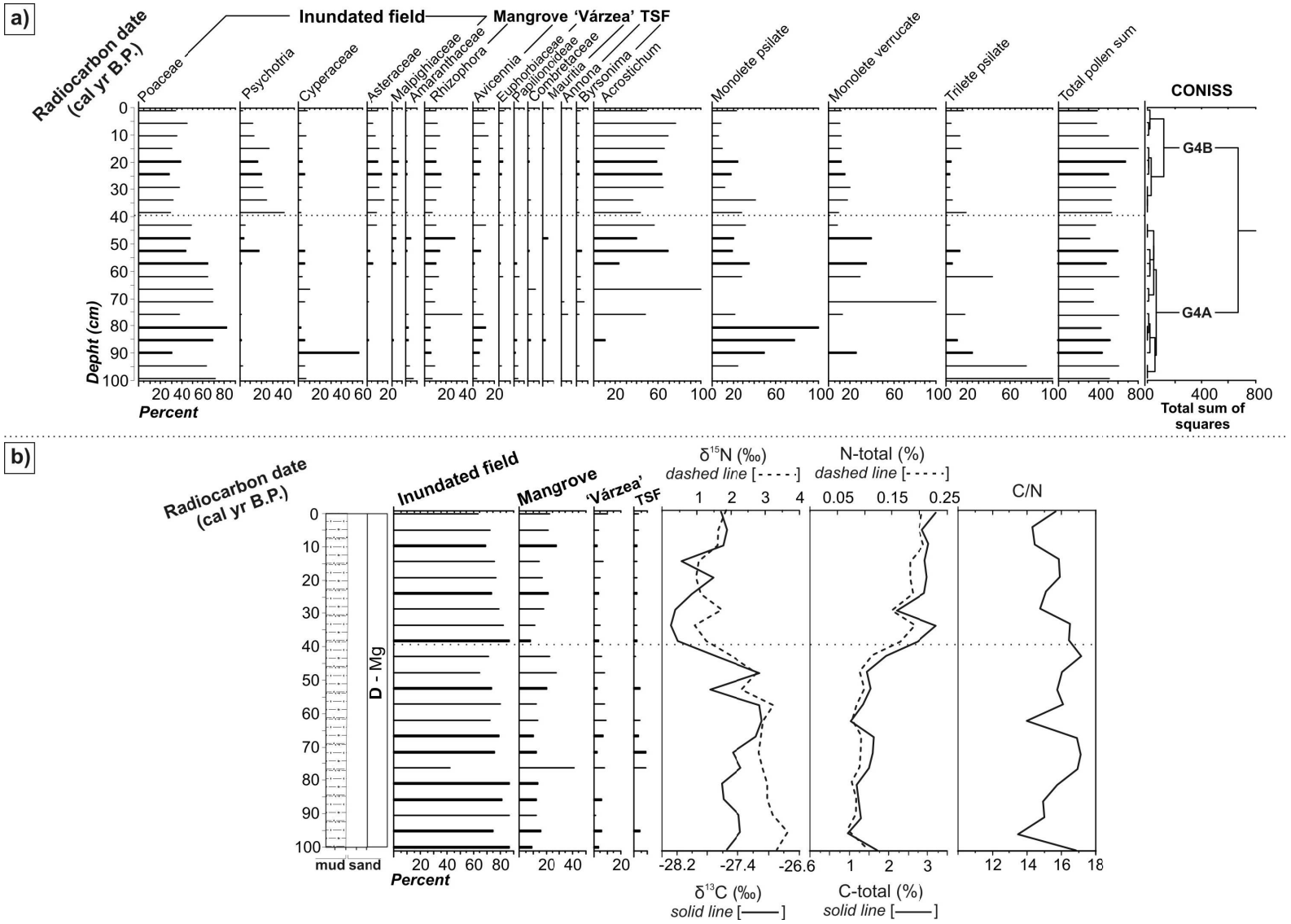

Figure 6. Integrated graphics, a) pollen diagram and b) interproxy records of G4 core.

Facies association B (Small-scale point-bar). The association B only occur in the GI exposed terrace and core (Figure 2). It consists of massive mud with basal quartz granules (facies Ml) and inclined laminae of mud and organic matter - OM films (facies Mi), which record a product of point-bar lateral accretion within a small-scale meandering creek with high suspended load draining tidal mudflats (e.g. Thomas et al., 1987).

Facies association C (Herbaceous field). This association occurs in the upper segment of the GI site (Figure 2), and in the lowest part of G2 (> 3170 - 2970 cal. yr BP; Figure 2 and 4a, b), G3 (2770 - 2710 until 1350 - 1290 cal. yr BP; Figure 2 and 5a,b) and GC sites (Figure 2). The association C presents mud with many fine root marks, herbaceous roots and oxidized features (facies Mb(h)), and peat material (facies Pt).

The pollen assemblages of association C are dominated by herbaceous pollen and correspond to Subzone $G2A_1$ (3170 - 2970 cal. yr BP; Figure 5a) and Zone G3A (2770 - 2710 to 1350 - 1290 cal. yr BP; Figure 5a). Subzone $G2A_1$ mainly presents Poaceae (50-90%), *Polygonum* (0-29%) and *Borreri*a (0-14%) pollen. Zone G3A is represented by the predominance of Poaceae (42-94%) and Cyperaceae (6-42%) pollen. *Avicennia* pollen (0-15%) can also be found, but with very low percentages.

The $\delta^{13}C$ values (-20.9‰ to -28‰) suggest higher contribution of C3 plants (-22‰ to -25‰; Peterson et al., 1994). The herbaceous field presents an increase trend of the C/N ration (6-27) and a decrease of $\delta^{15}N$ (-0.8‰ - 2.3‰) that suggests higher influence of terrestrial organic matter in relation to aquatic material (Figure 4b and 5b).

Facies association D (Mangrove). The association D can be found in the G2 (220 - 140 cal. yr BP until the present; Figure 2 and 4a, b), G3 (1350 - 1290 cal. yr BP until the present; Figure 2 and 5a, b) and along the G4 (Figure 2, 6a, b). The facies association consists of mud with many bioturbation features (facies Mb) such as woody roots, root marks and dwelling structures produced by the benthic fauna. Although the pollen profile of G4 indicates relatively low mangrove pollen (10-45%), it is represented by the *Avicennia* pollen that is entomophylous, very low pollen producer and the main tree that colonizes the sampled mangrove area.

This association corresponds to Zone G2B (Figure 4a), G3B (Figure 5a) and G4A/G4B (Figure 6a). Zone G2B (220 - 140 cal. yr BP until the present) is mainly composed by *Rhizophora* (5-70%) and *Avicennia* (5-60%). Poaceae (2-70%), Cyperaceae (0-30%), Papilionoideae and Mimosoideae (0-20%) represent the main families of herbaceous field and

"várzea" along this zone. Zone G3B (1350 - 1290 cal. yr BP until the present) exhibits *Avicennia* (10-36%) and *Rhizophora* (0-19%) pollen. Poaceae (10-70%) and Cyperaceae (0-28) are still present. Papilionoideae and Apocynaceae (0-10%) related to "Várzea" and TSF pollen, respectively, reveal lower percentages. Zone G4A/G4B is represented by mangrove pollen of *Rhizophora* (5-35%) and *Avicennia* (2-15%), and by Poaceae (27-80%) and Cyperaceae (0-55%) pollen.

The $\delta^{13}C$ values ranging between -25‰ to -28.3‰ suggest the contribution of C3 plants and marine and freshwater organic matter. The $\delta^{15}N$ values (0.9‰ to 5‰) indicate higher aquatic influence than in association C. The C/N values between 1 and 25 also indicate a mixture of aquatic and terrestrial materials (Figure 4b, 5b and 6b).

Facies association E (Chenier/tidal mixed flat). The deposit consists of erorive base, fine sand with low-angle (Sla) and ripple cross-laminations (facies Sc) produced by wave activity. Fine to very fine sand with bioturbation (facies Sb) and mottling features probably related to illuviation and vegetation development can also be observed in the upper chenier deposit (e.g. Retallack, 2001). Pollen was not found in the association E, which corresponds to Subzone $G2A_2$ (3170 - 2970 cal. yr BP and 220 - 140 cal. yr BP; Figure 4a).

The $\delta^{13}C$ values varied from -20.9‰ to -26.9‰, the $\delta^{15}N$ from 0.4‰ to 4‰ and the C/N values from 9 to 18. These may be indicative of a mixture of terrestrial and marine organic matter (Figure 4b).

Palaeoenvironmental interpretation

Proximal portion

This zone of the tidal flat is related to the transitional sector between the costal plateau and plain (Figure 7 and 8), where widespread paleochannel networks were indentified, probably developed during the evolution of the coastal plain (Guimarães et al., submitted). Therefore, the proximal portion interpretation is supported by the location of the sampling site on a meandering paleochannel in this sector. It represents the final filling stage of the concave-up feature formed by the abandoned channel that contributed to water accumulation under very low energy flows. Fern and other terrestrial vegetation composed the surroundings of the formed lake since 5280 - 5160 cal. yr BP. The source of mud ceased and autochthonous organic material became prevalent as well as the increase in contribution of freshwater DOC and C3 plants during the last 2840 - 2750 cal. yr BP (Figure 8). At present this lake is densely colonized by "várzea" vegetation.

The herbaceous field is characterized by very low drainage density related to the rapid shifting, abandonment and silting of tidal channels resulting in small-scale points bars, elongated lakes and lake belts associated to paleochannel settings. This setting may be a product of small accommodation space and high rates of vertical accretion with large concentration of muddy sediments continuously supplied by the Amazon River, which limited the tidal flat drainage by the silting of the tidal channels. Furthermore, its relative higher topography prevents the tidal influence and mangrove development. Thus, herbaceous field may be interely considered as supratidal environment (Guimarães et al., submitted).

Considering the topographic feedback on patterns of mud settling during the tidal excursion, processes of evaporation, dissection by intertidal drainage channels and colonization by mangroves; the linear bar-like features may be formed from a gradual accumulation of fluid mud inshore within a framework of predominantly tidal modulation of the vertical excursion of wave activity. These bars show marked cross-shore variations in the degree of consolidation that reflect three factors: intertidal elevation; trapping of fluid mud in depressions between the bars; and mud remobilization and fluidization by wave activity. Once in the supratidal zone, the bars become immobilized over fairly long phases of low wave energy, and, thus, progressively dry out. This involves changes in physical parameters, notably yield stress and pore-water salinity because of evaporation and dewatering (Fiot and Gratiot, 2006; Gardel et al., 2009).

Herbaceous field already colonized the tidal flat before 3170 - 2970 cal. yr BP on G2 site (Figure 7 and 8). The increase trend of C/N values to ~ 25 and $\delta^{15}N$ values ~ 2 of the herbaceous field phase corresponds to lower aquatic influence on G3 site (Figure 5), and afterward, around 1350-1290 cal. yr BP, the C/N values decrease and the $\delta^{15}N$ increase due to the aquatic influence. It marked the replacement of herbaceous field by the mangrove, probably, under brackish water influence.

Another possibility to herbaceous field development may be concerned in the influence of base level changes, regarding that herbaceous field, before 3170 - 2970 cal. yr BP, was at least 1 m below the current surface of intertidal zone (Figure 4, 5 and 7), would be reasonable to consider an old relative sea-level lower than the current one to allow the herbaceous field development without the tidal influence.

According to the G3 site (Figure 5), around 1350-1290 cal. yr BP, the herbaceous fields were replaced by the mangroves of about 1 m below the current mangrove surface, following the development of secondary channels. Thus, considering this hypothesis, during herbaceous field phase (>2770-2710 and 1350-1290 cal. yr B.P.) the sedimentation rate kept pace with

the relative sea-level rise until 1350-1290 cal. yr B.P., when the herbaceous field was replaced by mangroves due to a marine incursion. The RSL rise curves to Venezuela and Suriname during the Holocene were described by Milne et al. (2005), and according to Guimarães et al. (in press), during the late Holocene occurred an increase in the Amazon River discharge that produced significant vegetation changes along the Amapá littoral.

Considering the effects of the run-off and river discharge on the relative sea-level along the littoral (e.g. Mörner, 1996, 1999; Cohen et al., 2005), the RSL rise proposed to the Amapá littoral during the late Holocene may be related to the increase of Amazon River discharge.

Distal portion

This zone is mainly characterized by cheniers, and they are long, linear deposits representing the locations of ancient shorelines, changes in sediment supply, river discharge, sea level and storminess among others (Augustinus, 1989). Various studies have shown that they occur most commonly on low-relief coastal plains, their crests generally laying several meters above the surrounding marshland (Augustinus et al., 1989, Augustinus, 2004). They may occur singly or as multiple sets of ridges running roughly parallel to the shoreline, forming a chenier plain. These ridges can be further classified, in relation to the movement of the shoreline, as "transgressive" (landward migration) or "regressive" (seaward migration) (Curray, 1964).

The "transgressive" cheniers are characterized by thicker sediment with successive erosive episodes and intense landward migration that overlies the reworked chenier. The "transgressive" chenier implies strong erosive processes with intense shoreline retrogradation (Ramirez and Yáñes-Camacho, 2008).

Considering the studied site, part of distal portion of the tidal flat related to herbaceous field was eroded due to wave-winnowing of muddy sediments and subsequent concentration of coarser particles, with terrestrial and marine organic matter, to form chenier ridges/tidal mixed flat after 3170-2970 cal. yr BP and before 220-140 cal. yr BP in the distal portion (Figure 7 and 8). This erosive process may also have led the creation of the secondary channels that allowed the mangrove establishment in the study site between this time interval (see subsection *Proximal portion*).

According to Prost (1989) and Augustinus et al. (1989), the studied chenier ridges may be formed by decadal northwestern migration of shoreface-attached mud banks and interbanks, allowing the evolution of accretion (mudflat) and erosive (chenier ridges) profiles, respectively. The mud-bank formation is controlled by the physical oceanography of the continental shelf seaward of the mouth of the Amazon, which is an initial seafloor storage

area for much of the suspended sediment discharged by the river (Trowbridge and Kineke, 1994; Geyer and Kineke, 1995; Geyer et al., 2004). These authors have highlighted rapid and sustained fluid-mud concentration and trapping associated with freshwater/saltwater interaction and front activity over the shoreface, a precursor condition for the formation of the mud banks. This sediment is then remobilized and transported shoreward and then alongshore by a complex combination of wave forcing, tidal currents and wind-induced coastal currents.

The dynamic of the mud bank with the shore commonly creates an intertidal mudflat of several square kilometers in a few months, with very dense mangrove development in a few years, followed by rapid erosion of mangroves and their substrate during the inter-bank phase. The large mud supply also implies that in situ mangrove ecological dynamics are closely controlled by topographic changes brought by mud redistribution. Smothering of pneumatophores and suffocation of older mangroves commonly occur, for instance, as a result of fresh mud inputs that are driven ashore from the bank (Anthony et al., 2010). Thus, the littoral is easily eroded when the mud banks migrate (e.g. Allison et al., 2000; Augustinus, 2004). Nevertheless, Silveira (1998) suggested sedimentation and erosive process operating at larger temporal and spatial scale on chenier ridges development between 5000 and 3000 cal. yr BP between Cunani and Cassiporé River, north of Calçoene River. Additionally, the large-scale process of chenier formation presented in this work reinforce this interpretation.

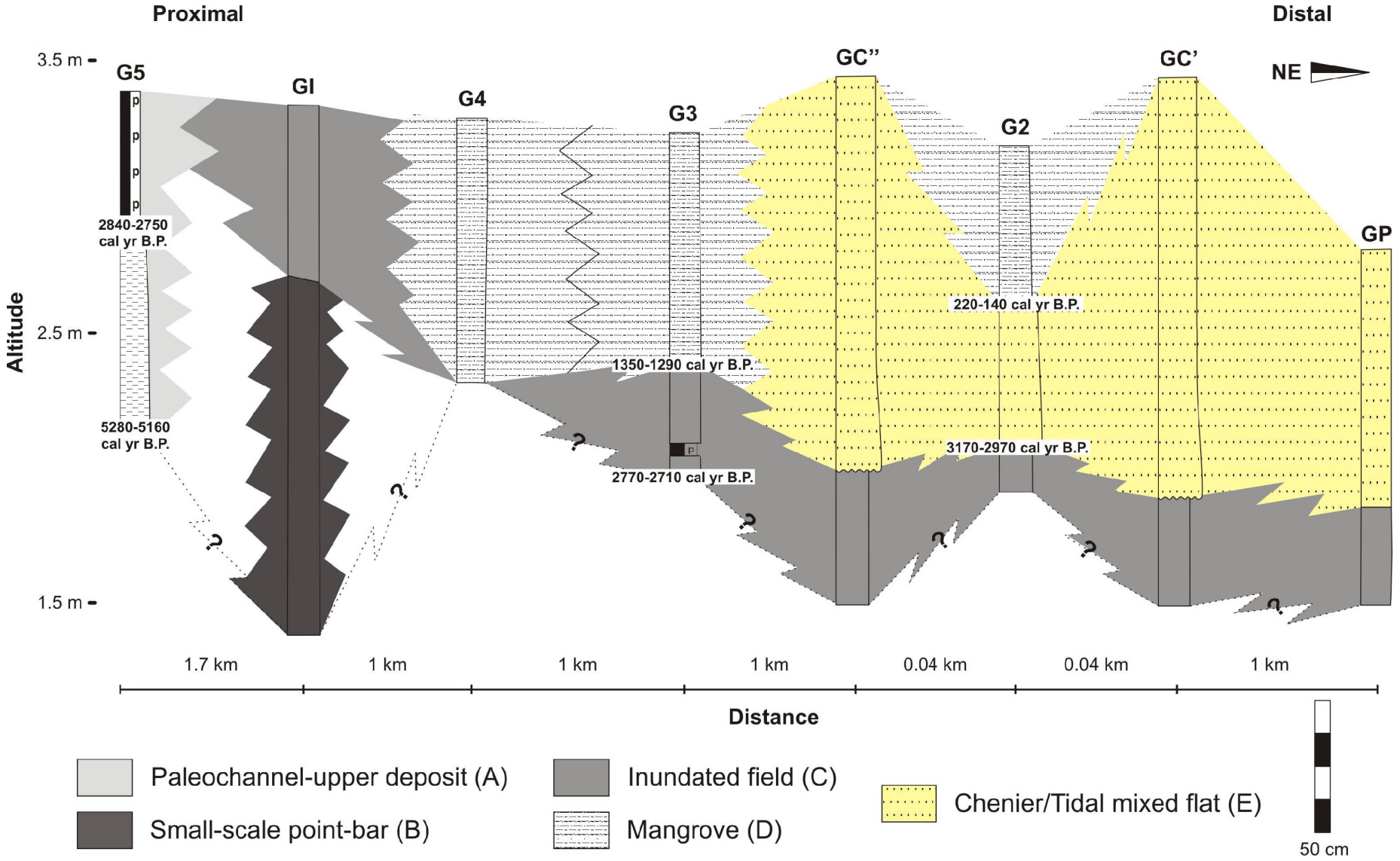

Figure 7. Correlation of the sedimentary profiles.

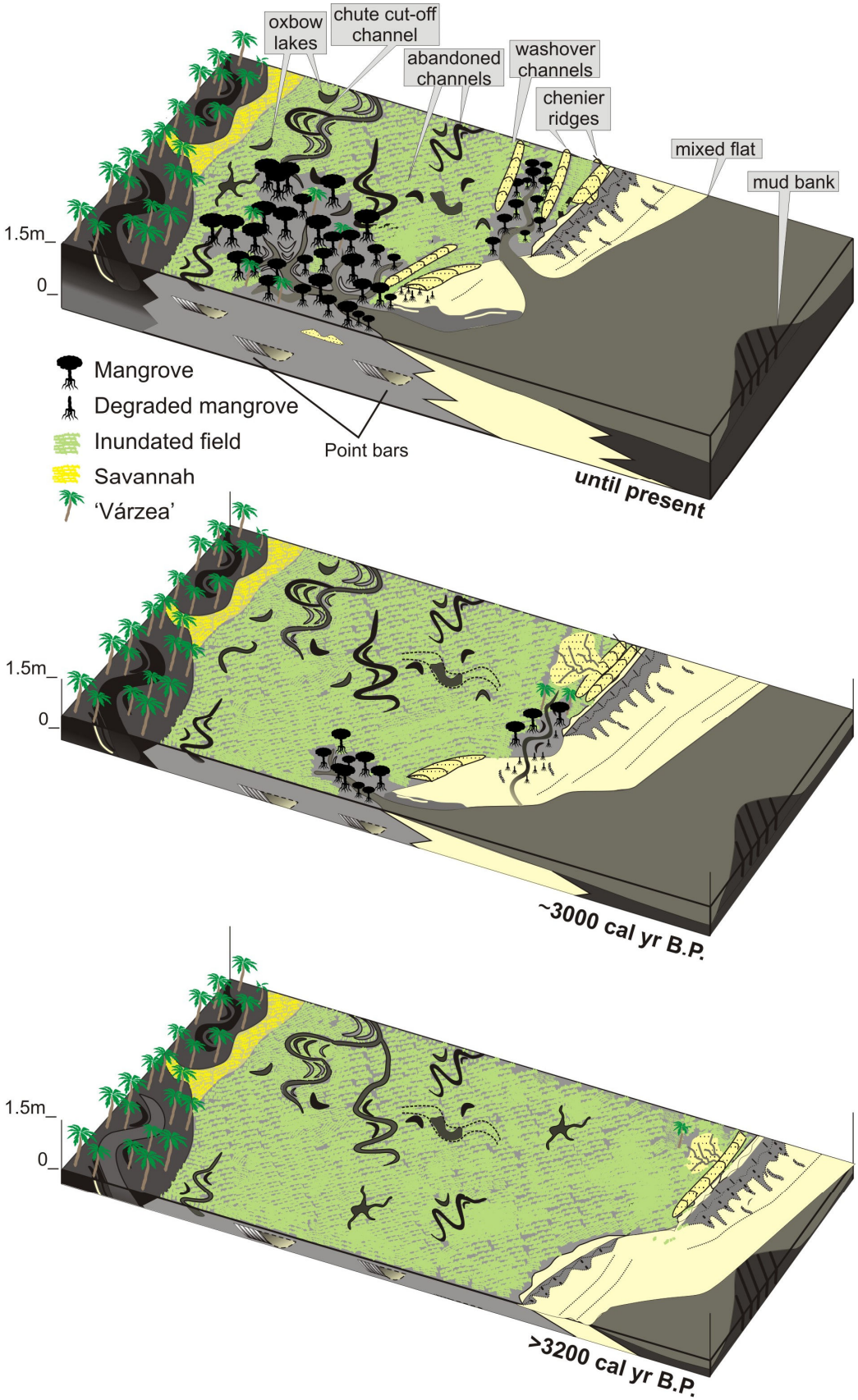

Figure 8. Evolutionay model showing main morphological and geobotanical units trough time of tidal flats near the mouth of the Amazon River

Conclusion

The integrated geomorphological, sedimentological, palynologycal, C/N ratio and isotope data indicate that vegetation development along the Calçoene Coastal Plain during the mid and late Holocene occurred basically influenced by the tidal channel dynamic, relative sea-level and chenier ridges formation. The data indicate a mud-rich tidal flat that presents alternations between supra and intertidal environments.

The proximal portion of the tidal flat is related to the transitional sector between the costal plateau and plain. It represents the final filling stage of the concave-up feature formed by the abandoned channel that contributed to water accumulation under very low energy flows, fern and other terrestrial vegetation establishment surrounding the formed lake since 5280 - 5160 cal. yr BP. The source of mud ceased and autochthonous organic material became prevalent as well as the increase in contribution of freshwater DOC and C3 plants, mainly represented by "várzea" vegetation, during the last 2840 - 2750 cal. yr BP. On the distal portion, the sediment accumulation during herbaceous field phase (>3170-2970 and 1350-1290 cal. yr BP) may kept pace with or without base level changes (e.g. relative sea-level). Subsequently, after 1350-1290 cal. yr BP, occurred a marine incursion by the evolution of secondary channels that allowed the mangrove development.

Part of distal portion of the tidal flat related to herbaceous field was eroded due to the formation of chenier ridges between 3170-2970 cal. yr BP and 220-140 cal. yr BP. Thus, This stacking pattern of sediments indicating a retrogradation, with distal facies over proximal facies, and gradual transition of herbaceous to mangrove sediment (e.g. G3 site) suggest that the creation of accommodation space may be produced during an increase of wave action, tidal inundation frequency and evolution of secondary channels in the study site with possible influence of relative sea-level rise.

Acknowledgements

The authors thank the members of the Laboratório de Dinâmica Costeira and Grupo de Grupo de Análises de Bacias Sedimentares da Amazônia - Universidade Federal do Pará, especially to Prof. Dr. Afonso César Rodrigues Nogueira for the numerous comments and suggestions that helped to significantly improve this manuscript and the Laboratório de Carbono 14 - Centro de Energia Nuclear na Agricultura, Universidade de São Paulo-USP.

Funding

This work was funded by CNPq (Project 562398/2008-2). The first and second authors hold a scholarship from CNPq (Process 143518/2008-9 and 302943/2008-0).

References

Absy ML, Clief A, Fournier M, Martin L, Servant M, Siffeddine A, Silva FD, Soubiès F, Suguio KT, Van der Hammen T (1991). Mise em évidence de Quatre phases d'ouverture de la forêt dense dans le sud-est de L'Amazonie au cours des 60,000 dernières années. Première comparaison avec d'autres régions tropicales. *Comptes Rendus Academie des Sciences Paris* 312: 673-678.

Allison MA, Nittrouer CA, Kineke GC (1995) Seasonal sediment storage on mudflats adjacent to the Amazon River. *Marine Geology* 125: 303-328.

Allison MA, Lee MT, Ogston AS, Aller RC (2000) Origin of Amazon mudbanks along the northeastern coast of South America. *Marine Geology* 163: 241-256.

Allison MA (2004) Sediment exchange between Amazon mudbanks and shore-fringing mangroves in French Guiana. *Marine Geology* 208: 169-190.

Alongi DM (2008) Mangrove forests: Resilience, protection from tsunamis, and responses to global climate change. *Estuarine, Coastal and Shelf Science* 76: 1-13.

ANA (2003) Hydrological information system. Brazilian National Water Agency. On line dataset, 14.3 MB, http://hidroweb.ana.gov.br/baixar/mapa/Bacia1.zip.

Anthony EJ, Gardel A, Gratiot N, Proisy C, Allison MA, Dolique F, Fromard F (2010) The Amazon-influenced muddy coast of South America: A review of mud-bank-shoreline interactions. *Earth-Science Reviews* 103: 99-121.

Augustinus PGEF (1989) Cheniers and chenier plains: a general introduction. *Marine Geology* 90: 219-229.

Augustinus PGEF, Hazelhoff L, Kroon A (1989) The chenier coast of Suriname: modern and geological development. *Marine Geology* 90: 269-281.

Augustinus PGEF (2004) The influence of the trade winds on the coastal development of the Guianas at various scale levels: a synthesis. *Marine Geology* 208: 145-151.

Azevedo RP (1991) Tectonic Evolution of Brazilian Equatorial Continental Margin Basins. PhD Thesis, Royal School of Mines Imperial College, London.

Beardsley RC, Candela J, Limeburner R, Geyer WR, Lentz SJ, Castro BM, Cacchione D, Carneiro N (1995) The M2 tide on the Amazon shelf. *Journal of Geophysical Research* 100: 2283-2319.

Behling H and Hooghiemstra H (2000). Holocene Amazon rain forest - savanna dynamics and climatic implications: high resolution pollen record Laguna Loma Linda in eastern Colombia. *Journal of Quaternary Science* 15, 687-695.

Behling H and Costa ML (2000). Holocene environmental changes from the Rio Curuá record in the Caxiuanã region, eastern Amazon Basin. *Quaternary Research* 53: 369-377.

Behling H, Cohen MCL, Lara RJ (2004) Late Holocene mangrove dynamics of Marajó Island in Amazonia, northern Brazil. *Vegetation History and Archaeobotany* 13: 73-80.

Bezerra PEL, Oliveira W, Regis WDE, Brazão JEM, Gavinho J, Coutinho RCP (1990) Amazônia legal: zoneamento das potencialidades e dos recursos naturais. In: Instituto Brasileiro de Geografia e Estatística, Superintendência de Desenvolvimento da Amazônia. Projeto zoneamento das potencialidades dos recursos naturais da Amazônia: geologia, solos e vegetação. Div. 5. Rio de Janeiro, pp. 9-89.

Blasco F, Saenger P, Janodet E (1996) Mangroves as indicators of coastal change. *Catena* 27: 167-178.

Boutton TW, Archer SR, Midwood AJ, Zitzer SF, Bol R (1998) $\delta^{13}C$ values of soil organic carbon and their use in documenting vegetation change in a subtropical savanna ecosystem. *Geoderma* 82: 5-41.

Bradley RS (1999) Paleoclimatology: Reconstructing Climates of the Quaternary. Academic Press. 613pp.

Bush MB, Silman MR, Listopad CMCS (2007) A regional study of Holocene climate change and human occupation in Peruvian Amazonia. *Journal of Biogeography* 34: 1342-1356.

Carvalho FP, Costa Neto SV, Costa WJP, Coutinho RS, Figueira ZR, Figueiredo SL, Martins MHA, Santos VF, Silva AQ, Silva LMA, Silva MS, Silveira OFM, Takyiama LR (2006) Atlas Zoneamento Costeiro Estuarino do Estado do Amapá. Macapá, PNMA/SQA/MMA. 77pp.

Cohen MCL (2003) Past and current mangrove dynamics on the Bragança peninsula, northern Brazil. PhD Thesis, Bremen, University of Bremen, Center for Tropical Marine Ecology. 110pp.

Cohen MCL and Lara RJ (2003) Temporal changes of vegetation boundaries in Amazonia: Application of GIS and Remote sensing techniques. *Wetlands Ecology and Management* 11: 223-231.

Cohen MCL, Behling H, Lara RJ (2005) Amazonian mangrove dynamics during the last millennium: The relative sea-level and the Little Ice Age. *Review of Palaeobotany and Palynology* 136: 93-108.

Cohen MCL, Lara RJ, Smith CB, Angélica RS, Dias BS, Pequeno T (2008) Wetland dynamics of Marajó Island, northern Brazil, during the last 1000 years. *Catena* 76: 70-77.

Cohen MCL, Lara RJ, Smith CB, Matos HRS, Vedel V (2009). Impact of sea-level and climatic changes on the Amazon coastal wetlands during the late Holocene. *Vegetation History and Archaeobotany* 18: 425-439.

Colinvaux PA, De Oliveira PE, Patiño JEM (1999) *Amazon Pollen Manual and Atlas - Manual e Atlas Palinológico da Amazônia*. Amsterdam: Hardwood Academic, 332 pp.

Costa JB, Hasui Y, Bemerguy RL, Soares-Júnior AV, Villegas J (2002) Tectonics and paleogeography of the Marajó Basin, northern Brazil. *Anais da Academia Brasileira de Ciências* 74: 519-531.

Costa Neto SV (2004) Relatório de vegetação: Subsídio ao diagnostico sócio ambiental. Relatório Técnico. Macapá, IEPA/GERCO, 32pp.

Costa Neto SV and Silva MS (2004) Vegetação do setor costeiro estuarino do estado do Amapá. Instituto de Pesquisas Científicas e Tecnológicas do Estado do Amapá. Governo do Estado do Amapá. Cap. 5. Projeto Zoneamento Econômico-Ecológico do setor costeiro estuarino: diagnóstico sócio ambiental participativo do setor costeiro estuarino, pp.72-96.

Costa Neto SV, Senna C, Tostes LCL, Silva SRM (2007) Macrófitas aquáticas das Regiões dos Lagos do Amapá, Brasil. *Revista Brasileira de Biociências* 5: 618-620.

CPRM (2010) *Geological information system.* Brazilian Geological Service. On line dataset, Folhas NA/SA-22 23 MB, http://geobank.sa.cprm.gov.br/.

Curray JR (1969) Shore zone sand bodies, barriers, cheniers and beach ridges. In: Stanley DJ and Curray JR (Eds.), *The New Concepts of Continental Margin Sedimentation*, Alexandria: American Geological Institute.

Dalrymple RW (1992) Tidal depositional systems. In: Walker RG and James NP (Eds.), Facies Models - Response to Sea Level Change. Ontario: Geological Association of Canada, 195-218.

Deines P (1980) The isotopic composition of reduced organic carbon. In: Fritz P and Fontes JC (Eds.), *Handbook of Environmental Isotope Geochemistry*. The Terrestrial Environment, vol.1. Amsterdam: A. Elsevier, 329-406.

Desjardins T, Filho AC, Mariotti A, Chauvel A, Girardin C (1996) Changes of the forest-savanna boundary in Brazilian Amazonia during the Holocene as revealed by soil organic carbon isotope ratios. *Oecologia* 108: 749-756.

Dott RH and Howard JK (1962) Convolute lamination in non-grained sequences. *Journal of Geology* 70: 114-120.

Duke NC, Ball MC, Ellison JC (1998) Factors influencing biodiversity and distributional gradients in mangroves. *Global Ecology and Biogeography Letters* 7: 27-47.

Eisma D, Augustinus PGEF, Alexander CR (1991) Recent and subrecent changes in the dispersal of Amazon mud. *Netherlands Journal Sea Research* 28: 181-192.

Faegri K and Iversen J (1989) Textbook of Pollen Analyses. Chichester: John Wiley and Sons LTD, 328pp.

Fiot J and Gratiot N (2006) Structural effects of tidal exposure on mud flats along the French Guiana coast. *Marine Geolology* 228: 25-37.

Freitas HA, Pessenda LCR, Aravena R, Gouveia SEM, Ribeiro AS, Boulet R (2001) Late Quaternary vegetation dynamics in the Southern Amazon Basin inferred from carbon isotopes in soil organic matter. *Quaternary Research* 55: 39-707.

Fromard F, Vega C, Proisy C (2004) Half a century of dynamic coastal change affecting mangrove shorelines of French Guiana. A case study based on remote sensing data analyses and field surveys. *Marine Geology* 208: 265-280.

Gallo MN and Vinzon S (2005) Generation of over tides and compound tides in Amazon estuary. *Ocean Dynamics* 55: 441-448.

Gardel A, Proisy C, Lesourd S, Philippe S, Caillaud J, Gontharet S, Anthony EJ, Brutier L (2009) A better understanding of mud cracking processes gained from in situ measurements on an intertidal mudflat in French Guiana. *Journal of Coastal Research* SI 56: 424-428.

Geyer WR and Kineke GC (1995) Observations of currents and water properties in the Amazon frontal zone. *Journal of Geophysical Research* 100: 2321-2339.

Geyer WR, Hill PS, Kineke GC (2004) The transport, transformati on and dispersal of sediment by buoyant coastal flows. *Continental Shelf Research* 24: 927-949.

Gornitz V (1991) Global coastal hazards from future sea level rise. *Palaeogeography*, *Palaeoclimatology*, *Palaeoecology* 89: 379-720.

Grimm EC (1987) CONISS: a FORTRAN 77 program for stratigraphically constrained cluster analysis by the method of the incremental sum of square. *Computer and Geosciences* 13: 13-35.

Guimarães JTF, Cohen MCL, França MC, Lara RJ, Behling H (2010) Model of wetland development of the Amapá coast during the late Holocene. *Anais da Academia Brasileira de Ciências* 82: 451-465.

Guimarães JTF, Cohen MCL, Pessenda LCR, França MC, Smith CB, Nogueira ACR (in press). Mid and late Holocene sedimentary process and palaeovegetation changes near the mouth of the Amazon River. *The Holocene*.

Guimarães JTF, Cohen MCL, França MC (submitted). Short-term morphological and geobotanical analysis of tidal flats near the mouth of the Amazon River. *Earth Surface Process and Landscape*.

Hesse M, Halbritter H, Zetter R, Weber M, Buchner R, Frosch-Radivo A, Ulrich S. 2008. *Pollen terminology*: *An illustrated handbook*. New York: Springer. 264pp.

Kao WY, Shih CN, Tsai TT (2004) Sensitivity to chilling temperatures and distribution differ in the mangrove species Kandelia candel and Avicennia marina. *Tree Physiology* 24: 859-864.

Keeley JE and Sandquist DR (1992) Carbon: freshwater plants. *Plant, Cell and Environment* 15: 1021-1035.

Klein GV (1971) A sedimentary model for determining paleotidal range. *Geological Society of America Bulletin* 82: 2585-2592.

Kjerfve B and Lacerda LD (1993) Mangroves of Brazil. In: *Conservation and sustainable utilization of mangroves forests in Latin America and Africa regions*. Part 1: Latin America. 1993. ITTO/ISME Project PD114/90(F), p. 245-272.

Krauss KW, Lovelock CE, McKee KL, López-Hoffman L, Ewe SML, Sousa WP (2008) Environmental drivers in mangrove establishment and early development: A review. *Aquatic Botany* 89: 105-127.

Lara RJ and Cohen MCL (2009) Palaeolimnological studies and ancient maps confirm secular climate fluctuations in Amazonia. *Climatic Change* 94: 399-408.

Latrubesse EM and Franzinelli E (2002) The Holocene alluvial plain of the middle Amazon River, Brazil. *Geomorphology* 44: 241-257.

Ledru MP (2001) Late Holocene rainforest disturbance in French Guiana. *Review of Palaeobotany and Palynology* 115: 161-176.

Lentz SJ (1995) The Amazon River plume during AMASSEDS: subtidal current variability and the importance of wind forcing. *Journal of Geophysical Research* 100: 2377-2390.

Lentz SJ and Limeburner R (1995) The Amazon River Plume during AMASSEDS: Spatial characteristics and salinity variability. *Journal of Geophysical Research* 100: 2355-2375.

Lima MIC, Bezerra PE, Araújo HJT (1991) Sistematização da Geologia do Estado do Amapá. In: *Simpósio de geologia da Amazônia*, vol. 3, Belém. Anais. SBG. pp. 322-335.

Marzo M and Puigdefábregas C (1993) *Alluvial Sedimentation.* Blackwell Scientific Publications, Oxford, 600 pp.

Maslin MA and Burns SJ (2000) Reconstruction of the Amazon Basin effective moisture availability over the past 14,000 years. *Science* 290: 2285-2287.

Mayle FE and Power MJ (2008) Impact of a drier Early-Mid-Holocene climate upon Amazonian forests. *Philosophical Transactions of the* Royal Society *B* 363: 1829-1838.

Meyers PA (1994) Preservation of elemental and isotopic source identification of sedimentary organic matter. *Chemical Geology* 114: 289-302.

Meyers PA (1997) Organic geochemical proxies of paleoceanographic, paleolimnologic and paleoclimatic processes. *Organic Geochemistry* 27: 213-250.

Miall AD (1978) Facies types and vertical profile models in braided river deposits: a summary. In: Miall AD (ed) *Fluvial sedimentology*. Calgary: Canadian Society of Petroleum Geologists, 597-604.

Milne GA, Long JA, Bassett SE. 2005. Modelling Holocene relative sea-level observations from the Caribbean and South America. *Quaternary Science Reviews* 24: 1183-1202.

Mörner NA (1996) Global change and interaction of earth rotation, ocean circulation and paleoclimate. *Anais da Academia Brasileira de Ciências* 68: 77-94.

Mörner NA (1999) Sea level and climate: rapid regressions at local warm phases. *Quaternary International* 60: 75-82.

Osmond CB, Valaane N, Haslam SM, Uotila P, Roksandic Z (1981) Comparisons of $\delta^{13}C$ values in leaves of aquatic macrophytes from different habitats in Britain and Finland; some implications for photosynthetic processes in aquatic plants. *Oecologia* 50: 117-124.

Pessenda LCR, Boulet R, Aravena R, Rosolen V, Gouveia SEM, Ribeiro AS, Lamote M (2001) Origin and dynamics of soil organic matterand vegetation changes during the Holocene in a forest-savanna transition zone, Brazilian Amazon region. *The Holocene* 11: 250-254.

Peterson BJ, Fry B, Hullar M, Saupe S, Wright R (1994) The distribution and stable carbon isotope composition of dissolved organic carbon in estuaries. *Estuaries* 17: 111-121.

Prost MT (1989) Coastal dynamics and chenier sands in French Guiana. *Marine Geology* 90: 259-267.

Pugh DT (1987) *Tides, surges and mean sea-level*: *a Handbook for Engineers and Scientists*. London: Wiley. 486 pp.

Ramirez A and Yáñes-Camacho CM (2008) Formation of chenier plain of the Doñana marshland (SW Spain): Observations and geomorphic model. *Marine Geology* 254: 187-196.

Reimer PJ, Baillie MGL, Bard E, Bayliss A, Beck JW, Bertrand CJH, Blackwell PG, Buck CE, Burr GS, Cutler KB, Damon PE, Edwards RL, Fairbanks RG, Friedrich M, Guilderson TP, Hogg AG, Hughen KA, Kromer B, McCormac FG, Manning SW, Ramsey CB, Reimer RW, Remmele S, Southon JR, Stuiver M, Talamo S, Taylor FW, Van der Plicht J, Weyhenmeyer CE (2004) IntCal04 Terrestrial radiocarbon age calibration, 26 - 0 ka BP. *Radiocarbon* 46: 1029-1058.

Retallack GJ (2001) *Soils of the past – An introduction to Paleopedology* (2nd ed.). Wiley-Blackwell. 512 pp.

Rosario RP, Bezerra MOM, Vinzon SB (2009) Dynamics of the saline front in the Northern Channel of the Amazon River - influence of fluvial flow and tidal range (Brazil). *Journal of Coastal Research* 2: 503-514.

Roubik DW and Moreno JE (1991) *Pollen and Spores of Barro Colorado Island*. Missouri Botanical Garden, 268 pp.

Semeniuk V (1994) Predicting the Effect of Sea-level Rise on Mangroves in Northwestern Australia. Journal of Coastal Research 10: 1050-1076.

Silveira OFM (1998) A Planície costeira do Amapá: dinâmica de ambiente costeiro influenciado por grandes fontes fluviais quaternárias. PhD Thesis. Programa de Pós-Graduação em Geologia e Geoquímica, Universidade Federal do Pará. 215 pp.

Smith CB, Cohen MCL, Pessenda LCR, França MC, Guimarães JTF, Rossetti DF, Lara, RJ (in press). Coastal vegetation changes at the mouth of the Amazon during the Holocene. *Review of Palaeobotany and Palynology*.

Souza EJ and Pinheiro RVL (2009) Relações entre as estruturas tectônicas do embasamento e o desenvolvimento da paisagem da região costeira do estado do Amapá uma investigação sobre reativações tectônicas e acumulação de hidrocarbonetos. Relatório técnico-científico, Brasília: ANP, 105 p.

Souza Filho PWM, Cohen MCL, Lara RJ, Lessa GC, Koch B, Behling H (2006) Holocene coastal evolution and facies model of the Bragança macrotidal flat on the Amazon mangrove coast, Northern Brazil, *Journal of Coastal Research* SI 39: 306-310.

Souza Filho PWM, Lara RJ, Silveira OFM, Miranda FP (2007) The Amazon Mangrove Coast: The Role of Geological Factors in its Evolution During the Quaternary. In:

American Geophysical Union AJoint Assembly, Acapulco. *Abstracts*. Washington D.C.: EOS Trans. AGU, 2007. v. 1. p. OS23D-04-OS23D-04.

Stuart SA, Choat B, Martin KC, Holbrook NM, Ball MC (2007) The role of freezing in setting the latitudinal limits of mangrove forests. *New Phytologist* 173: 576-583.

Szatmari P, Françolin JBL, Zanotto O, Wolff S (1987) Evolução tectônica da margem equatorial brasileira. *Revista Brasileira de Geociências* 17: 180-188.

Thomas RG, Smith DG, Wood JM, Visser J, Calverly-Range EA, Koster EH (1987) Inclined heterolithic stratification: terminology, description, interpretation and significance. *Sedimentary Geology* 53: 123-179.

Thornton SF and McManus J (1994) Applications of organic carbon and nitrogen stable isotope and C/N ratios as source indicators of organic matter provenance in estuarine systems: evidence from the Tay Estuary, Scotland. *Estuarine, Coastal and Shelf Science* 38: 219-233.

Toledo MB and Bush MB (2007) A mid-Holocene environmental change in Amazonian savannas. *Journal of Biogeography* 34: 1313-1326.

Trowbridge JH and Kineke GC (1994) Structure and dynamics of fluid muds on the Amazon continental shelf. *Journal of Geophysical Research Oceans* 99 (C1): 865-874.

Tyson RV (1995) *Sedimentary Organic Matter: Organic Facies and Palynofacies*. London: Chapman and Hall. 15 pp.

Vedel V, Behling H, Cohen MCL, Lara RJ (2006) Holocene mangrove dynamics and sea-level changes in Taperebal, northeastern Pará State, northern Brazil. *Vegetation History and Archaeobotany* 15: 115-123.

Vinzon BS, Vilela CPX, Pereira LCC (2008) Processos físicos na Plataforma Continental Amazônica. Relatório-Técnico, Potenciais Impactos Ambientais do Transporte de Petróleo e Derivados na Zona Costeira Amazônico. Petrobrás, Brasil, 31 pp.

Walker RG (1992) Facies, facies models and modern stratigrahic concepts. In: Walker RG and James NP (eds.), *Facies Models - Response to Sea Level Change*. Ontario: Geological Association of Canada, 1-14.

Weng C, Bush MB, Athens JS (2002) Two histories of climate change and hydrarch succession in Ecuadorian Amazonia. *Review of Palynology and Paleobotany* 120: 73-90.

Woodroffe CD, Chappell J, Thom BG, Wallensky E (1989) Depositional model of a macrotidal estuary and floodplains, South Alligator River, Northern Australia. *Sedimentology* 36: 737-756.

5 CONSIDERAÇÕES FINAIS

5.1 A EXPANSÃO DO MANGUEZAL E INFLUÊNCIA DE MATÉRIA ORGÂNICA MARINHA EM PLANÍCIE DE MARÉ ASSOCIADA AO RIO AMAZONAS DURANTE O HOLOCENO (MACAPÁ E AMAPÁ, ESTADO DO AMAPÁ)

A influência marinha e resultante expansão do manguezal ocorreram na área da cidade de Macapá, Amapá, entre 5560 - 5470 cal anos AP e ~ 5430 cal anos AP. Entre ~ 5430 e 5290-5150 cal anos AP, o manguezal retraiu e a vegetação de água doce expandiu, que sugere uma diminuição da influência marinha. Durante os últimos 3000 anos, a vegetação de água doce desenvolveu-se ao longo da planície de maré da cidade de Macapá. Entretanto, no litoral noroeste do Estado do Amapá (área da cidade do Amapá, Amapá), distante cerca de 150 km da foz do Rio Amazonas, as florestas de manguezal têm colonizado parte das planícies lamosas de maré durante os últimos 2350 - 2300 cal anos AP. Isto sugere que a influência marinha favoreceu a conservação desta vegetação, e o aumento do influxo fluvial não resultou em uma substituição completa do manguezal pela vegetação de água doce.

5.2 INFLÊNCIAS DO EL NIÑO E LA NIÑA NA GEOMORFOLOGIA COSTEIRA DOS ULTIMOS 30 ANOS (CALÇOENE, ESTADO DO AMAPÁ)

O planalto e a planície costeira são os dois compartimentos principais identificados através da análise geomorfológica da costa de Calçoene, Amapá. O planalto costeiro é limitado a oeste pelas colinas do Amapá e a leste pela planície costeira. Este compartimento possui elevações de aproximadamente 10 m, com predominância da várzea e cerrado que coexistem lateralmente próximos a extensos paleocanais meandrantes. A planície costeira apresenta canal fluvial influenciado pela maré, paleocanais, lagos e cinturão de lagos, várzea, campos herbáceos, manguezal, cadeias de *chenier*, barras lamosas alongadas de maré (BLAM), planícies lamosas e mistas de maré (não vegetadas). A análise temporal das unidades morfológicas e geobotânicas sugere uma estabilização relativa das áreas do cerrado (+1.4%), várzea (+0.2%) e manguezal (+2.2%), com a formação de extensas planícies lamosas de maré (+1800%) durante os períodos mais secos sob influência dos eventos El Niño. Os eventos La Niña são caracterizados por períodos mais úmidos que resultaram em um aumento das áreas de várzea (+2.9%) e lagos (+426%) sobre o cerrado (-9.6%), e expansão do manguezal (+14.7%) principalmente sobre os campos herbáceos (-2.6%). Assim, a diminuição do regime pluviométrico durante o El Niño pode ter reduzido o influxo do Rio Calçoene e favorecido a intensificação e propagação da maré, transporte e deposição de lama

ao longo do canal fluvial influenciado pela maré e seus canais secundários com subseqüente desenvolvimento de mangue no substrato lamoso próximo a linha de costa durante o La Niña.

5.3 MUDANÇAS GEOMORFOLÓGICAS E A RELAÇÃO CAMPOS HÉRBACEOS (SUPRAMARÉ) E MANGUEZAL (INTERMARÉ) DURANTE O HOLOCENO (CALÇOENE, ESTADO DO AMAPÁ)

A análise dos dados de morfologia, fácies sedimentares, palinologia, isótopos do carbono e nitrogênio, razão C/N e datação por ^{14}C dos sedimentos de uma planície de maré próxima à foz do Rio Amazonas indica que o desenvolvimento da vegetação durante o Holoceno médio e superior ocorreu de acordo com influência aquática e dinâmica de *chenier*. Os dados sugerem uma planície predominantemente lamosa que apresenta alternâncias entre ambientes de supra e intermaré. A porção proximal da planície de maré está relacionada ao setor transicional entre o planalto e a planície costeira, e representa o estágio final de preenchimento de um canal abandonado, que contribuiu para o acúmulo de água em fluxos de energia muito baixos, e a presença de samambaias e outra vegetação terrestre ao redor do lago formado desde 5280 - 5160 cal yr BP. Durante os últimos 2840 - 2750 cal yr BP, a fonte de lama cessou e matéria orgânica autóctone tornou-se predominante, assim como o aumento da contribuição de matéria orgânica terrestre (plantas C3), principalmente representado por vegetação de várzea. Os campos herbáceos já colonizavam a planície de maré no mínimo durante os últimos 3170 - 2970 cal yr BP. Entretanto, parte da porção distal da planície de maré relacionada com os campos herbáceos foi coberta por cadeias de *chenier* entre 3170-2970 e 220-140 cal yr BP. O estabelecimento do manguezal, caracterizado principalmente por matéria orgânica estuarina, pólen de *Rhizophora* e *Avicennia*, ocorreu após 1350-1290 cal yr B.P e 220-140 cal yr B.P. nas áreas G3 e G2, respectivamente. Este padrão de empilhamento dos sedimentos indica uma retrogradação, com fácies distais sobre fácies proximais, e transição gradual dos depósitos herbáceos para manguezal. Assim, a criação do espaço de acomodação foi produzida durante um aumento da ação de ondas, freqüência de inundação da maré e evolução de canais secundários na área de estudo, com provável influência de um aumento no nível relativo do mar.

REFERÊNCIAS

Absy, M.L., Clief, A., Fournier, M., Martin, L., Servant, M., Siffeddine, A., Silva, F.D., Soubiès, F., Suguio, K.T., Van der Hammen, T. 1991. Mise em évidence de Quatre phases d'ouverture de la forêt dense dans le sud-est de L'Amazonie au cours des 60,000 dernières années. Première comparaison avec d'autres régions tropicales. *Comptes Rendus Academie des Sciences Paris*, **312**: 673-678.

Allen, J.R.L. 1965. A review of the origin and characteristics of recent alluvial sediments. *Sedimentology*, **5**: 98-191.

Allen, J.R.L. 1990. The Severn Estuary in southwest Britain: its retreat under marine transgression and fine sediment regime. *Sedimentary Geology*, **66**: 13–28.

Allen, G.P. 1991. Sedimentary processes and facies in the Gironde estuary: a recent model for macrotidal estuarine systems. In: Smith D.G., Reinson G.E., Zaitlin B.A., Rahmani R.A. (Eds), *Clastic Tidal Sedimentology*, vol. 16. Canadian Society of Petroleum Geologists Memoir, Canada, p. 29-40.

Allison, M.A., Nitrouer, C.A., Faria, L.E.C. 1995. Rates and mechanisms of shoreface grogradation and retreatdowndrift of the Amazon river mouth. *Marine Geology*, **125**: 373-392.

Allison, M.A., Lee, M.T., Ogston, A.S., Aller, R.C. 2000. Origin of Amazon mudbanks along the northeastern coast of South America. *Marine Geology*, **163**: 241–256.

Allison, M.A. & Lee, M.T. 2004.Sediment exchange between Amazon mudbanks and shore-fringing mangroves in French Guiana. *Marine Geology*, **208**: 169-190.

Alongi, D.M., Tirendi, F., Clough, B.F. 2000. Below-ground decomposition of organic matter in forests of the mangrove Rhizophora stylosa and Avicennia marina along the arid coast of Western Australia. *Aquatic Botany*, **68**: 97–122.

Alongi, D.M. 2008. Mangrove forests: Resilience, protection from tsunamis, and responses to global climate change. *Estuarine, Coastal and Shelf Science*, **76**: 1-13.

Agência Nacional das Águas (ANA) 2003. Sistema de Informações Hidrológicas. Agência Nacional de Águas. Disponível em: http://hidroweb.ana.gov.br/baixar/mapa/Bacia1.zip. Acessado em 15 de janeiro de 2008.

Agência Nacional das Águas (ANA) 2010. Sistema de Informações Hidrológicas. Agência Nacional de Águas. Disponível em: http://hidroweb.ana.gov.br/Estacao.asp?Codigo=8250002. Acessado em 08 de setembro de 2010.

Anthony E.J., Gardel, A., Gratiot, N., Proisy, C., Allison, M.A., Dolique, F., Fromard, F. 2010. The Amazon-influenced muddy coast of South America: A review of mud-bank-shoreline interactions. *Earth-Science Reviews*, **103**: 99-121.

Augustinus, P.G.E.F. 1989. Cheniers and chenier plains: a general introduction. *Marine Geology*, **90**: 219-229.

Augustinus, P.G.E.F., Hazelhoff, L., Kroon, A. 1989. The chenier coast of Suriname: modern and geological development. *Marine Geology*, **90**: 269-281.

Augustinus, P.G.E.F. 2004. The influence of the trade winds on the coastal development of the Guianas at various scale levels: a synthesis. *Marine Geology*, **208**: 145-151.

Azevedo, R.P. 1991. Tectonic Evolution of Brazilian Equatorial Continental Margin Basins. Tese de Doutorado. Royal School of Mines Imperial College, London.

Balazs, R.J. & Klein, G.V. 1972. Roudness-mineralogical relations of some intertidal sands. *Journal of Sedimentary Petrology*, **42**: 425-433.

Baltzer, F. 1970. Etude sédimentologique du marais de Mara (Côte ouest de la Nouvelle Calédonie) et de formations quaternaires voisines. Mémoires expédition française sur les récifs coralliens de la Nouvelle Calédonie, Foundation Singer-Polignac 4, 146-169.

Basan, P.B. & Frey, R.W. 1978. Actual-paleontology and neoichnology of salt marches near Sapelo Island, Georgia. In: Crimes T.P. and Harper J.C. (Eds), *Trace fossils* 2. Geol Jour Spec Pub 9, p. 41-70.

Barth, J.A.C., Veizer, J., Mayer, B. 1998. Origin of particulate organic carbon in the upper St. Lawrence: isotopic constraints. *Earth and Planetary Science Letters*, **162**: 111-121.

Beardsley, R.C., Candela, J., Limeburner, R., Geyer, W.R., Lentz, S.J., Castro, B.M., Cacchione, D., Carneiro, N. 1995. The M2 tide on the Amazon shelf. *Journal of Geophysical Research*, **100**: 2283-2319.

Behling, H. & Costa, M.L. 2000. Holocene environmental changes from the Rio Curuá record in the Caxiuanã region, Eastern Amazon Basin. *Quaternary Research*, **53**: 369-377.

Behling, H. & Hooghiemstra, H. 2000. Holocene Amazon rain forest – Savanna dynamics and climatic implications: High resolution pollen record Laguna Loma Linda in eastern Colombia. *Journal of Quaternary Science*, **15**: 687-695.

Behling, H. & Costa, M.L. 2001. Holocene vegetation and costal environments changes from the Lago Crispim record in northeastern Pará State, eastern Amazonia. *Review of Palaeobotany and Palynology*, **114**: 145-155.

Behling, H., Cohen, M.C.L., Lara, R.J. 2001. Studies on Holocene mangroves ecosystem of the Bragança Peninsula in north-eastern Pará, Brazil. *Palaeogeography, Palaeoclimatology, Palaeoecology*, **167**: 225-242.

Behling, H., Cohen, M.C.L., Lara, R.J. 2004. Late Holocene mangrove dynamics of Marajó Island in Amazonia, northern Brazil. *Vegetation History and Archaeobotany*, **13**: 73-80.

Beta. 2010. Accelerator Mass Spectrometry Radiocarbon Dating. Beta Analytic. Disponível em: http://www.radiocarbon.com/accelerator-mass-spectrometry.htm. Acessado em 10 de abril de 2010.

Bezerra, P.E.L., Oliveira, W., Regis W.D.E., Brazão, J.E.M., Gavinho, J., Coutinho, R.C.P. 1990. Amazônia legal: zoneamento das potencialidades e dos recursos naturais. In: Instituto Brasileiro de Geografia e Estatística, Superintendência de Desenvolvimento da Amazônia. Projeto zoneamento das potencialidades dos recursos naturais da Amazônia: geologia, solos e vegetação. Div. 5. Rio de Janeiro, p. 9-89.

Blasco, F., Saenger, P., Janodet, E. 1996. Mangroves as indicators of coastal change. *Catena*, **27**: 167-178.

Boutton, T.W., Archer, S.R., Midwood A.J., Zitzer S.F., Bol R. 1998. $\delta^{13}C$ values of soil organic carbon and their use in documenting vegetation change in a subtropical savanna ecosystem. *Geoderma*, **82**: 5-41.

Bradley, R.S. 1999. *Paleoclimatology*: *Reconstructing Climates of the Quaternary*. Academic Press, 613 p.

Bush, M.B. & Colinvaux, P.A. 1988. A 7000yr vegetational history from lowland Amazon, Ecuador. *Plant Ecology*, **76**: 141-154.

Bush, M.B., Silman, M.R., Listopad, C.M.C.S. 2007. A regional study of Holocene climate change and human occupation in Peruvian Amazonia. *Journal of Biogeography*, **34**: 1342-1356.

Byrne, R., Ingram, L.B., Starratt, S., Malamud-Roam, F. 2001. Carbon-isotope, diatom, and pollen evidence for late Holocene salinity change in a brackish marsh in the San Francisco Estuary. *Quaternary Research*, **55**: 66-76.

Câmara, G., Souza, R.C.M., Freitas, U.M., Garrido, J. 1996. SPRING: Integrating remote sensing and GIS by object-oriented data modeling. *Computers & Graphics*, **20**: 395-403.

Carreira, L.M.M. & Barth, O.M. 2003. *Atlas de pólen da vegetação de canga da serra dos Carajás*. Museu Paraense Emílio Goeldi, Coleção Adolpho Ducke, Belém, 112 p.

Carvalho, F.P., Costa Neto, S.V., Costa, W.J.P., Coutinho, R.S., Figueira, Z.R., Figueiredo, S.L., Martins, M.H.A., Santos, V.F., Silva, A.Q., Silva, L.M.A., Silva, M.S., Silveira, O.F.M., Takyiama, L.R. 2006. *Atlas Zoneamento Costeiro Estuarino do Estado do Amapá*. Macapá, PNMA/SQA/MMA. 77 p.

Chappell, J.M.A. & Woodroffe, C.D. 1994. Macrotidal estuaries. In: Carter RWG and Woodroffe CD (Eds), *Coastal Evolution: Late Quaternary Shoreline Morpho-dynamics*. Cambridge University Press, Canberra, 539 p.

Chavez, P.S., Berlin, G.L., Sowers, L.B. 1982. Statistical method for selecting Landsat MSS ratios. *Journal of Applied Photographic Engineering*, **8**: 23-30.

Chavez, P.S. 1988. An improved dark-object subtraction technique for atmospheric scattering correction of multispectral data. *Remote Sensing of Environment*, **24**: 450-479.

Chivas, A.R., Garcia, A., Van der Kaars, S., Couapel, M.J.J., Holt, S., Reeves, J.M., Wheeler, D.J., Switzer, A.D., Murray-Wallace, C.V., Banerjee, D., Price, D.M., Wang, S.X., Pearson, G., Edger, N.T., Beaufort, L., De Deckker, P., Lawson, E., Cecil, C.B. 2001. Sea-level and environmental changes since the last interglacial in the Gulf of Carpentaria, Australia: an overview. *Quaternary International*, **83-85**: 19-46.

Clark, M.W., McConchie D.M., Lewis D.W., Saenger, P. 1998. Redox stratification and heavy metal partitioning in Avicennia-dominated mangrove sediments: A geochemical model. *Chemistry Geology*, **149**: 147-171.

Cloern, J.E., Canuel, E.A., Harris, D. 2002. Stable carbon and nitrogen isotope composition of aquatic and terrestrial plants of the San Francisco Bay estuarine system. *Limnology and Oceanography*, **47**: 713-729.

Coffin, R.B., Fry, B., Peterson, B.J., Wright R.T. 1989. Carbon isotopic compositions of estuarine bacteria. *Limnology and Oceanography*, **34**: 1305-1310.

Cohen, M.C.L. 2003. Past and current mangrove dynamics on the Bragança peninsula, northern Brazil. Tese de Doutorado. Bremen, University of Bremen, Center for Tropical Marine Ecology. 110 p.

Cohen, M.C.L. & Lara R.J. 2003. Temporal changes of mangrove vegetation boundaries in Amazonia: Application of GIS and remote sensing techniques. *Wetlands Ecology and Management*, **11**: 223-231.

Cohen, M.C.L., Behling, H., Lara, R.J. 2005a. Amazonian mangrove dynamics during the last millennium: The relative sea-level and the Little Ice Age. *Review of Palaeobotany and Palynology*, **136**, 93-108.

Cohen, M.C.L., Souza Filho, P.W.M., Lara, R.J, Behling, H., Ângulo, R.J. 2005b. A model of Holocene mangrove development and relative sea-level changes on the Bragança Peninsula (Northern Brazil). *Wetlands Ecology and Management*, **13**: 433-443.

Cohen, M.C.L., Lara, R.J., Smith, C.B., Angélica, R.S., Dias, B.S., Pequeno, T. 2008. Wetland dynamics of Marajó Island, northern Brazil during the last 1000 years. *Catena*, **76**: 70-77.

Cohen, M.C.L., Lara, R.J., Smith, C.B., Matos, H.R.S., Vedel, V. 2009. Impact of sea-level and climatic changes on the Amazon coastal wetlands during the late Holocene. *Vegetation History and Archaeobotany,* **18**: 425-439.

Collinvaux, P.A., De Oliveira, P.E., Patiño, J.E.M. 1999. *Amazon Pollen Manual and Atlas - Manual e Atlas Palinológico da Amazônia*. Hardwood Academic, Amsterdam, 332 p.

Collinson J., Mountney N., Thompson, D. 2006. *Sedimentary Structures*. (Third edition) Terra Publishing, 292 p.

Cooley, S.R., Coles, V.J., Subramaniam, A., Yager, P.L. 2007. Seasonal variations in the Amazon plume-related atmospheric carbon sink. *Global Biogeochemical Cycles*, **21**: GB3014.

Costa, J.B., Hasui, Y., Bemerguy, R.L., Soares-Júnior, A.V., Villegas, J. 2002. Tectonics and paleogeography of the Marajó Basin, northern Brazil. *Anais da Academia Brasileira de Ciências*, **74**: 519-531.

Costa Neto, S.V. 2004. Relatório de vegetação: Subsídio ao diagnostico sócio ambiental. Relatório Técnico. Macapá, IEPA/GERCO, 32 p.

Costa Neto, S.V. & Silva, M.S. 2004. Vegetação do setor costeiro estuarino do estado do Amapá. Instituto de Pesquisas Científicas e Tecnológicas do Estado do Amapá. Governo do Estado do Amapá. Cap. 5. *In*: Projeto Zoneamento Econômico-Ecológico do setor costeiro estuarino: diagnóstico sócio ambiental participativo do setor costeiro estuarino, p.72-96.

Costa Neto, S.V., Senna, C., Tostes, L.C.L., Silva, S.R.M. 2007. Macrófitas aquáticas das Regiões dos Lagos do Amapá, Brasil. *Revista Brasileira de Biociências*, **5**: 618-620.

Climate Prediction Center/*National Oceanic and Atmospheric Administration* (CPC/NOAA) 2010. Cold and Warm Episodes by Season. Climate Prediction Center. Disponível em: http://www.cpc.ncep.noaa.gov/products/analysis_monitoring/ensostuff/ensoyears. Acessado em 08 de novembro de 2010.

Companhia de Pesquisa de Recursos Mineirais (CPRM). 2010. Sistema de Informações Geológicas. Serviço Geológico Brasileiro. Folhas NA/SA-22 23 MB. Disponível em: http://geobank.sa.cprm.gov.br/. Acessado em 03 de janeiro de 2009.

Curray, J.R. 1969. Shore zone sand bodies, barriers, cheniers and beach ridges. In: Stanley DJ & Curray JR (Eds.), *The New Concepts of Continental Margin Sedimentation*, Alexandria: American Geological Institute.

Dalrymple, R.W., Knight, R.J., Lambiase, J.J. 1978. Bedforms and their hydraulic stability relationships in a tidal environment, Bay of Fundy, Canada. *Nature*, **275**: 293-307.

Dalrymple, R.W., Knight, R.J., Zaitlin, B.A., Middleton G.V. 1990. Dynamics and facies model of a macrotidal sand-bar complex, Cobequid Bay - Salmon River estuary (Bay of Fundy). *Sedimentology*, **37**: 577-612.

Dalrymple, R.W. 1992. Tidal depositional systems. In: Walker R.G. & James N.P. (Eds.), *Facies Models - Response to Sea Level Change*. Ontario, Geological Association of Canada, p. 195-218.

Dalrymple, R.W. 2006. Incised valleys in time and space: introduction to the volume and an examination of the controls on valley formation and filling. In: Dalrymple R.W., Leckie D.A., Tillman, R. (Eds), *Incised Valleys in Time and Space*. SEPM Special Publication, vol. 85, p. 5–12.

Dalrymple, R.W. & Choi K. 2007. Morphologic and facies trends through the fluvial-marine transition in tide-dominated systems: A schematic framework for environmental and sequence-stratigraphic interpretation. *Earth-Science Reviews*, **81**: 135-174.

Davis Jr., R.A. 1978. *Coastal sedimentary environments*. Springer Verlag, New York. 420 p.

Davis, M.B. 2000. Palynology after Y2K - understanding the source area of pollen in sediments. *Annual Review of Earth and Planetary Sciences*, **28**: 1-18.

Deines, P. 1980. The isotopic composition of reduced organic carbon. In: Fritz, P. & Fontes, J.C. (Eds.), *Handbook of Environmental Isotope Geochemistry*. The Terrestrial Environment, vol.1. A. Elsevier, Amsterdam, p. 329-406.

Desjardins, T., Filho, A.C., Mariotti, A., Chauvel, A., Girardin, C. 1996. Changes of the forest-savanna boundary in Brazilian Amazonia during the Holocene as revealed by soil organic carbon isotope ratios. *Oecologia*, **108**: 749-756.

Diretoria de Hidrografia e Navegação (DHN) 2009. Diretoria de Hidrografia e Navegacão, Tábuas de Marés do ano de 2009. Disponível em: http://www.mar.mil.br/dhn/chm/tabuas/index.htm. Acessado em 20 de janeiro de 2008.

Departamento Ncional de Produção Mineral (DNPM) 1971. Levantamento de recursos naturais, v. 21, 23 e 24. Folhas NA22 MACAPÁ. Projeto In: Projeto RADAMBRASIL. Rio de Janeiro, MME/DNPM.

Dott, R.H. & Howard, J.K. 1962. Convolute lamination in non-grained sequences. *Journal of Geology* **70**: 114-120.

Duke, N.C., Ball, M.C., Ellison, J.C. 1998. Factors influencing biodiversity and distributional gradients in mangroves. *Global Ecology and Biogeography Letters*, **7**: 27-47.

Dott, R.H. & Howard, J.K. 1962. Convolute lamination in non-grained sequences. *Journal of Geology*, **70**: 114-120.

Eisma, D., Augustinus, P.G.E.F., Alexander, C.R. 1991. Recent and subrecent changes in the dispersal of Amazon mud. *Netherlands Journal Sea Research*, **28**: 181-192.

Empresa Brasileira de Pesquisa Agraecuária (EMBRAPA) 2006. *Sistema Brasileiro de Classificação de Solos*. Empresa Brasileira de Pesquisa Agropecuária - 2.ed. Rio de Janeiro, Embrapa Solos. Centro Nacional de Pesquisa de solos. 306 p.

Engelhart, S.E., Horton, B.P., Roberts, D.H., Bryant, C.L., Corbett, D.R. 2007. Mangrove pollen of Indonesia and its suitability as a sea-level indicator. *Marine Geology*, **242**: 65-68.

Erdtman, G. 1947. Suggestion for the classification of fossil ann recent grains ans spores. *Svensk Botanisk Tidskrift*, **41**: 104-114.

Erdtman, G. 1952. *Pollen Morphology and Plant Taxonomy*. Angiosperms. Almqvist and Wiksell, Stockholm.

Erdtman, G. 1960. Pollen walls and Angiosperm phylogeny. *Bot. Notis*., **113**: 41-45.

ESRI. 2006. ArcGIS Version 9.0 Software. Redland, California.

Evans, 1965. Intertidal flat sediments and their environments of deposition in The Wash. *Quaterly Journal of the Geological Society of London*, **121**: 209-241.

Faegri, K. & Iversen, J. 1950. *Textbook of modern pollen analysis*. Munksgaard, Copenhagen. 168 p.

Faegri, K. 1956. *Recent trends in palynology*. *Bot. Rev*., **22**: 639-664.

Faegri, K. & Iversen J. 1989. *Textbook of Pollen Ana*lyses. John Wiley and Sons LTD, Chichester, 328 p.

Fiot, J. & Gratiot N. 2006. Structural effects of tidal exposure on mud flats along the French Guiana coast. *Marine Geolology*, **228**: 25-37.

Freitas, H.A., Pessenda, L.C.R., Aravena, R., Gouveia, S.E.M., Ribeiro, A.S., Boulet, R. 2001. Late Quaternary vegetation dynamics in the Southern Amazon Basin inferred from carbon isotopes in soil organic matter. *Quaternary Research*, **55**: 39-707.

Freycon, V., Krencker, M., Schwartz, D., Nasi, R., Bonal, D. 2009. The impact of climate changes during the Holocene on vegetation in northern French Guiana. *Quaternary Research*, **73**: 220-225.

Fromard, F., Vega, C., Proisy, C. 2004. Half a century of dynamic coastal change affecting mangrove shorelines of French Guiana. A case study based on remote sensing data analyses and field surveys. *Marine Geology*, **208**: 265-280.

Gallo, M.N. & Vinzon, S. 2005. Generation of over tides and compound tides in Amazon estuary. *Ocean Dynamics*, **55**: 441-448.

Gardel, A., Proisy, C., Lesourd, S., Philippe, S., Caillaud, J., Gontharet, S., Anthony, E.J., Brutier, L. 2009. A better understanding of mud cracking processes gained from in situ measurements on an intertidal mudflat in French Guiana. *Journal of Coastal Research*, **SI 56**: 424-428.

Geyer, W.R. & Kineke G.C. 1995. Observations of currents and water properties in the Amazon frontal zone. *Journal of Geophysical Research*, **100**: 2321-2339.

Geyer, W.R., Hill, P.S., Kineke, G.C. 2004. The transport, transformati on and dispersal of sediment by buoyant coastal flows. *Continental Shelf Research*, **24**: 927-949.

GLOBAL Mapper LLC. 2009. Global Mapper Version 9.0 Software. Colorado, Parker.

Gonçalves-Alvim, S.J., Vaz dos Santos, M.C.F., Fernandes, G.W. 2001. Leaf gall abundance on Avicennia germinans (Avicenniaceae) along an interstitial salinity gradient. *Biotropica*, **33**: 69-77.

Gornitz, V. 1991. Global coastal hazards from future sea level rise. *Palaeogeography*, *Palaeoclimatology*, *Palaeoecology*, **89**: 379-720.

Gouveia, S.E.M., Pessenda, L.C.R., Aravena, R., Boulet, R., Roveratti, R., Gomes, B.M. 1997. Dinâmica de vegetações durante o Quaternário recente no sul do Amazonas indicada pelos isótopos do carbono (^{12}C, ^{13}C e ^{14}C). *Geochimica Brasiliensis*, **11**: 355-367.

Graham, M.C., Eaves, M.A., Farmer, J.G., Dobson, J., Fallick, A.E. 2001. A study of carbon and nitrogen stable isotope and elemental ratios as potential indicators of source and fate of organic matter in sediments of the Forth Estuary, Scotland. Estuarine, Coastal and Shelf Science, **51**: 375-380.

Grimm, E.C. 1987. CONISS: a FORTRAN 77 program for stratigraphically constrained cluster analysis by the method of the incremental sum of square. *Computer and Geosciences*, **13**: 13-35.

Guimarães, J.T.F., Cohen, M.C.L., França, M.C., Lara, R.J., Behling, H. 2010. Model of wetland development of the Amapá coast during the late Holocene. *Anais da Academia Brasileira de Ciências*, **82**: 1-15.

Guimarães, J.T.F., Cohen, M,C.L., Pessenda, L.C.R., França, M.C., Smith, C.B., Nogueira A.C.R. No prelo. Mid and late Holocene sedimentary process and palaeovegetation changes near the mouth of the Amazon River. *The Holocene*.

Guimarães, J.T.F., Cohen, M,C.L., França, M.C. Submetido. El Niño and La Niña effects on tidal flats near the mouth of the Amazon River. *Earth Surface Process and Landscape*.

Haines, E.B. 1976. Stable carbon isotope ratios in biota, soils and tidal water of a Georgia salt marsh. *Estuarine and Coastal Marine Science*, **4**: 609-616.

Harris P.T. & Collins M.B. 1985. Bedform distributions and sediment transport paths in the Bristol Channel and Severn Estuary, UK. *Marine Geology*, **62**: 153-166.

Hayakawa, E.H., Rossetti, D.F., Valeriano, M.M. 2010. Applying DEM-SRTM for reconstructing a late Quaternary paleodrainage in Amazonia. *Earth and Planetary Science Letters*, **297**: 262-270.

Heslop-Harrison, J. 1971. *Pollen: Development and Physiology*. Butterworth, Londres. 378 p.

Hesse M., Halbritter, H., Zetter, R., Weber, M., Buchner, R., Frosch-Radivo, A., Ulrich S. 2008. *Pollen terminology: An illustrated handbook, Springer*. New York. 264 p.

Hesse, P.R. 1961. Some differences between the soils of Rhizophora and Avicennia mangrove swamp in Sierra Leone. *Plant Soil*, **14**: 335-346.

Hoefel, F.G. 1998. Morfodinâmica de praias arenosas oceânicas: uma revisão bibliográfica. Editora da Univali. Itajaí. 92 p.

Hofton, M., Dubayah, R., Blair, J.B., Rabine, D. 2006. Validation of SRTM elevations over vegetated and non-vegetared terrain using medium footprint Lidar. *Photogrammetric Engineering & Remote Sensing*, **72**: 279-285.

Holmgren, M., Scheffer, M., Ezcurra, E., Gutiérrez, J.R., Mohren, G.M.J. 2001. El Niño effects on the dynamics of terrestrial ecosystems. *Trends in Ecology & Evolution*, **16**: 89-94.

Horbe, A.M.C., Behling, H., Nogueira, A.C.R., Mapes, R. 2011. Environmental changes in the western Amazônia: morphological framework, geochemistry, palynology and radiocarbon dating data. *Anais da Academia Brasileira de Ciências*, **83**: 863-874.

Horikava, E.H. 2003. Relatório de Etapa Projeto Pedra Branca, Área Amaparí Brownfield. Estado do Amapá. Relatório interno Anglo Gold.

Horton, B.P., Gibbard, P.L., Milne, G.M., Morley, R.J., Purintavaragul, C., Stargardt, J.M. 2005. Holocene sea levels and palaeoenvironments of the Malay-Thai Peninsula, southeast Asia. *The Holocene*, **15**: 1199-1213.

Howard, J.D. & Frey R.W. 1975. Estuaries of the Georgia coast, USA: Sedimentology and Biology. II. Regional animal-sediment characteristics of Georgia estuaries: *Senchenberiana merti.*, **7**: 33-103.

Hutchings P. e Saenger P. 1987. Ecology of Mangroves. Queensland University Press, 388 p.

Instituto Brasileiro de Geografia e Estatística (IBGE). 2008. Mapa Geomorfológico do Estado do Amapá. Instituto Brasileiro de Geografia e Estatística – Coordenação de Pesquisas Naturais e Estudos Ambientais. Disponível em ftp://geoftp.ibge.gov.br/mapas/tematicos/tematico_estadual/AP_geomorfologia.pdf. Acessado em 05 de outubro de 2009.

Kao, W.Y., Shih, C.N., Tsai, T.T. 2004. Sensitivity to chilling temperatures and distribution differ in the mangrove species Kandelia candel and Avicennia marina. *Tree Physiology*, **24**: 859-864.

Keeley, J.E. & Sandquist, D.R. 1992. Carbon: freshwater plants. *Plant, Cell and Environment*, **15**: 1021-1035.

Kjerfve, B. & Lacerda, L.D. 1993. Mangroves of Brazil. In: *Conservation and sustainable utilization of mangroves forests in Latin America and Africa regions*. Part 1: Latin America. 1993. ITTO/ISME Project PD114/90(F), p. 245-272.

Klein, G.V. 1963. Bay of Fundy intertidal zone sediments. *Journal of Sedimentary Petrology*, **33**: 844-854.

Klein, G.V. 1967. Paleocurrent analysis in relation to modern marine dispersal patterns. *Geological Society* of *America* Bulletin, **51**: 366-382.

Klein, G.V. 1970a. Depositional and dispersal dynamics of intertidal sand bars. *Journal of Sedimentary Petrology*, **40**: 1095-1127.

Klein, G.V. 1970b. Tidal origin of a Precambrian quartzite – the Lower Fine-Grained Quartzite (Middle Dalradian) of Islay, Scotland. *Journal of Sedimentary Petrology*, **40**, 973-985.

Klein, G.V. 1971. A sedimentary model for determining paleotidal range. *Geological Society of America Bulletin*, **82**: 2585-2592.

Klein, G.V. 1977. *Clastic tidal facies*. Continuing Education Publication Company, Champaign, Illinois, 149 p.

Knight, R.J. & Dalrymple, R.W. 1975. Intertidal sediments from the south shore of Cobequid Bay, Bay of Fundy, Nova Scotia, Canada. In: Ginsburg, R.N. (Ed) *Tidal deposits: a*

casebook of recent examples and fossil counterparts. Springer-Verlag, New-York, p. 47-55.

Komar, P.D. 1976. *Beach process and sedimentation*. Prentice Hall Editors, New Jersey, 429 p.

Krauss, K.W., Lovelock, C.E., McKee, K.L., López-Hoffman, L., Ewe, S.M.L., Sousa, W.P. 2008. Environmental drivers in mangrove establishment and early development: A review. *Aquatic Botany*, **89**: 105-127.

Krauss, K.W., Lovelock, C.E., McKee, K.L, López-Hoffman, L., Ewe, S.M.L., Sousa, W.P. 2008. Environmental drivers in mangrove establishment and early development: A review. *Aquatic Botany*, **89**: 105-127.

Kremp, G.O.W. 1965. *Morphologic Encyclopedia of Palynology*. University of Arizona Press. Tucson. 263 p.

Lacerda, L.D., Ittekkot V., Patchineelam S.R. 1995. Biogeochemistry of mangrove soil organic matter: A comparison between Rhizophora, Avicennia soils in south-eastern Brazil. *Estuarine, Coastal and Shelf Science*, **40**: 713-720.

Lamb, A.L., Wilson, G.P., Leng, M.J. 2006. A review of coastal palaeoclimate and relative sea-level reconstructions using $\delta^{13}C$ and C/N ratios in organic material. *Earth-Science Reviews*, **75**: 29-57.

Lara, J.R. & Cohen, M.C.L. 2006. Sediment porewater salinity, inundation frequency and mangrove vegetation height in Bragança, North Brazil: An ecohydrology-based empirical model. *Wetlands Ecology and Management*, **14**: 349-358.

Lara, R.J. & Cohen, M.C.L. 2009. Palaeolimnological studies and ancient maps confirm secular climate fluctuations in Amazonia. *Climatic Change*, **94**: 399-408.

Latrubesse, E.M. & Franzinelli, E. 2002. The Holocene alluvial plain of the middle Amazon River, Brazil. *Geomorphology*, **44**: 241-257.

Ledru, M.P. 2001. Late Holocene rainforest disturbance in French Guiana. *Review of Palaeobotany and Palynology*, **115**: 161-176.

Lentz, S.J. 1995. The Amazon River plume during AMASSEDS: subtidal current variability and the importance of wind forcing. *Journal of Geophysical Research*, **100**: 2377-2390.

Lentz, S.J. & Limeburner, R. 1995. The Amazon River Plume during AMASSEDS: Spatial characteristics and salinity variability. *Journal of Geophysical Research*, **100**: 2355-2375.

Leopold, L.B. & Wolman, M.G. 1957. *River channel patterns: braided, meandering and straight*. Physiographic and hydraulic studies of rivers. *US Geological Survey Professional Paper*, **282B**: 39-85.

Lesourd, S., Lesueur, P., Brun-Cottan, J.C., Garnaud, S., Poupinet, N. 2003. Seasonal variations in the characteristics of superficial sediments in a macrotidal estuary (the Seine inlet, France). *Estuarine, Coastal and Shelf Science*, **58**: 3-16.

Libby, W.F. 1955. *Radiocarbon dating*. 2.ed. Chicago: University of Chicago Press. 175 p.

Lima, M.I.C., Montalvão, R.M.G. de., Oliveira, A.daS., Basei, M.A.S., Araújo, J.F.V. de., Silva G.G. 1974. Geologia Folha NA/22 (Macapá). In: Projeto RADAM, Departamento Nacional de Produção Mineral, Rio de Janeiro. Levantamento de Recursos Naturais 6, p.1-120.

Lima, M.I.C, Bezerra, P.E., Araújo H.J.T. 1991. Sistematização da Geologia do Estado do Amapá. In: Simpósio de geologia da Amazônia, vol. 3, Belém. *Anais*. SBG. p. 322-335.

Lima, M.I.C., Oliveira, E.P., Tassinari C.C.G. 1992. Cinturões granulíticos da porção setentrional do Cráton Amazônico. In: SBG, Simpósio de Geologia da Amazônia, 1, Belém, *Atas*, v. 1, p.147-162.

Long, S.P. 1999. Environmental responses. In: Sage, R.F. & Monson, R.K. (Eds), *C4 plant biology*. Academic Press, San Diego, p. 215-249.

Imbrie, J.& Buchanan, H. 1965. Sedimentary structures in modern carbonate sands of the Bahamas. In: Middleton, G.V. (Ed.), *Primary sedimentary structures and their hydrodynamic interpretation*. Society of Economic Paleontologists and Mineralogists Special Publication 12, p. 149-172.

Iversen, J. e Troels-Smith, J. 1950. Pollenmorphologishe Definitionen Typen. *Danm. Geol. Unders. Ser.*, **4**,**3**: 1-54.

Macar, P. & Antun, P. 1950. Pseudonodules et glisserment sousanquatique dans L'Emsian Inferieur de l'Oesing. *Soc. Geol. Belgiques Ann.*, **73**: 121-151.

Macar, P. & Ek, C. 1965. Un curieux phenomena d'erosion Fammeinnienne: Les "Pains de gres" de Chambrailes (Ardenne, Belde). *Sedimentology*, **4**: 53-64.

Marzo, M. & Puigdefábregas, C. 1993. *Alluvial Sedimentation*. Blackwell Scientific Publications, Oxford, 600 p.

Maslin, M.A. & Burns, S.J. 2000 Reconstruction of the Amazon Basin effective moisture availability over the past 14,000 years. *Science*, **290**: 2285-2287.

Mayle, F.E. & Power, M.J. 2008. Impact of a drier Early-Mid-Holocene climate upon Amazonian forests. *Philosophical Transactions of the* Royal Society *B*, **363**: 1829-1838.

Mead, R.H., Dunee, T., Richey, J.E., Santos, U.M., Salati, E. 1985. Storage and remobilization of suspended sediment in the lower Amazon River of Brazil. *Science*, **228**: 488-490.

Medina, E., Cuevas, E., Popp, M., Lugo, A. 1990. Soil salinity, sun exposure, and growth of Acrostichum aureum, the mangrove fern. *Botanical Gazette*, **151**: 41-49.

Menezes, M., Berger, U., Worbes, M. 2003. Annual growth rings and long-term growth patterns of mangrove trees from the Bragança peninsula, North Brazil. *Wetlands Ecology and Management*, **11**: 233-242.

Meyers, P.A. 1994. Preservation of elemental and isotopic source identification of sedimentary organic matter. *Chemical Geology*, **114**: 289-302.

Meyers, P.A. 1997. Organic geochemical proxies of paleoceanographic, paleolimnologic, and paleoclimatic processes. *Organic Geochemistry*, **27**: 213-250.

Miall, A.D. 1978. Facies types and vertical profile models in braided river deposits: a summary. In: Miall, A.D. (Ed.), *Fluvial sedimentology*. Calgary: Canadian Society of Petroleum Geologists, p. 597-604.

Miall, A.D. 1992. Alluvial Models. In: Walker, R.G. & James, N.P. (Eds) *Facies Models - Response to sea-level change*. Geological Association of Canada, Newfoundland, p 119-142.

Middelburg, J.J. & Nieuwenhuize, J. 1998. Carbon and nitrogen stable isotopes in suspended matter and sediments from the Schelde Estuary. *Marine Chemistry*, **60**: 217-225.

Milne, G.A., Long, J.A., Bassett, S.E. 2005. Modelling Holocene relative sea-level observations from the Caribbean and South America. *Quaternary Science Reviews*, **24**: 1183-1202.

Mörner, N.A. 1996. Global change and interaction of earth rotation, ocean circulation and paleoclimate. *Anais da Academia Brasileira de Ciências*, **68**: 77-94.

Möner, N.A. 1999. Sea level and climate: Rapid regressions at local warm phases. *Quaternary International*, **60**: 75-82.

Ng, P.K.L., Sivasothi, N., Morgany, T., Murphy, D.H. 2002. *A Guide to the Mangroves of Singapore* 1: The Ecosystem & Plant Diversity. Singapore Science Centre, Rev. Edition, 160 p.

O´Leary, M.H. 1988. Carbon isotopes in photosynthesis. *BioScience*, **38**: 328-336.

Osmond, C.B., Valaane N., Haslam S.M., Uotila P., Roksandic Z. 1981. Comparisons of $\delta^{13}C$ values in leaves of aquatic macrophytes from different habitats in Britain and Finland; some implications for photosynthetic processes in aquatic plants. *Oecologia*, **50**: 117-124.

Pessenda, L.C.R., Gouveia, S.E.M., Aravena, R., Gomes, B.M., Boulet, R., Ribeiro, A.S. 1998. ^{14}C dating and stable carbon isotopes of soil organic matter in forest–savanna boundary areas in southern Brazilian Amazon region. *Radiocarbon*, **40**: 1013-1022.

Pessenda, L.C.R., Boulet, R., Aravena, R., Rosolen, V., Gouveia, S.E.M., Ribeiro, A.S., Lamote, M., 2001. Origin and dynamics of soil organic matterand vegetation changes during the Holocene in a forest-savanna transition zone, Brazilian Amazon region. *The Holocene*, **11**: 250-254.

Pessenda, L.C.R., Ribeiro, A.S., Gouveia, S.E.M., Aravena, R., Boulet, R., Bendassoli, J.A., 2004a. Vegetation dynamics during the late Pleistocene in the Barreirinhas region, Maranhão State, northeastern Brazil, based on carbon isotopes in soil organic matter. *Quaternary Research*, **62**: 183-193.

Pessenda, L.C.R., Gouveia, S.E.M., Aravena, R., Boulet, R., Valencia, E.P.E. 2004b. Holocene fire and vegetation changes in southeastern Brazil as deduced from fossil charcoal and soil carbon isotopes. *Quaternary International*, **114**: 35-43.

Peterson, B.J., Fry, B., Hullar, M., Saupe, S., Wright, R. 1994. The distribution and stable carbon isotope composition of dissolved organic carbon in estuaries. *Estuaries*, **17**: 111-121.

Pimentel, M.M., Ferreira Filho, C.F., Spier, C.A. 2002. Estudo Sm-Nd do Complexo Máfico-Ultramáfico Bacuri, Amapá: idade da intrusão, metamorfismo e natureza do magma original. *Revista Brasileira de Geociências*, **32**: 371-376.

Prentice, I.C. 1985. Pollen representation, source area, and basin size: toward a unified theory of pollen analysis. *Quaternary Research*, **23**: 76-86.

Prost, M.T. 1989. Coastal dynamics and chenier sands in French Guiana. *Marine Geology*, **90**: 259-267.

Punt, W., Blackmore S., Nilson S., Le Thomas A. 1994. *Glossary of pollen and spore terminology*. LPP Foundation, Utrecht, LPP Contributions Series n. 1, Ultrecht, 71 p.

Pugh, D.T. 1987. *Tides, surges and mean sea-level: a Handbook for Engineers and Scientists*. London: Wiley. 486 p.

Ramani, B., Reeckb, T., Debezc, A., Stelzerd, R., Huchzermeyera, B., Schmidta, A. 2006. Aster tripolium L. and Sesuvium portulacastrum L.: Two halophytes, two strategies to survive in saline habitats. *Plant Physiology and Biochemistry*, **44**: 395-408.

Ramirez, A. & Yáñes-Camacho, C.M. 2008. Formation of chenier plain of the Doñana marshland (SW Spain): Observations and geomorphic model. *Marine Geology*, **254**: 187-196.

Raven, P.H., Evert, R.F., Eichorn, S. 1996. *Biologia vegetal*. Rio de Janeiro: Guanabara Koogan. 728 p.

Raymond, P.A. & Bauer, J.E. 2001. Use of ^{14}C and ^{13}C natural abundances for evaluating riverine, estuarine, and coastal DOC and POC sources and cycling: A review and synthesis. *Organic Geochemistry*, **32**: 469-485.

Reading, H.G. 1996. *Sedimentary Environments and Facies*. Blackwell Scientific Publications. 688 p.

Reimer, P.J., Baillie, M.G.L., Bard, E., Baylis, A., Beck, J.W., Bertrand, C.J.H., Blackwell, P.G., Buck, C.E., Burr, G.S., Cutler, K.B., Damon, P.E., Edwards, R.L., Fairbanks, R.G., Friedrich, M., Guilderson, T.P., Hogg, A.G., Hughen, K.A., Kromer, B., McCormac, F.G., Manning, S.W., Ramsey, C.B., Reimer, R.W., Remmele, S., Southon, J.R., Stuiver, M., Talamo, S., Taylor, F.W., Van der Plicht, J., Weyhenmeyer, C.E. 2004. IntCal04 Terrestrial radiocarbon age calibration 26 - 0 ka B.P. *Radiocarbon*, **46**: 1029-1058.

Reineck, H.E. 1958. Longitudinale schrägschicht in Watt. *Geologische Rundschau*, **47**: 73-82.

Reineck, H.E. 1963. Sedimentgefuge im Bereich der Sudliche Nordsee. *Abhandl. Sencken. Nat. Gesell.*, 505: 1-138.

Reineck, H.E. 1967. Layered sediments of tidal flats, beaches and shelf bottoms of the North Sea. In: Lauff, G.H. (Ed.), *Estuaries*. The American Association for the Advancement of Science, Special Publication 83, p. 191-206.

Reineck, H.E. & Wunderlich F. 1968. Classification and origin of flaser and lenticular bedding. *Sedimentology*, **11**: 99-104.

Reineck, H.E. 1975. German North Sea tidal flats. In: Ginsburg, R.N. (Ed.), *Tidal deposits: a casebook of recent examples and fossil counterparts*. Springer-Verlag, New York, p. 5-12.

Reineck, H.E. & Singh, I.B. 1980. *Depositional Sedimentary Environments with Reference to Terrigenous Clastics* 2nd ed. Springer-Verlag, Berlin, Germany. 542 p.

Reinson, G.E. 1992. Transgressive Barrier Island and estuarine systems. In: Walker, R.G. & James, N.P. (Eds), *Facies Models - Response to Sea Level Change*. Ontario, Geological Association of Canada, p. 179-194.

Retallack, G.J. 2001. Soils of the Past - An Introduction to Paleopedology (Second edition). Wiley-Blackwell, 512 p.

Rhoads, D.C. 1967. Biogenic reworking of intertidal and subtidal sediments in Barnstable Harbor and Buzzards Bay, Massachusetts. *Journal of Geology*, **75**: 461-476.

Rosario, R.P., Bezerra, M.O.M., Vinzon, S.B. 2009. Dynamics of the saline front in the Northern Channel of the Amazon River - influence of fluvial flow and tidal range (Brazil). *Journal of Coastal Research*, **2**: 503-514.

Rossetti, D.F., Almeida, S., Amaral, D.D., Lima, C.M., Pessenda, L.C.R. 2010. Coexistence of forest and savanna in an Amazonian area from a geological perspective. *Journal of Vegetation Science*, **21**: 120-132.

Roubik, D.W. & Moreno, J.E. 1991. *Pollen and Spores of Barro Colorado Island*. Missouri Botanical Garden, 268 p.

Sage R.F. & Monson R.K. 1999. *C4 Plant Biology*. Academic Press. 596 p.

Salgado-Labouriau, M.L. 1962. *Palinologia - fundamentos, técnicas e algumas perspectivas*. *Revista Brasileira de Geografia*, **4**: 107-129.

Salgado-Labouriau, M.L. 2007. *Critérios e técnicas para o Quaternário*. Edgard Blücher, São Paulo, São Paulo. 387 p.

Sangster, A.G. & Dale, H.M. 1961. A preliminary study of differential pollen grain preservation. *Canadian Journal of Botany*, **39**: 35-43.

Sangster, A.G. & Dale, H.M. 1964. Pollen grain preservation of underrepresented species in fossil spectra. *Canadian Journal of Botany*, **42**: 437-449.

Santos, V.F., Costa, W.J.P., Silva, M.S., Silveira, O.F.M., Torres, A.M., Silva, A.Q., Martins, M.H.A. 2004. Geologia do setor costeiro estuarino do estado do Amapá. Instituto de Pesquisas Científicas e Tecnológicas do Estado do Amapá. Governo do Estado do Amapá. Cap. 2. In: Projeto Zoneamento Econômico-Ecológico do setor costeiro estuarino: diagnóstico sócio ambiental participativo do setor costeiro estuarino, p. 24-42.

Santos, V.F. 2006. *Ambientes Costeiros Amazônicos: avaliação de Modificações por Sensoriamento Remoto. Curso de Pós-Graduação em Geologia e Geofísica Marinha, Universidade Federal Fluminense*. Tese de Doutorado. 306 p.

Schidlowski, M., Hayes, J.M., Kaplan, I.R. 1983. Isotopic inferences of ancient biochemistries: carbon, sulphur, hydrogen and nitrogen. In: Scholf, J.W. (Ed.), *Earth's Earliest Biosphere, Its Origin and Evolution*. Princeton University Press, Princeton, p. 149-186.

Schumm, S.A. 1977. *The Fluvial System*. John Wiley 7 Sons, New York, 338 p.

Semeniuk, V. 1994. Predicting the effect of sea-level rise on mangroves in northwestern Australia. *Journal of Coastal Research*, **10**: 1050-1076.

Sifeddine, A., Fröhlich, F., Fournier, M., Martin, L., Servant, M., Soubiés, F. 1994. La sédimentation lacustre indicateur de changements des paléoenvironnements au cous des 30000 dernières annèes (Carajas, Amazonie, Brésil). *Comptes rendus de l'Académie des sciences*, **318**: 1645-1652.

Sifeddine, A., Martin, L., Turcq, B., Ribeiro, C.V., Soubiès, F., Cordeiro, R.C. 2001. Variations of the Amazonian rainforest environment: A sedimentological record covering 30,000 years. *Palaeogeography, Palaeoclimatology, Palaeoecology*, **168**: 221-235.

Silveira, O.F.M. 1998. *A Planície costeira do Amapá: dinâmica de ambiente costeiro influenciado por grandes fontes fluviais quaternárias. Programa de Pós-Graduação em Geologia e Geoquímica, Universidade Federal do Pará*. Tese de Doutorado. 215 p.

Smith, C.B., Cohen, M.C.L., Pessenda, L.C.R., França, M.C., Guimarães, J.T.F., Rossetti, D.F., Lara, R.J. (No prelo). Coastal vegetation changes at the mouth of the Amazon during the Holocene. *Review of Palaeobotany and Palynology*.

Snedaker, SC. 1978. Mangroves: Their value and perpetuation. *Natural Resources*, **16**: 179-188.

Soares-Filho, B.S., Nepstad, D., Curran, L., Voll, E., Cerqueira, G., Garcia, R.A., Ramos, C.A., Mcdonald, A., Lefebvre, P., Schlesinger, P. 2006. Modeling conservation in the Amazon basin. *Nature*, **440**: 520-523.

Souza, E.J. & Pinheiro, R.V.L. 2009. Relações entre as estruturas tectônicas do embasamento e o desenvolvimento da paisagem da região costeira do estado do Amapá uma investigação sobre reativações tectônicas e acumulação de hidrocarbonetos. Relatório técnico-científico, Brasília: ANP, 105 p.

Souza, E.J. 2010. *Geologia da região costeira do Amapá com ênfase na estratigrafia, morfotectônica e geomorfologia*. Monografia de Conclusão de Curso, Faculdade de Geologia, Universidade Federal do Pará. 118 p.

Souza Filho, P.W.M., Cohen, M.C.L., Lara, R.J., Lessa, G.C., Koch, B., Behling, H. 2006. Holocene coastal evolution and facies model of the Bragança macrotidal flat on the Amazon mangrove coast, Northern Brazil. *Journal of Coastal Research*, **SI 39**: 306-310.

Souza Filho, P.W.M., Lara, R.J., Silveira, O.F.M., Miranda, F.P. 2007. The Amazon Mangrove Coast: The Role of Geological Factors in its Evolution During the Quaternary. In: American Geophysical Union AJoint Assembly, Acapulco. *Abstracts*. Washington D.C.: EOS Trans. AGU, 2007. v. 1. p. OS23D-04-OS23D-04.

Stockmarr, J. 1971. Tablets with spores used in absolute pollen analysis. *Pollen et Spores*, **8**: 615-621.

Stuart, S.A., Choat, B., Martin, K.C., Holbrook, N.M., Ball, M.C. 2007. The role of freezing in setting the latitudinal limits of mangrove forests. *New Phytologist*, **173**: 576-583.

Stuart, S.A., Choat, B., Martin, K.C., Holbrook, N.M., Ball, M.C. 2007. The role of freezing in setting the latitudinal limits of mangrove forests. *New Phytologist*, **173**: 576-583.

Stuiver, M. & Polach, H.A. 1977. Reporting of ^{14}C Data. Radiocarbon 19, 355-363

Sugita, S. 1993. A model of pollen source area for an entire lake surface. *Quaternary Research*, **39**: 239-244.

Szatmari, P., Françolin, J.B.L., Zanotto, O., Wolff, S., 1987. Evolução tectônica da margem equatorial brasileira. *Revista Brasileira de Geociências*, **17**, 180-188.

Tanner, W.F. 1958. An occurrence of flat-topped ripple marks. *Journal of Sedimentary Petrology*, **28**: 95-96.

Thomas, R.G., Smith, D.G., Wood, J.M., Visser, J., Calverly-Range, E.A., Koster, E.H. 1987. Inclined heterolithic stratification: Terminology, description, interpretation and significance. *Sedimentary Geology*, **53**: 123-179.

Thompson, R.W. 1975. Tidal flat sediments of the Colorado delta, northwestern Gulf of California. In: Ginsburg, R.N. (Ed) *Tidal deposits: a casebook of recent examples and fossil counterparts*, Springer-Verlag, New-York, p. 57-65.

Thornton, S.F. & McManus, J. 1994. Applications of organic carbon and nitrogen stable isotope and C/N ratios as source indicators of organic matter provenance in estuarine systems: evidence from the Tay Estuary, Scotland. *Estuarine, Coastal and Shelf Science*, **38**: 219-233.

Toledo, M.B. & Bush, M.B. 2007. A mid-Holocene environmental change in Amazonian savannas. *Journal of Biogeography*, **34**: 1313-1326.

Traverse, A. 2007. *Paleopalynology*. 2nd ed., Springer, Dordrecht. 813 p.

Trowbridge, J.H. & Kineke, G.C. 1994. Structure and dynamics of fluid muds on the Amazon continental shelf. *Journal of Geophysical Research Oceans*, **99 (C1)**: 865-874.

Tyson, R.V. 1995. *Sedimentary Organic Matter: Organic Facies and Palynofacies*. Chapman and Hall, London. 15 p.

United States Department of Agriculture (USDA). 1999. *Soil Taxonomy: a basic system of soil classification for making and interpreting soil surveys*. United State Department of Agriculture. Natural Resources Conservation Service. Soil Survey Staff. 2ed. Washington. 169 p.

Vedel, V., Behling, H., Cohen, M.C.L., Lara, R.J. 2006. Holocene mangrove dynamics and sea-level changes in Taperebal, northeastern Pará State, northern Brazil. *Vegetation History and Archaeobotany*, **15**: 115-123.

Van der Hammen, T. 1974. The Pleistocene changes of vegetation and climate in tropical South America. *Journal of Biogeography*, **1**: 3-26

Van Straaten, L.M.J.U. 1952. Biogene textures and the formation of shell beds in the Dutc Wadden Sea. *Koninkl. Nederlandse. Akad. Wetensch. Proc., Ser. B*., **55**: p. 500-516.

Van Straaten, L.M.J.U. 1954. Sedimentology of recent tidal flat deposits and the Psammites du Condroz. *Geologie en Mijnbouw*, **16**: 25-47.

Van Straaten, L.M.J.U. & Kuenen Ph.H. 1957. Accumulation of fine-grained sediments in the Dutch Wadden Sea. *Geol. En. Mijnb.*, **19**: 329-354.

Van Straaten, L.M.J.U. 1961. Sedimentation in tidal flat areas. *Alberta Soc Petrol Jour*., **9**: 203-226.

Viles, H.A. & Goudie, A.S. 2003. Interannual, decadal and multidecadal scale climatic variability and geomorphology. *Earth-Science Reviews*, **61**: 105-131.

Vinzon, B.S., Vilela, C.P.X., Pereira, L.C.C. 2008. Processos físicos na Plataforma Continental Amazônica. Relatório-Técnico, Potenciais Impactos Ambientais do Transporte de Petróleo e Derivados na Zona Costeira Amazônico. Petrobrás, Brasil, 31 p.

Walker, R.G. 1992. Facies, facies models and modern stratigrahic concepts. In: Walker, R.G. & James, N.P. (Eds.), *Facies Models - Response to Sea Level Change*. Ontario: Geological Association of Canada, p. 1-14.

Walsh, G.E. 1974. Mangroves, a review. In: Reimold, R.J. & Queens, W.H. (Eds.) *Ecology of Halophytes*. Academic Press, 51-174.

Weimer, R.J., Howard, J.D. Lindasay, D.R. 1982. Tidal flats and associated tidal channels. In: Scholle, P.A. & Spearing, D. (Eds.), *Sandstone Depositional Environments*. The American Association of Petroleum Geologists, Wisconsin, p. 191-245.

Weng, C., Bush, M.B., Athens, J.S. 2002. Two histories of climate change and hydrarch succession in Ecuadorian Amazonia. *Review of Paleobotany Palynology*, **120**: 73-90.

Wilson, G.W., Lamb, A.L., Leng, M.J., Gonzalez, S., Huddart, D. 2005a. Variability of organic $\delta^{13}C$ and C/N in the Mersey Estuary, UK and its implications for sea-level reconstruction studies. *Estuarine, Coastal and Shelf Science*, **64**: 685-698.

Wilson, G.P., Lamb, A.L., Leng, M.J., Gonzalez, S., Huddart, D. 2005b. $\delta^{13}C$ and C/N as potential coastal palaeoenvironmental indicators in the Mersey Estuary, UK. *Quaternary Science Reviews*, **24**: 2015-2029.

Wolanski, E., Mazda, Y., King, B., Gay, S. 1990. Dynamics, flushing and trapping in Hinchinbrook Channel, a giant mangrove swamp, Australia. *Estuarine, Coastal and Shelf Science*, **31**: 555-579.

Woodroffe, C.D., Chappell, J., Thom, B.G., Wallensky, E. 1989. Depositional model of a macrotidal estuary and floodplains, South Alligator River, Northern Australia. *Sedimentology*, **36**: 737-756.

Wunderlich, F. 1970. Genesis and development of the "Nellenkopfenschichten" (Lowe Emsian, Rheinian Devonian) at locus typicus in comparison with modern coastal environments of the German Bay. *Journal of Sedimentary Petrology*, **40**: 102-130.

Youssef, T. & Saenger, P. 1999. Mangrove zonation in Mobbs Bay, Australia. *Estuarine, Coastal and Shelf Science*, **49**: 43-50

UNIVERSIDADE FEDERAL DO PARÁ
INSTITUTO DE GEOCIÊNCIAS
PROGRAMA DE PÓS-GRADUAÇÃO EM GEOLOGIA E GEOQUÍMICA

PARECER

Sobre a Defesa Pública da Tese de Doutorado de JOSÉ TASSO FELIX GUIMARÃES

A banca examinadora da tese de doutorado de **JOSÉ TASSO FELIX GUIMARÃES,** intitulada **"GEOMORFOLOGIA, MUDANÇAS NAS FONTES DE MATÉRIA ORGÂNICA E DA VEGETAÇÃO EM PLANÍCIES DE MARÉ PRÓXIMAS A FOZ DO RIO AMAZONAS DURANTE O HOLOCENO"**, composta pelos Professores Doutores **Marcelo Cancela L. Cohen** (Orientador-UFPA), **Afonso Cesar R. Nogueira** (UFPA), **Maria Inês F. Ramos (**MPEG**)**, **Susy Eli Marques Gouvea** (UFPA) e **Luiz Carlos Ruiz Pessenda** (USP) após a apresentação oral e arguição do candidato, emite o seguinte parecer:

O candidato apresentou contribuição relevante ao conhecimento sobre a dinâmica e desenvolvimento das planícies de maré do litoral do Amapá no que se refere a sua geomorfologia, vegetação, aporte de matéria orgânica, e estruturas sedimentares desenvolvidas durante o Holoceno. O candidato mostrou segurança durante a exposição de seu trabalho, com uma apresentação clara, didática, bem estruturada e de conteúdo relevante, demonstrando conhecimento da literatura e dos dados palinológicos, isotópicos e sedimentológicos apresentados. Na arguição o candidato defendeu muito bem sua Tese, respondendo as várias questões gerais e específicas. O documento está bem redigido e bem estruturado, no qual seu conteúdo se encontra na forma de três artigos, sendo um já publicado, um segundo em revisão e um terceiro submetido. Destaca-se o fato do candidato ter defendido sua Tese em 36 meses, portanto antes do prazo estipulado de 48 meses.

Com base no exposto, a banca examinadora decidiu por unanimidade aprovar a Tese de doutorado, "COM DISTINÇÃO".

Belém, 11 de novembro de 2011.

Prof. Dr. Marcelo Cancela L. Cohen
(Orientador-UFPA)

Prof. Dr. Afonso Cesar R. Nogueira
(Membro-UFPA)

Prof.ª Dr.ª Maria Inês F. Ramos
(Membro-MPEG)

Prof.ª Dr.ª Susy Eli Marques Gouvea
(Membro-UFPA)

Prof. Dr. Luiz Carlos R. Pessenda
(USP)